



UNIVERSITÀ
DI PAVIA



UNIVERSITY OF PAVIA
FACULTY OF ENGINEERING

UNIVERSITY SCHOOL OF ADVANCED
STUDIES - IUSS PAVIA

**Seismic design and loss assessment of base-isolated structures
using a PBEE framework**

A Thesis Submitted in Partial Fulfilment of the Requirements
for the Degree of Master of Science (Laurea Magistrale) in

Civil Engineering for the Mitigation of Risk from Natural Hazards

by

Federico Damiani

Supervisors:

Gerard O'Reilly, Ricardo Monteiro

Scuola Universitaria Superiore IUSS Pavia, Italy

21 December, 2020



UNIVERSITÀ
DI PAVIA



ABSTRACT

The work of thesis focuses on the improvement that seismic isolation provides to a reinforced concrete (RC) frame's structural performance when subjected to earthquake action; a new conceptual seismic design (CSD) approach is used within the framework of performance-based earthquake engineering (PBEE) in order to justify the choice for seismic isolation, showing how it is a feasible and recommended design solution, as opposed to a fixed-base structure.

This study considers a case study model, represented by a bi-dimensional RC moment resisting frames and performance objectives are now defined in terms of a target expected annual loss (EAL). The CSD approach is used to identify the most suitable structural solution capable of respecting a predefined EAL limit, via feasible initial period range definition. It is shown how, for a fixed-base configuration, a solution compatible with the EAL target does not exist while for a base-isolated configuration, using friction pendulum bearings (FPB) isolators it is, in fact, possible.

Two different solutions of isolation are evaluated: (i) medium friction and (ii) low friction FPBs. The building is then designed for both cases (i.e. fixed base and base isolated) following the Italian national design code (NTC18) requirements, assessing their seismic performance in order to validate the conclusion initially provided by the CSD approach. Static pushover analysis (SPO) and non-linear response history analysis (NRHA) using 11 sets of 40 ground motion records, corresponding to 11 different intensity measure levels, are performed. In order to estimate the seismic induced losses, maximum inter-storey drift ratios (IDR) and peak floor accelerations (PFA) are selected as engineering demand parameters (EDP) and are used to derive the floor median expected loss using available story-specific EDP-DV functions.

Finally, the seismic performance is evaluated through the comparison of vulnerability and loss between the fixed-base case and base-isolated cases. Moreover, medium to low friction FPB isolators variability is also examined to see the impact that the friction coefficient has on the structural response. EAL is computed as the governing performance index to demonstrate how using a base-isolated structural solution leads to the fulfilment of the performance objectives, i.e. having an EAL below the imposed target, while the fixed base does not, validating what was anticipated by the CSD approach.



UNIVERSITÀ
DI PAVIA



ACKNOWLEDGMENTS

For the realization of this work of thesis I want first to thank Professor Ricardo Monteiro and Dr Gerard O'Reilly for all the availability and help towards me in these months. An additional mention goes to the PhD student Gianrocco Mucedero for the given contribution at the beginning of the work. Thanks also to my parents and my brother for having supported me in this period and during these last two years Master. Finally, a special thanks goes to all my friends and classmates I met in these five years of university; it has been a pleasure for me to work with you and to share with you these fantastic years.



UNIVERSITÀ
DI PAVIA



TABLE OF CONTENTS

ABSTRACT	i
ACKNOWLEDGMENTS	i
TABLE OF CONTENTS	iii
LIST OF FIGURES	v
LIST OF TABLES	xi
1. INTRODUCTION	1
2. SEISMIC DESIGN OF RC BUILDINGS	3
2.1. TRADITIONAL NTC18 SEISMIC DESIGN	3
2.2. PBEE CONSIDERATIONS: CSD AND COMPARISON WITH NTC18	9
2.2.1. CSD limitations and drawbacks	19
2.2.2. Specific aspects for base isolation	21
3. SEISMIC ISOLATION	23
3.1. PRESENTATION OF THE TECHNIQUE	23
3.1.1. Performance aspects and comparison with FB configuration	24
3.1.2. Design requirements according to NTC18	26
3.2. DIFFERENT POSSIBLE DEVICES	29
3.2.1. Lead rubber bearings	30
3.3. FRICTION PENDULUM BEARINGS	32
3.3.1. Numerical modelling	36
3.3.2. Friction pendulum bearings NTC18 requirements	38
4. CASE STUDY	41
4.1. PRESENTATION OF THE CASE STUDY BUILDING	41
4.1.1. Fixed-base configuration modelling	44

4.1.2.	Friction pendulum bearings modelling.....	52
4.2.	CSD APPROACH APPLICATION.....	55
4.2.1.	Performance objectives definition.....	55
4.2.2.	SLS requirements	61
4.3.	NTC18 FIXED-BASE CONFIGURATION DESIGN.....	67
4.3.1.	NTC18 capacity design requirements	71
4.4.	NTC18 BASE ISOLATED CONFIGURATION DESIGN.....	79
5.	SEISMIC PERFORMANCE ASSESSMENT	85
5.1.	STATIC PUSHOVER ANALYSIS.....	86
5.2.	NON LINEAR RESPONSE HISTORY ANALYSIS	93
5.2.1.	Ground motion records selection	94
5.2.2.	Results discussion.....	96
6.	LOSS ESTIMATION PROCEDURE.....	105
6.1.	AVAILABLE LOSS ESTIMATION PROCEDURES	107
6.2.	STOREY-BASED BUILDING SPECIFIC LOSS ESTIMATION METHOD	
	111	
6.2.1.	EDP-DV functions.....	116
7.	APPLICATION TO THE CASE STUDY BUILDING.....	119
7.1.	EXPECTED FLOOR LOSSES DISCUSSION	121
7.2.	LOSS CURVES AND EAL DEFINITION	130
8.	CONCLUSIONS AND FUTURE DEVELOPMENTS	133
	REFERENCES.....	137
	APPENDIX A	141
	APPENDIX B	147
	APPENDIX C	149
	APPENDIX D	151
	APPENDIX E	157
	APPENDIX F	161



LIST OF FIGURES

Figure 2.1: Limit state exceedance consideration in a probabilistic or deterministic fashion	12
Figure 2.2: Approximated and refined loss curves used to estimate (EAL)	13
Figure 2.3: Storey loss functions for different occupancies with indication of damageable components weighting coefficients.....	14
Figure 2.4: Feasible initial secant to yield period range at SLS	17
Figure 2.5: Identification of feasible backbone curves space at ULS	19
Figure 2.6: Limitation of CSD approach which assumes uniform demand over building height	20
Figure 2.7: Total losses evolution with increasing damage, also indirect losses are evaluated here	20
Figure 2.8: Situation in which SLS performance objectives cannot be met, alternative solution as base isolation are required	21
Figure 3.1: Isolator period and damping effect in acceleration and displacement response spectra	25
Figure 3.2: Lead rubber bearing typical configurations.....	30
Figure 3.3: Laminated rubber bearing and lead rubber bearing hysteretic loop comparison	31
Figure 3.4: Lead rubber bearing bilinear constitutive law.....	31
Figure 3.5: Normal pendulum and friction pendulum bearing behaviour comparison ..	33
Figure 3.6: FIP series isolator typical configuration	34
Figure 3.7: FIP-D series isolator typical configuration	34
Figure 3.8: Friction coefficient - vertical load ratio relationship for low and medium friction cases	36
Figure 3.9: Friction pendulum bearing typical bi-linear constitutive law	36
Figure 4.1: Front view of the case study building to be modelled	42

Figure 4.2: Design elastic response spectra for NTC18 limit states referred to L'Aquila site	43
Figure 4.3: Beams and columns material and geometrical initial properties.....	44
Figure 4.4: Experimental data from cyclic and monotonic tests of two identical RC columns	47
Figure 4.5: Assumed cantilever model of RC beam and column experimental tests	47
Figure 4.6: Idealized tri-linear end moment versus chord rotation constitutive law.....	48
Figure 4.7: Selected low and medium friction pendulum bearings from FIP catalogue with a displacement capacity of 250mm	52
Figure 4.8: Coulomb friction model selected for the isolators due to friction coefficient velocity independence	54
Figure 4.9: L'Aquila INGV model hazard curve in terms of PGA.....	55
Figure 4.10: Approximated and refined loss curve comparison.....	57
Figure 4.11: SLS point identification on the hazard curve coming from INGV model.	58
Figure 4.12: NTC18 SLS elastic design response spectrum	58
Figure 4.13: Structural drift sensitive and non-structural drift sensitive components loss curves	59
Figure 4.14: Non-structural acceleration sensitive components loss curve	59
Figure 4.15: Displaced shape values for the examined RC frame	61
Figure 4.16: Displaced shape plot for the examined RC frame.....	62
Figure 4.17: A feasible and spectrum compatible solution space for fixed-base configuration cannot be determined.....	63
Figure 4.18: Elastic and overdamped design response spectra comparison	65
Figure 4.19: Feasible solution space and feasible initial period range determined thanks to seismic isolation.....	66
Figure 4.20: NTC18 Table 7.3.II for basic behaviour factor estimation.....	68
Figure 4.21: L'Aquila life safety reduced design spectrum	69
Figure 4.22: Bending moment-axial load interaction diagram	75
Figure 4.23: Capacity design nodal check.....	78
Figure 4.24: SLO average response spectrum to be compared with the L'Aquila-site limit-state corresponding one	81

Figure 4.25: SLD average response spectrum to be compared with the L'Aquila-site limit-state corresponding one	81
Figure 4.26: SLV average response spectrum to be compared with the L'Aquila-site limit-state corresponding one	81
Figure 4.27: SLC average response spectrum to be compared with the L'Aquila-site limit-state corresponding one	82
Figure 4.28: NTC18 limit state checks for both medium and low friction cases.....	83
Figure 5.1: Capacity curve obtained from pushover analysis for the fixed base configuration.....	86
Figure 5.2: Inter-storey drift envelope for fixed base configuration, from pushover analysis.....	88
Figure 5.3: Structural profile for the fixed base configuration, from pushover analysis.	88
Figure 5.4: Inter-storey drift envelope for fixed base configuration, when maximum base shear is reached	89
Figure 5.5: Structural profile for the fixed base configuration, when maximum base shear is reached	89
Figure 5.6: Capacity curves comparison for fixed base, base isolated with medium friction bearings and base isolated with low friction bearings.....	90
Figure 5.7: Inter-storey drift ratio comparison for fixed base, base isolated with medium friction bearings and base isolated with low friction bearings.....	92
Figure 5.8: Structural profile comparison for fixed base, base isolated with medium friction bearings and base isolated with low friction bearings.....	92
Figure 5.9: Fixed base conditioned mean spectrum method for 0.1 probability of exceedance in 50 years	96
Figure 5.10: : Base isolated conditioned mean spectrum method for 0.1 probability of exceedance in 50 years	96
Figure 5.11: Peak floor displacements and inter-storey drift ratios envelope comparison for all the three examined structural configurations, i.e. fixed base, base isolated with medium friction pendulum bearings and base isolated with low friction pendulum bearings; 140 years return period is considered.....	97
Figure 5.12: Peak floor accelerations envelope comparison for all the three examined structural configurations, i.e. fixed base, base isolated with medium friction pendulum bearings and base isolated with low friction pendulum bearings; 140 years return period is considered	98

Figure 5.13: Peak floor displacements and peak inter-storey drift ratios envelope comparison for all the three examined structural configurations, i.e. fixed base, base isolated with medium friction pendulum bearings and base isolated with low friction pendulum bearings; 72 years return period is considered	99
Figure 5.14: Peak floor accelerations envelope comparison for all the three examined structural configurations, i.e. fixed base, base isolated with medium friction pendulum bearings and base isolated with low friction pendulum bearings; 72 years return period is considered	100
Figure 5.15: : Peak floor displacements and peak inter-storey drift ratios envelope comparison for all the three examined structural configurations, i.e. fixed base, base isolated with medium friction pendulum bearings and base isolated with low friction pendulum bearings; 19975 years return period is considered	101
Figure 5.16: Peak floor accelerations envelope comparison for all the three examined structural configurations, i.e. fixed base, base isolated with medium friction pendulum bearings and base isolated with low friction pendulum bearings; 19975 years return period is considered.....	101
Figure 6.1: Simplified PEER framework according to storey-based building specific loss estimation procedure.....	112
Figure 6.2: Building cost distribution assuming commercial office occupancy, from RS Mean Square Root Costs (2007).....	117
Figure 6.3: Components cost distribution for a typical floor in a commercial office building.....	118
Figure 7.1: 1st floor EDP-DV function for commercial office building occupancy to be used for case study model configurations, from Ramirez (2009).....	120
Figure 7.2: Drift sensitive structural (left) and non-structural (right) component expected floor losses, for 475-year return period IM level	121
Figure 7.3: Acceleration sensitive non-structural components expected floor losses, for 475-year return period IM level	122
Figure 7.4: Total expected floor losses for 475-year return period IM level	123
Figure 7.5: Drift sensitive structural (left) and non-structural (right) component expected floor losses, for 72-year return period IM level.....	124
Figure 7.6: Acceleration sensitive non-structural components expected floor losses, for 72-year return period IM level	124
Figure 7.7: Total expected floor losses for 72-year return period IM level	124

Figure 7.8: Drift sensitive structural (left) and non-structural (right) component expected floor losses, for 19975-year return period IM level	125
Figure 7.9: Acceleration sensitive non-structural components expected floor losses, for 19975-year return period IM level.....	126
Figure 7.10: Total expected floor losses for 19975-year return period IM level.....	126
Figure 7.11: Total building expected losses for the fixed base configuration	128
Figure 7.12: Total building expected losses for the base isolated configuration, using medium friction pendulum bearings.....	128
Figure 7.13: Total building expected losses for the base isolated configuration, using low friction pendulum bearings.....	128
Figure 7.14: Vulnerability curves comparison for the three case-study model configurations.....	129
Figure 7.15: Loss curves comparison for the three case-study model configurations ..	131



UNIVERSITÀ
DI PAVIA



LIST OF TABLES

Table 2.1: Probability of exceedance values, in the reference period for the seismic action, associated to each limit state	5
Table 3.1: Minimum friction coefficient values.....	35
Table 4.1: Distributed load values for typical floor and for the roof.....	43
Table 4.2: Seismic hazard parameters for L'Aquila site, for each limit state, from INGV model	43
Table 4.3: Design spectral parameters from INGV model, corresponding to the SLS return period	58
Table 4.4: Weighting coefficients and consequently obtained expected loss ratio for the three damageable components	60
Table 4.5: Fixed-base period range values corresponding to the spectral displacement and acceleration, used to enter the ADRS	63
Table 4.6: Base-isolated period range values corresponding to the spectral displacement and acceleration, used to enter the ADRS	65
Table 5.1: Considered intensity measures return periods and corresponding probability of exceedance in the reference period for the seismic action	93



UNIVERSITÀ
DI PAVIA



1. INTRODUCTION

This thesis focuses on the improvements that seismic isolation provides to the structural performance of reinforced concrete (RC) frames when subjected to earthquake action with respect to the traditional fixed-base configurations. A new conceptual seismic design (CSD) approach is utilised inside the framework of performance-based earthquake engineering (PBEE) in order to validate the choice for seismic isolation, showing how it is a recommended and feasible design solution, when compared to the fixed-base one, if some designers-defined performance objectives are respected. This method, by definition, provides only a conceptual and not detailed seismic design, coming up with the basic geometrical dimensions of the frame, given the material parameters. Its use in this work is to provide a proof or demonstration of how, in order to respect the aforementioned performance requirements, seismic isolation can be seen as the recommended design solution, as opposed to relying on engineering judgement.

The work is mainly divided in three parts:

1. The case study model is presented as a bi-dimensional RC moment resisting frame and the performance objectives that drive the seismic design are set in terms of expected loss ratios, associated with three different limit states, corresponding to three ground motion return periods, and target expected annual loss (EAL). Here the CSD approach is used in order to define the most suitable structural system able to meet them, by means of a feasible initial period range definition at the serviceability limit state (SLS) showing how, for a fixed-base structural solution this cannot be verified, while for a base-isolated one, it can. Two different typologies of friction pendulum bearing (FPB) isolators are selected from an available technical catalogue in the literature: medium and low friction ones. The model is then designed in the fixed-base case, firstly, for the seismic hazard at L'Aquila, in agreement with the capacity design requirements in NTC18 and then in the two configurations (medium & low friction) of the base isolated one. Vertical capacity is the parameter which drives the friction pendulum bearing selection whose performance has to be checked under four sets of 7 ground motion records each, compatible with the site hazard, referred to the four limit states defined by NTC18: operational limit state (SLO), damage limit state (SLD), life safety limit state (SLV) and collapse limit state (SLC);

2. The analysis in which the seismic performance of the model in its different configurations is evaluated, in order to validate the conclusion driven by the CSD approach, through static pushover analysis (SPO) and non-linear response history analysis (NRHA). For the latter, 11 sets, corresponding to 11 different intensity measure levels, of 40 ground motion records each, selected with the conditional mean spectrum method, with respect to the spectral acceleration (SA) at the fundamental structural period of the examined configuration, are used. Maximum inter-storey drift ratios (IDR) and peak floor accelerations (PFA) are selected as the engineering demand parameters (EDP) representing the structural response at each floor level;
3. The estimation of seismically induced expected losses by means of a storey-based building-specific loss estimation method: three damageable component groups are assumed to be present: (1) structural drift sensitive, (2) non-structural drift sensitive and (3) non-structural acceleration sensitive. For each one of them, floor dependant EDP-DV functions available in the literature are used to estimate the mean expected loss (EL), normalized by the storey replacement value. Vulnerability curves are obtained by summing the floor losses to obtain a total building loss for each IM level. Loss curves are created putting together the total building loss and the corresponding IM level mean annual frequency of exceedance. Seismic performance is then evaluated through the comparison of these curves and the aforementioned EDP envelopes that result from both fixed-base and base-isolated solutions. Moreover, medium to low friction FPB variability is examined to see the impact that the friction coefficient has on the structural response. EAL is computed as the governing performance metric to demonstrate how the use of a base-isolated structural solution leads to the fulfilment of the above defined performance objectives, i.e. having an EAL below the imposed target, while the fixed-base one does not, confirming what was anticipated by the CSD approach.

The conclusion of the work focuses, firstly, on the utility of the CSD approach as a discriminant method between feasible and unfeasible structural solutions, though still in a preliminary stage of the seismic design, as well as to underline how this is proved by the actual behaviour of a base-isolated structure, mainly improved in terms of response parameters and losses, with respect to the traditional fixed-base one. Furthermore, some future developments are addressed, resulting in a more practical quantification of the feasible period range values at the SLS, so that the designed isolated structure will have a first period actually inside this range, providing the CSD approach a more practical sense and not just a theoretical one.



UNIVERSITÀ
DI PAVIA



2. SEISMIC DESIGN OF RC BUILDINGS

This chapter deals with the NTC18 definition of the design seismic action according to the considered site and associated seismic hazard, together with an overview of the NTC18 methods and procedures to perform the seismic design of modern RC buildings. The general framework and main applicative steps of the CSD approach are then presented inside PBEE, focusing also on the actual developments for fixed-base structures together with the limitations and drawbacks that can be improved. Moreover, final considerations on how base isolation can be inserted in this framework in order to ensure a structural solution that respects the designers-defined performance objectives, are presented.

2.1. TRADITIONAL NTC18 SEISMIC DESIGN

The design of a structural system must generally comply with the following relationship:

$$E_d \leq R_d \quad (2.1)$$

meaning that the demand E_d , due to the different type of actions present on the structure, has to be less or equal than its capacity R_d , function mainly of the materials mechanical parameters and how their actual behaviour is modelled by means of constitutive laws which can ensure a completely elastic structural response or eventually an excursion in the plastic field, when reached a certain demand threshold. In the latter case the structural resistance becomes dependant also on the structural dissipative capacity through hysteretic cycles and its ability to resist the action not only in a strength-based way, but also in a displacement-based one, being able to displace in order to attenuate the demand, according to the so-called ductility capacity μ_{Ed} :

$$\mu_{Ed} = \frac{\Delta_y}{\Delta_u} \quad (2.2)$$

where:

Δ_y is the yielding displacement defining the transition from the elastic domain to the plastic one;

Δ_u is the ultimate displacement of the structure;

On the other hand, the different actions constituting the demand, are classified in the third chapter of the Italian code, NTC18 §3; among them and in parallel with the scope of the presented work, the seismic action plays a role of paramount importance. It is also relevant to underline how this action, in order to come up with its rigorous estimation, has to be treated in a probabilistic rather than deterministic way. However, in this section, the attention is mainly paid to how seismic action and design are addressed by the Italian code.

The widespread idea among all existing codes is to evaluate structural performance under earthquake action through the definition of different limit states: each one is associated to a certain intensity measure level associated to a specific ground shaking return period T_R . From the structural response point of view, for all of them, a number of requirements that the structure has to fulfil and respect, in order to be characterized by a suitable performance level, are set up. The Italian code prescribes the definition of four limits states; the first twos are termed as serviceability limit states, due to the fact that they are mainly related to the maintenance of structural functionality during ground shaking while the last twos are defined as ultimate limit states since they are related to structural collapse and occupant safety. NTC18 §3.2.1 provides their general description:

1. Operational limit state (SLO): due to earthquake action, the whole structure, including structural and non-structural components and the equipment relevant to its function, must not suffer significant damage and interruption in their functionality;
2. Damage limit state (SLD): due to earthquake action, the whole structure, including structural and non-structural components and the equipment relevant to its function, suffers damage that does not provide risk for users and does not significantly compromise the resistance and stiffness capacity with respect to vertical and horizontal actions, remaining immediately available even in the interruption of part of equipment usage;
3. Life safety limit state (SLV): due to earthquake action, the building undergoes breakages and collapses of the non-structural and plant components and significant damage of the structural components which is associated with a significant loss of stiffness with respect to horizontal actions; the structure instead maintains a part of the strength and stiffness for vertical actions and a safety margin against collapse due to horizontal actions;
4. Collapse prevention limit state (SLC): due to earthquake action, the building undergoes relevant breakages and collapses of the non-structural and plant components and serious damage to the structural components; the construction

still maintains a safety margin for vertical actions and a small safety margin against collapse for horizontal actions.

As mentioned before, each one of these presented limit states, is referred to a certain intensity measure level which can be expressed also, due to the probabilistic nature of the earthquake phenomenon, in terms of probability of exceedance in a given time window. In seismic design, the considered time window is also called reference period for the seismic action V_R , function of the structural nominal life and its occupancy according to the relationship taken from NTC18 §2.4.3:

$$V_R = V_N * C_U \quad (2.3)$$

where:

V_N is the structural nominal life, set up at 50 years for ordinary structures and,

C_U is the usage coefficient, function of the structural occupancy, taken from Table 2.4.II;

NTC18 Table 3.2.1 presents the limit states corresponding probability of exceedance in the reference period for the seismic action:

Table 2.1: Probability of exceedance values, in the reference period for the seismic action, associated to each limit state

Limit states	Probability of exceedance
SLO	81%
SLD	63%
SLV	10%
SLC	5%

The return period T_R is so defined:

$$T_R = -\frac{V_R}{\ln(1 - P_{VR})} \quad (2.4)$$

where:

V_R is the defined reference period for the seismic action;

P_{VR} is the probability of exceedance in this period;

The limit states corresponding to the design seismic action can be defined in different ways according to the type of analysis the designer wants to perform; however, in all of them, the starting point is represented by the (i) the seismic hazard of the considered site, and by (ii) the topographic soil conditions, which determine the local site seismic response. The first term (i) is described by the peak ground acceleration (PGA), at free field conditions on a rigid reference site with a horizontal topographic surface. In Italy, this is determined using the National Institute of Geophysics and Volcanology (INGV) model which divides the country in different seismic hazard level zones, based on the PGA values. The second one (ii) is evaluated through the use of code-defined coefficients, according to the soil type (Tab 3.2. II, NTC18) and topographic conditions (Tab. 3.2.III, NTC18) that, in most cases, are inside category T1.

Three translational components characterize the seismic action: two horizontal components, in X and Y direction, orthogonal with respect to each other, and one vertical along Z direction, considered independently. The last one, has to be considered only in some particular cases and for the effects that can have on non-structural rocking-susceptible elements. A seismic response spectrum is of paramount importance inside this framework and, according to the considered site with associated seismic hazard, it is defined starting from three site-dependant and limit-state dependant parameters:

a_g site peak ground acceleration

F_0 horizontal spectrum maximum value of amplification factor

T_C^* reference period for the horizontal spectrum constant velocity range

The design response spectrum expressions to be used are presented below, in accordance with NTC18 §3.2.3.2.1; these can be used for structures with fundamental period less or equal than 4.0 [s] while, in other cases, seismic action must be defined through the use of ground motion records.

$$0 \leq T \leq T_B \quad S_e(T) = a_g * \eta * F_0 * \left(\frac{T}{T_B} + \frac{1}{\eta * F_0} * \left(1 - \frac{T}{T_B} \right) \right)$$

$$T_B \leq T \leq T_C \quad S_e(T) = a_g * S * \eta * F_0 \quad (2.5)$$

$$T_C \leq T \leq T_D \quad S_e(T) = a_g * S * \eta * F_0 * \left(\frac{T_C}{T} \right)$$

$$T_D \leq T \leq 4[s] \quad S_e(T) = a_g * S * \eta * F_0 * \left(\frac{T_C * T_D}{T^2} \right)$$

where:

$S = S_S * S_T$ is the soil category and topographic condition coefficient, function of stratigraphic amplification S_S (Tab. 3.2.IV, NTC18) and topographic one S_T (Tab. 3.2.V, NTC18)

η is the reduction factor defining the transition from elastic to inelastic response spectrum, in the first case is set equal to 5%, differently is computed as follows:

$$\eta = \sqrt{\frac{10}{5+\zeta}} \geq 0.55 \quad (2.6)$$

with ζ [%] is the structural dependant equivalent viscous damping coefficient

T_C is the reference period for the beginning of spectrum constant velocity range:

$$T_C = C_c * T_C^* \quad (2.7)$$

with C_c coefficient function of the soil category (Tab.3.2.IV, NTC18)

T_B is the reference period for the beginning of spectrum constant acceleration range:

$$T_B = \frac{T_C}{3} \quad (2.8)$$

T_D is the reference period for the beginning of spectrum constant displacement range;

According to each considered limit state, the corresponding design response spectrum has to be selected to define the seismic action; for the serviceability limit states (SLO and SLD) the elastic ones, and a damping coefficient $\zeta = 5\%$ can be used. Differently, for the ultimate limit states (SLV and SLC), when the seismic action is not defined through the use of ground motion records, the structural dissipative capacity can be considered by means of the elastic force reduction, coming up with a reduced design response

spectrum. These considerations are due to the fact that, structural behaviour and response under seismic action, may be distinguished in two categories:

- elastic (non dissipative) structural behaviour: in the evaluation of the demand, all the members and the connections remain in the elastic or substantially elastic domain; the demand arising from the seismic action and other actions is calculated, according to the limit state to which it refers, but regardless of the structural type and without taking into account the non-linearity of the material, through an elastic mode;
- inelastic (dissipative) structural behaviour: in the evaluation of the application a large number of members and / or connections evolve in the plastic field, while the remaining part of the structure remains in the elastic or substantially elastic range; the demand arising from the seismic action and other actions is calculated, according to the limit state to which it refers and the structural type, taking into account the dissipative capacity linked to the non-linearity of the material.

Assuming a structural dissipative behaviour, the design has to comply with one of the two presented ductility classes:

1. high ductility class (class A): with high dissipative capacity
2. medium ductility class (class B): with medium dissipative capacity

The difference between these two is mainly due to the amount of allowed plastic deformation at the design stage, at both local and global level.

The actual non-linear structural behaviour can be detected with the use of constitutive laws which describe in a detailed way the excursion of the structure in the plastic domain where certain amount of displacements, and provided damage, are accepted in accordance with the maintenance of a suitable structural performance. Alternatively, the structural dissipative capacity can be evaluated in an implicit way, through the definition of the so called behaviour factor q . It allows the definition of an equivalent linear model and is function of the structural typology, of how it has been designed and of the material dissipative capacity, through this relationship:

$$q = q_0 * K_R \quad (2.9)$$

where:

q_0 is the basic behaviour factor value at SLV, whose values are reported in Tab.7.3.II of NTC18 depending on ductility class, structural typology and $\frac{\alpha_u}{\alpha_1}$ ratio with:

α_u seismic action multiplier for which the structure develops a collapse mechanism, and

α_1 seismic action multiplier for which the first structural element reaches the plastic domain through yielding.

K_R is a structural in height regularity dependant factor, equal to 1 for regular structures or 0.8 for non-regular ones.

At the ultimate limit states so, seismic demand can be still expressed using the design response spectrum, but reduced as already anticipated, by this behaviour factor q , substituting η with $1/q$.

NTC18 §7.3 defines all the possible structural analyses that can be performed together with the structural response verification criteria at each limit states. The idea of the Italian code is to provide a set of prescriptive requirements in terms of strength and ductility that must be respected in order to come up with acceptable structural performance. This goes under the name of “capacity design”, according to which a hierarchy of strength is defined, allowing the development of some failure mechanisms rather than others and protecting from collapse the structural stability governing elements; structure collapse becomes something accepted but only in accordance with the criteria below:

- distinction of elements and mechanisms in local and global, in brittle and ductile ones;
- brittle mechanisms must be completely avoided as they lead to a non-acceptable structural performance. In the case of RC frames, columns must be stronger than beams in order to protect them from failure ensuring the development of the so-called strong column weak beam ductile mechanism;
- according to the used structural scheme, dissipative zones are defined and correctly designed according to prescribed requirements in order to ensure a correct and efficient energy dissipation.

NTC18 §7.4 presents specific indications for the seismic design of RC structures to which the presented work is mainly addressed. Going inside the specific checks that must be performed, NTC18 §7.4.6 can be consulted for all the structural member prescriptions and verifications that must be fulfilled.

2.2. PBEE CONSIDERATIONS: CSD AND COMPARISON WITH NTC18

Performance based earthquake engineering (PBEE) was introduced around 1995 and had a great influence on the development and modification of the seismic design idea and process: structural performance is assessed in terms of engineering demand parameters-

related damage, due to increasing level of ground motion intensity measures. Different ground shaking return periods are selected to define corresponding limit states with respect to which structural response has to be evaluated. Structural performance rigorous assessment, such as PBEE, is of paramount importance, since it allows designers to understand how the structure behaves under ground motion thus verifying the suitability of the performed design. Current codes, widespread all over Europe and other countries, among which also the Italian one (NTC18), as discussed in the previous section, check building performance simply through the provision of inter-storey drift limits and member verifications, among other requirements, in a completely prescriptive way. Damage states and seismically induced losses are not present inside these codes but they can be really helpful in the description of the structural performance, not only from an engineer's point of view, but also when describing the building performance to the owner and its occupants; on the other side quantities like inter-storey drift or peak floor acceleration, have relatively little significance for them. From a building occupant point of view, structural safety and risk of casualties are of immediate concern; these aspects form part of what has been known as the Pacific Earthquake Engineering Center (PEER) PBEE methodology, outlined by (Cornell CA, 2000), representing an evolution to the initial meaning of PBEE in more probabilistic performance-definition way.

Inspired by this framework, the conceptual seismic design (CSD) is presented as an innovative approach focusing on new metrics, such as seismic induced economic losses, that define performance objectives to be respected by the chosen structural system. This is addressed mainly at the first stage of the seismic design, which, according to (O'Reilly GJ, 2019), can be summarized in three principal phases:

1. identification of a suitable lateral-load resisting system and its associated geometrical layout, given the material properties;
2. detailing of structural members for forces and deformations, identified using one of the many available seismic design methods; and
3. performance verification of the resulting design with respect to the design requirements using either linear or non-linear, static or dynamic analysis.

Existing codes tend to be more focused on the second and third point while the selection of a suitable structural typology is not dealt with with enough attention and though it is a primary step in the seismic design process, they do not provide any detailed indication on suitable choices of lateral load resisting system at the outset of the design process. Conceptual seismic design proposes as a method of conceptual design (meaning so not a rigorous and detailed one) able to come up with the most feasible design solution for a given scenario, in which, and it is here that most of the innovation and changes lay, new metrics and variables drive the design and the selection of this structural system, such as

EAL, i.e. the enclosed area by the loss curve, expected loss ratio at certain limit states, given a certain engineering demand parameter, and also mean annual frequency of exceedance of these limit states. Performance objectives, described in terms of the aforementioned metrics, are set out as the starting point of the conceptual design which has the scope to come up with a feasible solution able to respect these new requirements.

Differing from the existing codes, the attention is shifted from a structural performance merely described by engineering demand parameters and fulfilment of corresponding requirements, to something which, introducing concept of economic losses, can also be addressed and understood to building owners or occupants. Another important point to be underlined is the change in how seismic action is considered probabilistically, meaning its uncertainty is propagated into the structural response to give more risk-consistent designs. The innovation of this approach is not due merely to the use of EAL in an engineering scenario, since it has been already adopted in seismic assessment and for the seismic classification introduced in Italy, but to the fact that it is now chosen as the governing metric driving seismic design and with respect to which seismic performance and the feasibility of different structural solutions is evaluated.

Conceptual seismic design flow is divided in two main parts: (i) definition of performance objectives and (ii) identification of feasible structural solutions. The first step, is to identify, for the considered site, the corresponding seismic hazard coming up with the required parameters to define the seismic action through design response spectrum, as outlined in the previous section (NTC18 §3.2.2). Then, the definition of the building performance objectives to be respected by structural response comes into play; these are set up in terms of expected loss ratio at a certain number of limit states. Expected loss ratio (ELR) is the expected value of direct monetary loss arising from building damage, normalised by its replacement cost; for each limit state a corresponding mean annual frequency of exceedance (MAFE) is defined in order to build up the loss curve (ELR along horizontal axis, MAFE along vertical one, as shown in figure 1), whose enclosed area represents the EAL the building must comply with. It is important not to confuse the mean annual frequency of exceeding a certain limit state with the mean annual frequency of exceeding a certain ground shaking level (hazard curve) while in the past, as said by (O'Reilly GJ, 2019), the first one has typically been assumed to correspond to the reciprocal of the return period for which it was designed, actually this should be the ground shaking MAFE not the limit state one. This, indeed, implies that the design problem becomes deterministic and that no variability is accounted for; (Cornell CA, 2002), proposed an expression to relate these two parameters:

$$\lambda = H(s) * e^{(0.5*k_1^2*\beta^2)} \quad (2.10)$$

where:

λ is the limit state mean annual frequency of exceedance;

$H(s)$ is the ground shaking mean annual frequency of exceedance, with s median value of the selected intensity measure, at the considered limit state: $H = \frac{1}{T_R}$

k_1 is a parameter function of the considered country and β is the assumed dispersion;

As illustrated in Figure 2.1, from deterministic ($MAFE = H$) to probabilistic approach ($\lambda = MAFE$), there is a shift upward due to the amplification of limit state mean annual frequency of exceedance with respect to ground shaking one. A study by (Pinto PE, 2014) pointed out how λ can be expected to be ~ 2.25 times greater than H ; actually this ratio varies with the considered limit state and site hazard conditions.

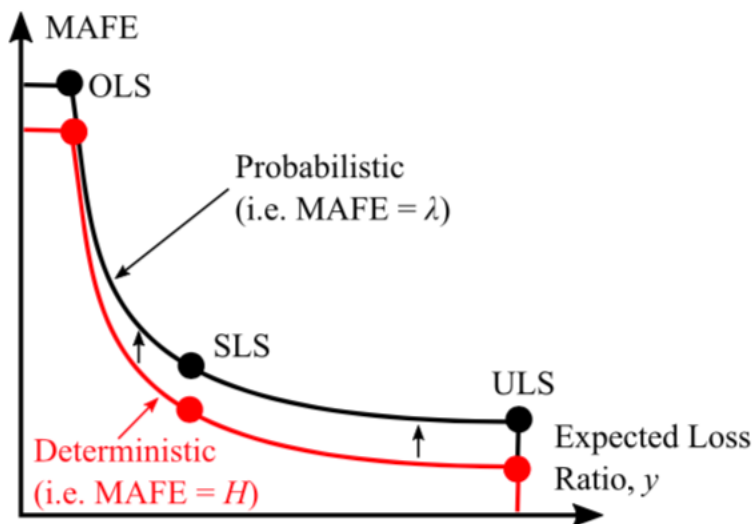


Figure 2.1: Limit state exceedance consideration in a probabilistic or deterministic fashion

When defining the loss curve, different limit states can be considered in a discretised manner, leading to an approximated curve; since this is a conceptual design, three limit states appear reasonable. These are:

- fully operational limit state (OLS), usually associated to an expected loss ratio of 1% as the performance point where direct monetary losses begin to accumulate due to building damage;

- serviceability limit state (SLS) whose corresponding loss ratio is not strictly defined, usually $\sim 15\%$, value that can be modified in order to reach different EAL targets
- ultimate limit state (ULS) for which an expected loss ratio of 100% is adapted, meaning that the structure has sustained losses becoming completely unreparable and must be replaced: the replacement cost has been saturated.

As anticipated, the enclosed area stands for EAL; it is sensitive to how loss curve is defined by means of the number of considered limit states. Having considered just three of them, the actual EAL is not computed as the area beneath the approximated loss curve, but a more refined function, as shown in Figure 2.2, is considered:

$$\lambda = c_0 * e^{-c_1 \ln(y) - c_2 \ln(y)^2} \quad (2.11)$$

where:

y stands for the considered expected loss ratio normalized by the replacement cost;

c_0, c_1, c_2 are simply fitted to pass through the three limit states.

This aspect requires careful consideration since the difference in area between approximated and refined loss curve leads to an overestimation of up to 50% of the first case when compared to the refined one:

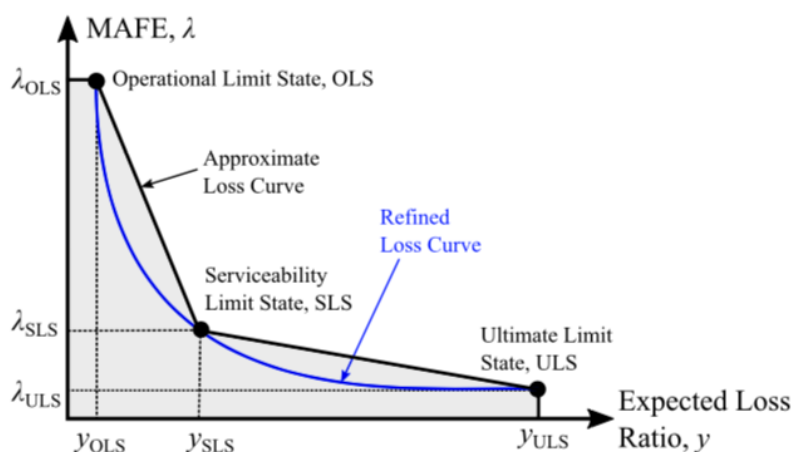


Figure 2.2: Approximated and refined loss curves used to estimate (EAL)

Once performance objectives at different limit states are set up, corresponding maximum allowable engineering demand parameters at SLS and ULS are determined by means of the so called storey-loss functions or engineering demand parameter-damage variable (EDP-DV) functions defined by (Ramirez, 2009). Considering a general building level, three damageable component groups are assumed to be present and to contribute to the total floor expected loss ratio:

- structural drift sensitive components (S_{PSD});
- non-structural drift sensitive components (NS_{PSD});
- non-structural acceleration sensitive components (NS_{PFA});

According to the structural occupancy, each one of them, for the considered floor, has an impact on the total floor expected loss ratio, represented by a “weighting coefficient”: the summation of them must saturate at 1:

$$Y_{S,PSD} + Y_{NS,PSD} + Y_{NS,PFA} = 1.0 \quad (2.12)$$

where these are the weighting coefficient, function of the building occupancy, respectively defined for the three damageable components presented before. An example of storey-loss functions is reported in Figure 2.3:

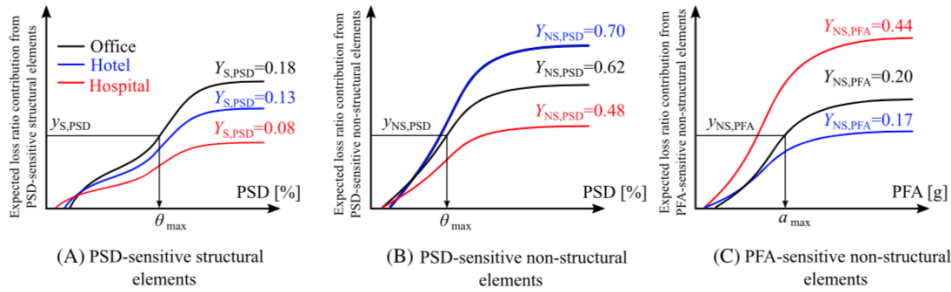


Figure 2.3: Storey loss functions for different occupancies with indication of damageable components weighting coefficients

These curves must be entered with the limit state expected loss ratio of the considered component that is determined as follows. As an example, it is reported the expression for structural drift sensitive components but this is valid also for all the others:

$$y_{S,PSD} = y * Y_{S,PSD} \quad (2.13)$$

where:

y is the total limit state expected loss ratio, defined in the loss curve;

$Y_{S,PSD}$ is the “weighting coefficient” associated to structural drift sensitive components;

$y_{S,PSD}$ is the limit state expected loss ratio for the structural components, that must be used to enter the corresponding storey-loss function;

Entering these curves with the limit state expected loss ratios for all the three damageable components, three structural parameters are obtained:

- $\vartheta_{S,PSD}$ maximum drift for structural components
- $\vartheta_{NS,PSD}$ maximum drift for non-structural drift sensitive components
- $a_{NS,PFA}$ maximum floor acceleration for non-structural acceleration sensitive components.

In order to obtain these parameters at the SLS, the maximum drift representing the maximum allowable building response is taken as the minimum between the structural and non-structural ones. These engineering demand parameters must be converted into spectral values of displacement and acceleration in order to find a feasible initial period range, in the Acceleration Displacement Response Spectrum (ADRS) format, inside which the first period of the designed structural configuration must fall. Starting with the maximum peak storey drift (PSD), this is transformed into spectral displacement by means of the single degree of freedom approximation (SDOF), employed to characterise the multi degree of freedom (MDOF) structural response, under the first-mode dominated assumption. This is similar to the approach adapted in the direct displacement based design (DDBD), developed by (T.J. Sullivan, 2012), obtaining the below defined value of design spectral displacement at serviceability limit state:

$$\Delta d_{SLS} = \frac{\sum m_i * \Delta_i^2}{\sum m_i * \Delta_i} \quad (2.14)$$

where:

i is the index going from 1 to the building number of stories;

m_i is the present floor mass, actually this cannot be known since the structure has not been designed yet, but it is assumed as a function of the acting load, combination of the live load and dead one;

Δ_i is the displaced shape, function of the considered structural typology. For the scope of the presented work, the one referred to RC frames is reported below:

$$\Delta_i = \omega_\theta * PSD * H_i * \frac{4*H_n - H_i}{4*H_n - H_1} \quad (2.15)$$

with:

ω_θ is a reduction factor included for possible storey drift amplification due to higher mode effects;

PSD is the maximum allowable peak storey drift defined just before;

H_i is the current floor level height, H_n the top one and H_1 the first level height.

Relating the peak floor acceleration (PFA) to spectral acceleration at serviceability limit state is not as simple as just done for the maximum drift-spectral displacement relationship, due to the fact that peak floor acceleration cannot be assumed as first-mode dominated. However, since the process of identifying spectral acceleration for various building assumes that the response remains in the elastic domain, some simplifications can be done when computing the j_{th} mode contribution to the PFA at the i_{th} floor level:

$$a_{i,j} = \phi_{i,j} * \Gamma_j * S_a(T_j) \quad (2.16)$$

where:

$\phi_{i,j}$ is the j_{th} mode shape value at floor i ;

Γ_j is the j_{th} mode's participation factor given by the following expression:

$$\Gamma_j = \frac{\sum m_i * \phi_{i,j}}{\sum m_i * \phi_{i,j}^2} \quad (2.17)$$

$S_a(T_j)$ is the spectral acceleration at j_{th} mode period of vibration;

As said by (O'Reilly GJ, 2019), the individual Γ values remain somewhat constant since they depend on storey stiffness and floor mass distribution; knowing the number of storeys and structural typology, the expression above can be simplified summarising the various terms in a unique coefficient γ :

$$\alpha_{SLS} \sim \gamma * PFA \quad (2.18)$$

where:

α_{SLS} is the spectral acceleration at the serviceability limit state;

γ is the summarising coefficient, assumed of the order of 0.60 for low-rise RC frame structures;

The two obtained spectral values Δd_{SLS} and α_{SLS} have then to be used to enter the ADRS, function of the considered site and associated seismic hazard, for the serviceability limit state at the elastic response stage, in order to identify a feasible initial secant to yield period range, as shown in Figure 2.4:

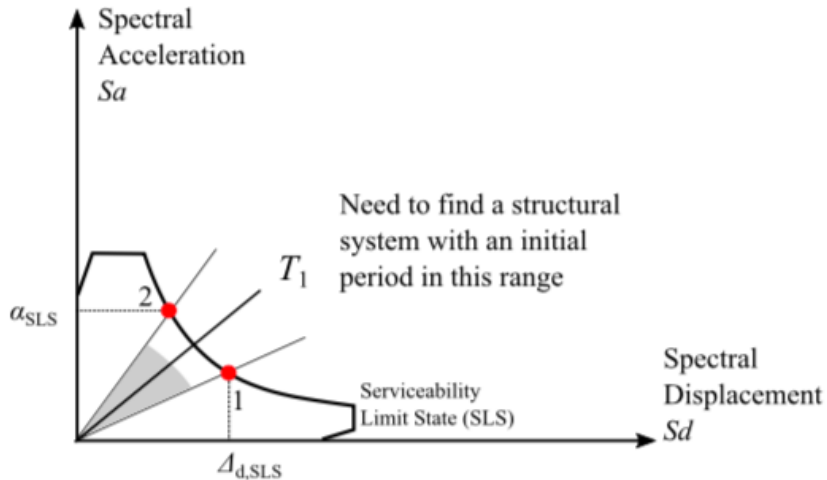


Figure 2.4: Feasible initial secant to yield period range at SLS

Performance objectives at the serviceability limit states are fulfilled if the chosen structural solution has a first period of vibration T_1 that falls within the zone highlighted in grey and bound by the points identified by spectral displacement and spectral acceleration. This implies that the structure must have enough stiffness to not undergo excessive deformations and must be flexible enough not to generate excessive floor accelerations.

Once the range of feasible initial periods has been determined, ultimate limit state (ULS) performance objectives must be fulfilled, finding a feasible structural backbone curve,

characterised by an elastic perfectly plastic behaviour modelling. Actually, ULS considerations are beyond the scope of this work and they are briefly presented herein just for completeness.

Spectral displacement is obtained with the same approach of SLS, while the spectral acceleration is now changed by trial and error attempts in order to obtain the final feasible backbone curve for the chosen lateral-load resisting system. The main difference with respect to SLS is that, now, non-linear structural behaviour must be accounted for through the use of a reduced spectrum, whose required reduction factor is determined below:

$$\eta = \frac{\Delta d_{ULS}}{S_d(T_e)} \quad (2.19)$$

where:

Δd_{ULS} is the spectral displacement at the ultimate limit state and;

$S_d(T_e)$ is the spectral displacement value read at the structural effective period T_e given by:

$$T_e = 2\pi * \sqrt{\frac{\Delta d_{ULS}}{\alpha_{ULS}}} \quad (2.20)$$

The yielding displacement is the parameter of paramount importance that drives all the considerations at ULS together with the spectral acceleration; it is changed till the assumed value and the obtained one, at the end of the process as a function of the determined geometrical dimensions, have a difference that is close to zero. With the assumed Δ_y , the provided ductility is computed, as the ratio between the ultimate and yielding displacement values. With this last value and according to the chosen lateral-load resisting system, the provided reduction factor is computed and the reduced inelastic spectrum is obtained; it has to be used in order to find the grey shaded area representing the space for all feasible backbone curves, as represented in Figure 2.5:

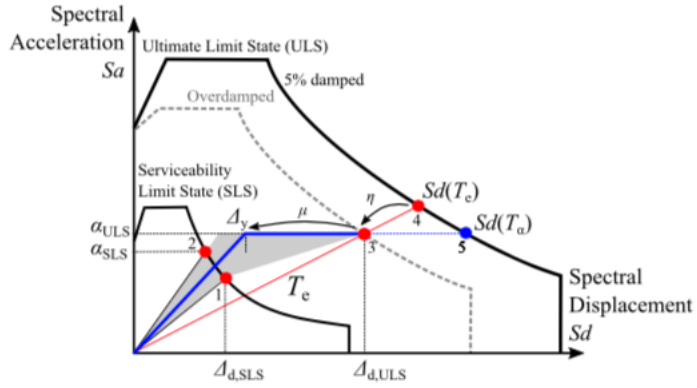


Figure 2.5: Identification of feasible backbone curves space at ULS

As a last step, the geometrical dimensions (frame bay width and beam depth considering, as an example, a RC frame as lateral-load resisting system) are determined and from them, the provided yielding displacement is computed, recalling how it is only function of the geometrical and material properties but not of the structural strength, and compared with the required one, assumed just before. When the difference between these two values is close to zero, conceptual seismic design is performed successfully and the suitable lateral-load resisting system is determined. This is, indeed, able to fulfil the SLS performance objectives having a first fundamental period inside the determined range and respect the ULS ones thanks to the defined elastic perfectly plastic backbone curve.

2.2.1. CSD limitations and drawbacks

The framework described above outlines how feasible structural systems can be identified to meet the targeted performance defined in terms of EAL. However, since it is a quite simplified approach, allowing the designer to come up with just a conceptual design rather than a detailed one, some limitations are presented. One is related to the fact that constant demand, at the considered limit states, over the entire building height, are evaluated when using storey-loss functions to determine the corresponding maximum allowable engineering demand parameter for a certain damageable component, starting from the limit state expected loss ratio.

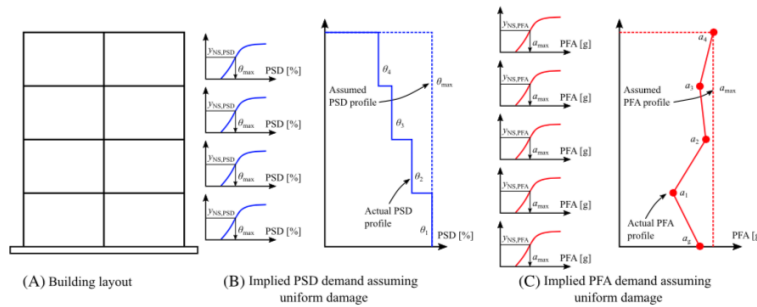


Figure 2.6: Limitation of CSD approach which assumes uniform demand over building height

Actually, this is a quite conservative assumption because when performing subsequent design verifications, using the same storey loss functions ELRs are going to decrease hence the starting point was conservative, from a safety point of view. Moreover, the impact of this assumption is no longer so much relevant for structural systems characterized by a more uniform demand distribution over their height. Some future developments may be performed in this direction.

Indirect losses, such as downtime, may also be incorporated through a more refined ELR definition at each limit state, depending on the building occupancy and its importance and relevance in the society (function of the design nominal life). From Figure 2.7, it is possible to understand how the impact of indirect loss increase with the development of structural damage, moving so from operational limit state, where no indirect losses are present, to the ULS where the direct economic loss saturates at the replacement cost, while the indirect one may significantly increase due to the complete structural collapse.

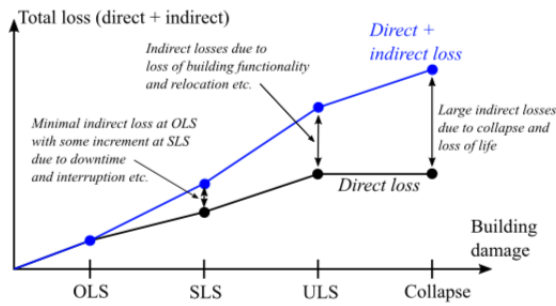


Figure 2.7: Total losses evolution with increasing damage, also indirect losses are evaluated here

2.2.2. Specific aspects for base isolation

Base isolation is a widespread structural solution, especially in recent years, in countries with high seismic risk, in order to improve structural performance under earthquake action resulting in a damage reduction and in a super-structure response (part of the structure above the isolator level) similar to a rigid-body one, due to the low level of inter-storey drift demand. The use of seismic isolation is something that, often, is decided by engineers based on their experience or as a consequence of the difficulty in finding a feasible solution from the initial analysis. This can lead to a not always justified use of base isolation, providing some performance advantages with respect to the more traditional fixed-base configuration that are not very evident, if compared also with the economic drawbacks associated to the realization of such a structural system.

Inside the CSD framework, this decision would be more direct and simpler for designers due to the fact that structures must fulfil well defined performance objectives. For example, it could happen that SLS demand, represented by the associated design response spectrum (elastic), is too large and for the considered traditional structural system, a suitable period range is not possible to be identified via intersection with the design spectrum: this means that it is not able to comply with the performance objectives defined at SLS, since no feasible initial period can be found. Base isolation comes into play reducing the seismic demand through the definition of an overdamped design spectrum, characterized by the use of an equivalent damping coefficient ζ , function of the added isolators type. This design situation is represented in the Figure 2.8:

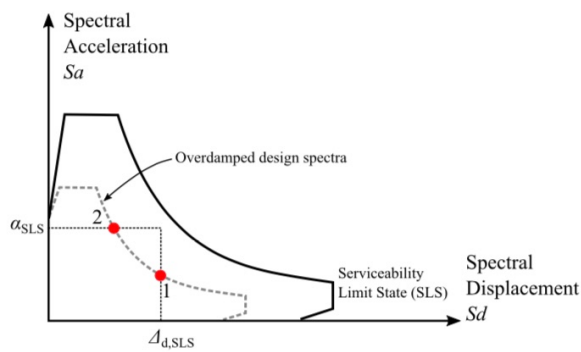


Figure 2.8: Situation in which SLS performance objectives cannot be met, alternative solution as base isolation are required

It is important to underline how the CSD approach still has to be extended to base-isolated structures in further research. Therefore, the idea of this study is to use this method as a validation instrument for the choice of using base isolation rather than a traditional fixed-base structural system, when some performance objectives have to be

met. In these terms, the process followed is the general one described previously for an application case of the CSD approach, with some aspects specified for the RC frames. However, it is important to underline, for a better understanding of the reader, how in this work, the CSD approach has not been directly extended, as it remains the focus of future research, but rather as an instrument to prove and validate the selection of base isolation as a required structural configuration if some performance requirements need to be respected. These are defined in terms of a target EAL that must not be overcome to ensure an acceptable structural performance. Two RC frame configurations are considered: a fixed-base one and a base-isolated one using friction pendulum bearings with first low, and then medium friction. As anticipated, considerations are done only at the serviceability limit state, where the CSD approach is used to show how, for the first structural solution a feasible range of initial periods cannot be found while for the base-isolated one, it can. Both of them are then designed according to NTC18 requirements and their performance assessed using NRHA with different sets of ground motions of increasing intensity measure; EAL is computed showing actually that the base isolated option is below the imposed target, while the fixed base one is not. This underlines how CSD is herein used not strictly in a quantitative way but rather to justify the use of base isolation as structural solution. Future developments may be performed in the direction of defining a detailed procedure for base isolated structures to be applied also in a practical and quantitative manner.



UNIVERSITÀ
DI PAVIA



3. SEISMIC ISOLATION

In this chapter base isolation is described as a possible structural solution, pointing out its main principles and improvements with respect to the traditional fixed base configurations, in terms of structural response and seismic performance. NTC18 design requirements and limit state checks to be verified, are presented. Then, a general overview of all possible devices is given with only a brief description of lead rubber bearings since the main focus is on friction pendulum bearings (FPB) which are used in the case study application. Their behaviour and modelling are discussed referring to the Italian catalogue “FIP Industriale”, from which medium and low friction isolators are selected for the examined case.

3.1. PRESENTATION OF THE TECHNIQUE

While in the past, fixed-base solution was the mostly developed for RC moment resisting frames, designed according to the existing codes, more recently, together with the rise of performance based earthquake engineering and capacity design requirements (NTC18), in order to improve structural response to earthquake action, seismic isolation becomes a quite developed and chosen technique by designers. This happens, particularly, in high seismic risk countries where, despite the use of the innovative provisions mentioned before, structural performance of buildings did not reach acceptable level for designers. The technique of base isolation can both be used for the design of new structures or for the retrofit of existing ones. As already mentioned in the previous chapter, sometimes designers decide for the use of isolators merely according to their experience or as a result of difficulty in finding a feasible structural solution at the design outset: it is important to underline how the isolation solution is able to significantly improve structural response and seismic performance under ground shaking, but a certain trade-off between these advantages and the economic drawbacks due to the higher realization costs (for example with respect to a traditional fixed-base configuration) needs to be considered when selecting the most suitable structural solution. In practical terms, it consists in the use of different type of devices that separate the structural system in two parts: (i) the superstructure, intended as the part above the isolator level which has to be protected and improved in its performance, and (ii) the substructure, defined as the one below the isolator level, mainly constituted by structural foundations. Seismic isolation seeks to completely change the design perspective since, utilising this structural subdivision, earthquake action is not resisted through a systematic increase of the

structural capacity, but by reducing the demand now concentrated at the isolators level. To ensure this structural behaviour, isolators design needs to be performed really carefully, finding the optimal solution for the examined structural system; the devices are selected from available catalogues where their most relevant mechanical parameters and features are presented. Sometimes iterations in the design are needed, trying different types of isolators to see the impact they have on structural response, in order to come up with the optimal solution mentioned before. In fact, this is something that goes beyond the scope of this work where a certain isolation layout is designed and checked with respect to existing code requirements without looking for the absolute optimal solution; the attention is mainly focused on the performance comparison between fixed-base and base-isolated configurations and on the validation of the isolators choice as feasible structural solution when performance objectives have to be met.

3.1.1. Performance aspects and comparison with FB configuration

The introduction of isolating devices has the main function of dividing the building in two parts where ground shaking and structural displacement are decoupled, resulting in a global reduction of the demand in the superstructure with a concentration of demand in the lower isolated layer. Going inside the main principles of this innovative technique, the improvements that can be reached in terms of structural performance with respect to more traditional solutions, are also different. A brief presentation is reported below:

- The first thing that has to be emphasized is superstructure's protection from seismic induced demands and subsequent damage: the isolator presence ensures an elastic response for this part, similar to a rigid body one, reducing significantly inter-storey drifts if compared with the ones present in a fixed-base configuration. This has also a good impact on the structural performance, decreasing the damage associated with drift sensitive structural and non-structural components which, on the other side, have a quite relevant impact on the overall damage state of a traditional building. As a consequence, the use of isolators can lead to a better control of seismic induced direct economic losses, resulting in the fulfilment of prescribed performance objectives, typically not controlled directly with traditional structural solutions;
- The introduction of isolators leads to an increase of the structure fundamental period up to values usually around 2 or 3 seconds, depending also on the selected device typology. The first mode period from modal analysis and associated structural mode of vibration mainly refers to the isolator behaviour. The second one, instead, refers to the superstructure elastic response. The provided increase of fundamental period causes a change in spectral acceleration and displacement values read from the corresponding design spectrum: the first one decreases, together with the inertial forces transmitted to the superstructure

while the latter increases. Seismic isolation essentially represents a trade-off between force reduction and increased displacement across the isolation system. This is well shown in Figure 3.1:

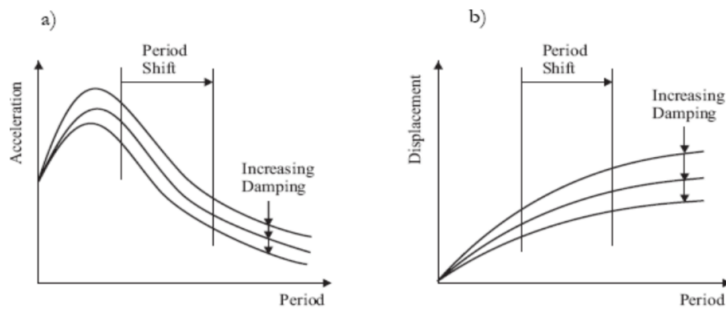


Figure 3.1: Isolator period and damping effect in acceleration and displacement response spectra

In fixed base traditional RC frames, plastic behaviour is mainly associated to the member dissipative capacity and, according to the capacity design requirements a strong-column weak-beam mechanism is looked for, allowing the formation of plastic hinges (and so the development of a dissipative zone) along beams rather than on columns, in order to ensure a ductile failure mechanism in favour of a brittle one. With the addition of isolators, superstructure and all its members remain in the elastic domain and all the energy dissipation is concentrated at the isolators level given their hysteretic behaviour, that can be modelled with the definition of an equivalent damping coefficient ζ . This plays an equivalent role to the behaviour factor q , since as can be seen in Figure 3.1, it leads to a reduction in the spectral demand according to an “overdamped” design spectrum: in this way a spectral displacement reduction can also be appreciated.

- In order to sustain seismic induced displacement demand, together with the dissipative behaviour just described, isolators need to be characterized by a reasonable horizontal flexibility and ultimate horizontal displacement capacity (depending on the isolator typology used); on the other side, along the vertical direction the behaviour has to be stiff enough so that gravity loads, coming from the superstructure, can be sustained without any problems or tension state development and consequent isolator uplift. Due to the high flexibility characterising the isolators, particular attention must also be paid to the evaluation of structural relative movements under non-seismic loading, such as wind action.
- The use of seismic isolation, in general, provides a more regular structural response with respect to traditional solutions, particularly in terms of peak floor acceleration and inter-storey drift envelopes: this will also reflect in a more

uniform direct economic losses distribution among the damageable components present at each superstructure level. In order to emphasize on the concept of response regularity, there are some particular devices characterized by a self-centring or re-centring capacity which completely reduces the amount of residual displacements and drifts; actually the dissertation of such a typology of isolators is beyond the scope of the presented work.

Based on all these considerations, structural response and seismic performance improvements provided by seismic isolation are clearly evident. In order to comply with this described behaviour, isolators need to be carefully selected and designed in agreement with existing codes.

3.1.2. Design requirements according to NTC18

NTC18 §7.10 provides criteria and requirements for the design of new buildings and for the retrofitting of existing ones, in which a seismic isolation system is added under the structure itself, in order to improve the response to horizontal seismic actions. For the scope of this work, the design of new RC frames with base isolation is addressed.

According to NTC18 §7.10.2, this system is composed of isolation and possibly dissipation devices, each of which performs one or more of the following functions:

1. supporting vertical loads with high stiffness along vertical direction and low stiffness or strength in the horizontal direction, allowing considerable horizontal displacements, in agreement with the devices ultimate displacement capacity;
2. energy dissipation with hysteretic and/or viscous mechanisms;
3. re-centring of the structural system;
4. lateral restraint, with adequate stiffness under horizontal (non-seismic) service loads, in order to reduce structural relative movements.

Some additional requirements, indicated in NTC18 §7.10.4, must be respected to ensure a complete functionality of the isolation system:

- the superstructure centre of mass projection on the isolators plan layout has to approximately coincide with the base isolation centre of stiffness in order to avoid excessive torsional effects;
- vertical compression forces coming from the superstructure have to be as uniform as possible not to create too much discrepancy between isolators' behaviour;

- the isolator plane must have a rigid behaviour under seismic action to avoid the development of relative displacements. (See NTC18 §7.10.4.3 for more specifications).

As pointed out in the previous section, the use of isolation devices allows the superstructure to behave essentially in the elastic domain while all energy dissipation is concentrated at the isolators level: how this behaviour is actually modelled is something really relevant that can also affect the global structural response. NTC18 §7.10.5.2 deals with this topic.

In the most rigorous case, the isolation system can be modelled, in relation to its mechanical characteristics, with a linear viscoelastic or nonlinear constitutive law. Isolators vertical deformability must be taken into account only when:

$$\frac{K_v}{K_{esi}} < 800 \quad (3.1)$$

where:

K_v is the isolators vertical stiffness;

K_{esi} is the equivalent horizontal stiffness;

For the sake of simplicity, equivalent linear modelling characterized by equivalent stiffness, referred to the examined limit state total design displacement, can be assumed. Globally, the total equivalent stiffness of the isolation system K_{esi} , is given by the individual devices stiffness sum, and the corresponding dissipative capacity must be expressed in terms of an equivalent viscous damping coefficient ζ_{esi} , evaluated with respect to the amount of energy dissipated by the system through cycles with frequency in the natural frequency range of the modes considered. If K_{esi} and ζ_{esi} significantly depend on the design displacement, an iterative procedure must be applied until the difference between the assumed value and the calculated one is not less than 5%.

This can be done if all the following conditions are met:

- the equivalent stiffness of the isolation system is at least equal to 50% of the secant stiffness for cycles with displacement equal to 20% of the reference displacement;
- the equivalent linear damping, as defined above, is less than 30%;

- the force-displacement characteristics of the system do not vary by more than 10% due to variations in the strain rate in a range of $\pm 30\%$ around the design value, and the vertical action on the devices, in the range of project variability;
- the increase in force in the isolation devices for displacements between $0.5d_c$ and d_{dc} , being d_{dc} the displacement of the center of stiffness due to seismic action, is at least equal to 2.5% of the total weight of the superstructure.

If a non-linear model is adopted, the isolators constitutive law must adequately reproduce their behaviour in the field of strains and velocities that occur during the seismic action, also in relation to the correct representation of the energy dissipated in the hysteresis cycles.

Once the isolation system has been modelled, structural analysis must be performed in order to evaluate structural response, according to what prescribed by NTC18 §7.10.5.3. Linear static analysis can be applied if the following requirements are met:

1. the isolation system can be modelled as linear, in accordance with the previous NTC18 § 7.10.5.2;
2. the equivalent period T_{is} of the isolated structures must be between $3T_{fb}$ and 3.0 [s] , where T_{fb} is the period of the superstructure assumed on a fixed basis, estimated with an approximate expression;
3. isolators vertical stiffness K_v is at least 800 times greater than the equivalent horizontal one, K_{esi} ;
4. the period along the vertical direction $T_v = 2\pi \sqrt{\frac{M_{tot}}{K_v}}$ is less than 0.1 seconds;
5. due to the combined effects of seismic action and vertical loads, no tension is present in the isolators.

NTC18 §7.10.5.3. contains further specifications for the application of the linear static procedures or other alternative methods of analysis; for the scope of the presented work, non-linear response history analysis (NRHA) will be performed to evaluate the case study configurations structural performance.

According to the PBEE framework that governs the Italian code, isolation system performance must be checked with respect to the defined limit states, as shown in NTC18 §7.10.6. This part will be directly addressed in the following section with respect to the friction pendulum bearings (FPB), used in the case study isolated structural solution.

3.2. DIFFERENT POSSIBLE DEVICES

During design outset, it is not possible to establish, a priori, which could be the best isolation system to be used to comply with limit states requirements and additional performance objectives. There are multiple types of isolators available in the market with corresponding catalogues, from which the most suitable for the structure to be designed is selected with all its mechanical parameters. However, some common features must always be present for all isolation devices:

- horizontal flexibility to accommodate seismic induced displacement at isolators level;
- dissipative capacity to attenuate seismic demand both in terms of induced spectral accelerations and displacements;
- rigid behaviour along the vertical direction to sustain vertical load coming from the superstructure, both at rest and during ground shaking (support function);
- horizontal restraint with respect to non-seismic lateral load, such as wind action.

Different can be, for example, the characteristic constitutive law assumed to model the isolator dissipative behaviour, or the presence of an additional self-centring capacity leading to negligible residual displacements or drifts at the end of ground shaking. Two main categories of devices can be identified:

1. elastomeric isolators which exploit the rubber high elastic deformation capacity and sometimes can also be combined with a central lead plug obtaining the so called lead rubber bearings;
2. friction pendulum bearings (FPB), used as the isolation solution of the examined case study, presented in the following section.

Some additional devices could also be considered, together with the isolators themselves, in order to provide additional dissipative capacity, restraint against non-seismic lateral loads and self-centring property. They can be:

- hysteretic-based devices, using the presence of metals such as plug or steel, with non-linear velocity-independent behaviour;
- viscous devices with a deformation velocity-dependant behaviour, based on the extrusion of highly viscous fluids inside a cylinder with piston equipped with suitably dimensioned openings;
- linear or quasi linear devices with a viscoelastic-like behaviour, based on special polymers shear deformation.

This is just a brief presentation and description of all the different available possibilities, there is no intention in going deep inside this topic. As an example, and due to the fact that they are one of the most widespread isolator types, lead rubber bearings are presented.

3.2.1. Lead rubber bearings

These kind of isolators combine a laminated rubber bearing with a cylindrical lead plug, placed in the centre:

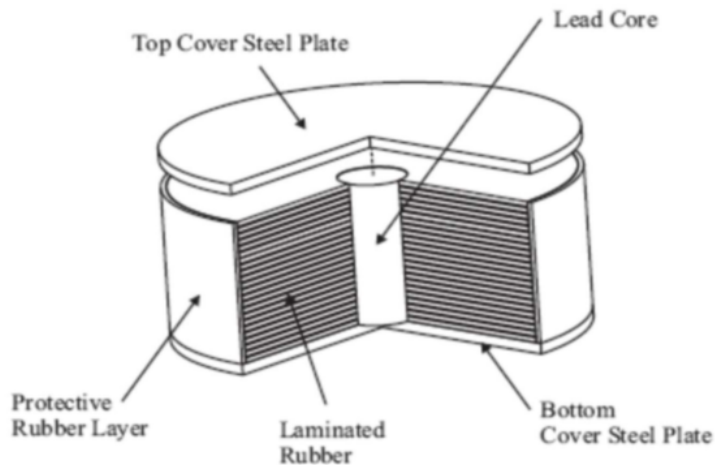


Figure 3.2: Lead rubber bearing typical configurations

The lead core is introduced in order to exploit lead hysteretic properties that it provides due to the shear deformation giving increased damping and dissipative capacity to strongly attenuate the transmitted seismic induced demand to the superstructure.

There are several metals that can be used to realize the core, lead is selected for some reasons:

- at room temperature, it behaves like an elastic-plastic material;
- reaches shear yielding at low stress around 10 [MPa]
- lead properties are restored when cycled in the inelastic range and it has a good fatigue resistance.

The associated advantages can be appreciated in Figure 3.3, where lead rubber bearing hysteretic behaviour (continuous line) is compared with the laminated rubber one (dotted line):

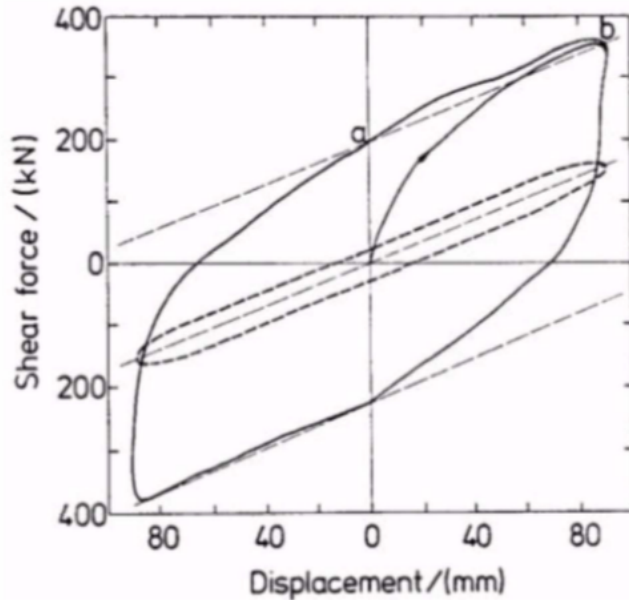


Figure 3.3: Laminated rubber bearing and lead rubber bearing hysteretic loop comparison

As it can be seen, lead rubber bearings provide more energy dissipation and damping with respect to laminated rubber ones, due to the larger area enclosed by the corresponding hysteresis loop. This validates the widespread use of these devices rather than others.

A reasonable model for lead rubber bearings hysteretic behaviour can be the bilinear one represented in Figure 3.4:

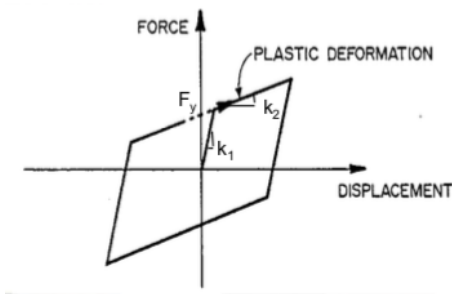


Figure 3.4: Lead rubber bearing bilinear constitutive law

where:

$k_1 = \frac{1}{h_r} * (G_p A_p + G_r A_r)$ is the elastic stiffness with;

h_r total rubber height;

A_p lead plug area; A_r rubber area;

$G_p \approx 150 [MPa]$ lead shear modulus at room temperature;

$G_r \approx 0.5 \div 1 [MPa]$ rubber shear modulus;

$k_2 = k_b = \frac{G_r A_r}{h_r}$ is the post-yield stiffness, equal to rubber lateral shear stiffness;

Having a lower shear modulus with respect to lead the rubber contribution is indeed predominant in the plastic domain: its stiffness becomes the representative constitutive law. For practical size bearings, the elastic stiffness can be estimated as ten times the rubber one.

$$k_1 \approx 10k_b \quad (3.2)$$

Yield force F_y is set equal to the shear force required to yield the lead plug plus the elastic force carried by the rubber at the corresponding yield displacement:

$$F_y = \tau_{py} A_p \left(1 + \frac{G_r A_r}{G_p A_p} \right) \quad (3.3)$$

with:

$\tau_{py} \approx 10 [MPa]$ lead shear yield strength.

For practical size bearings, only the lead contribution is actually relevant at this stage, so that:

$$F_y \approx \tau_{py} A_p \quad (3.4)$$

3.3. FRICTION PENDULUM BEARINGS

This particular kind of isolation devices exploit the pendulum mechanism of motion in order to sustain the seismic induced lateral displacements; indeed, the horizontal component of gravity load is used as restoring force:

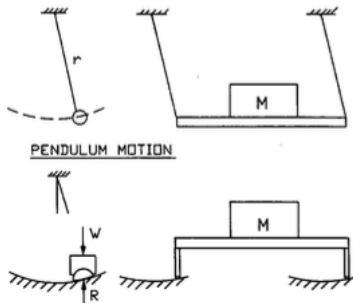


Figure 3.5: Normal pendulum and friction pendulum bearing behaviour comparison

As illustrated in Figure 3.5, friction pendulum bearings behaviour is similar to the “normal” pendulum one for which the period of vibration does not depend on the involved mass but only on the pendulum length. In this case, the fundamental period of vibration of a base-isolated structure with friction pendulum bearings under motion is a function of the sliding surface’s radius of curvature and is independent of the structural mass. The amount of dissipated energy and associated damping, to attenuate seismic induced demand, is given by the during-sliding developed friction while the sliding surface curvature gives the devices a quite good self-centring property, reducing so residual drifts and displacements. These isolators, in general, can be realized in two different ways: (i) with a single primary sliding surface allowing horizontal displacement or (ii) with a double sliding surface.

The Italian catalogue “FIP Industriale” denotes them, respectively, FIP (Friction Isolation Pendula) and FIP-D: this catalogue is mentioned here as the reference one for the selection and design of the isolation devices in the considered case study model.

FIP devices are characterized by three components:

- an element (top in Figure 3.6) with a primary concave sliding surface whose radius of curvature determines the period of oscillation, and which allows horizontal displacement;
- a base member with a secondary concave sliding surface that allows rotation;
- a central element with two convex surfaces suitably shaped to couple with the concave surfaces of the other two elements. The device can also be installed upside down, with the primary sliding surface at the bottom instead of at the top.



Figure 3.6: FIP series isolator typical configuration

Instead, FIP-D devices, also termed sliding isolators with double curved surface, are characterized by two concave sliding surfaces with the same radius of curvature; both allow both horizontal displacement and rotation (which turns into horizontal displacement).

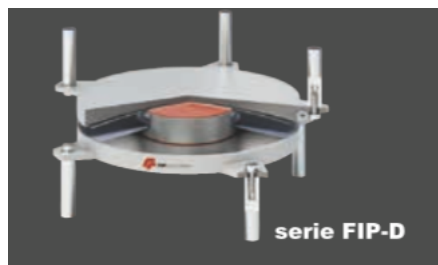


Figure 3.7: FIP-D series isolator typical configuration

In this case, each single curved surface is designed for only half of the horizontal displacement, so that the plan dimensions of the devices can be considerably reduced compared to those of the FIP series. A further advantage of the FIP-D series compared to the FIP series can be identified: the halving of the eccentricity of the vertical load ($P-\Delta$ effect), equal to half the displacement rather than the entire displacement.

The choice of the sliding material is essential in order to give the curved sliding surface isolators an optimal behaviour in terms of:

- bearing capacity;
- friction coefficient and corresponding energy dissipation;
- stability of the force-displacement hysteretic cycle both with temperature and during repeated cycles;
- durability and resistance to fatigue.

According to the Italian catalogue mentioned before, the sliding material used in the primary sliding surface of the FIP series isolators and in both sliding surfaces of the FIP-D series isolators, is the FFM (FIP Friction Material), an ultra-high molecular weight polyethylene (Ultra-High Molecular Weight Poly-Ethylene -UHMWPE) characterized by exceptional properties in terms of load capacity, fatigue resistance, stability and durability. Other important characteristics of the FFM are the absence of the stick-slip phenomenon and the low ratio between first release friction and dynamic friction. These properties have been verified through numerous experimental tests, including those required by the European Standard UNI EN 15129. The FFM is used without lubrication. The material used in the secondary sliding surface of the FIP series devices is SMF (Sliding Material FIP), which is also UHMWPE, but nosed and lubricated.

The parameter of paramount importance in order to correctly model friction pendulum bearings behaviour and for engineers when designing isolation systems with these devices, is the dynamic friction coefficient μ . For any sliding material, the friction coefficient is a function of both velocity and applied pressure. Velocity dependence usually is not significant in the velocity range associated with the seismic excitation of an isolated structure. On the other hand, it is known from the literature, and confirmed by the experimental results, that the dependence on pressure is not negligible: in particular, the friction coefficient decreases with increasing vertical load.

The table shows the minimum values of the dynamic coefficient of friction of the FFM, respectively for FFM type L (low friction) and FFM type M (medium friction), corresponding to the maximum vertical design load N_{Ed} of the isolator, representing its capacity along vertical direction:

Table 3.1: Minimum friction coefficient values

FFM type	Low friction	Medium friction
Minimum friction coefficient	2.5 %	5.5 %

The dynamic friction coefficient varies with the acting vertical load N_{sd} , coming from the superstructure above the isolator plane, in particular it is function of the ratio between N_{sd} (usually considered constant and equal to the quasi-permanent load) and the isolator vertical design load N_{Ed} , taken from the tables for device selection, present in the catalogue. The latter is the maximum vertical load that isolators can sustain at ultimate limit state load combinations including the earthquake, or in any case in any load combination that includes horizontal displacement. The functions that define this variation are represented in Figure 3.8, for both low and medium friction cases:

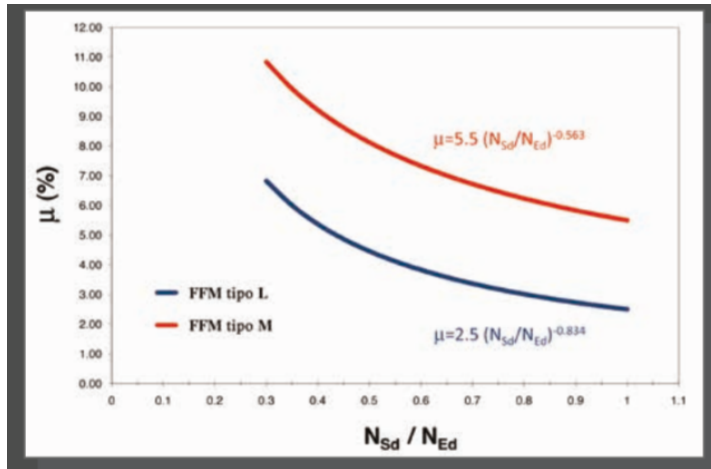


Figure 3.8: Friction coefficient - vertical load ratio relationship for low and medium friction cases

3.3.1. Numerical modelling

The most effective numerical model able to capture the actual behaviour of friction pendulum bearings, with curved sliding surface, of both FIP and FIP-D series, is represented by the bi-linear constitutive law shown in Figure 3.9:

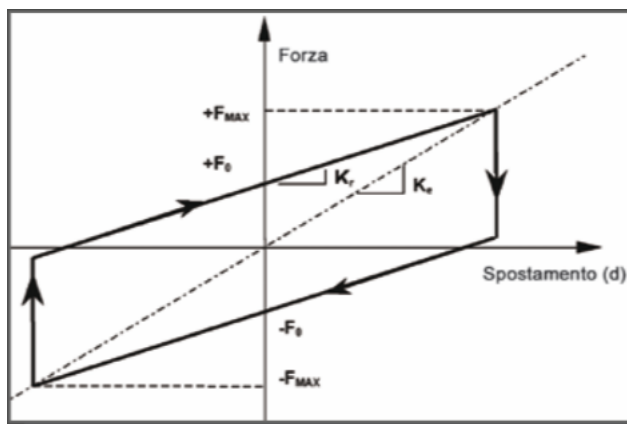


Figure 3.9: Friction pendulum bearing typical bi-linear constitutive law

The most relevant parameters are:

$F_0 = \mu * N_{sd}$ friction force developed by the isolator given by the acting vertical load multiplied by the corresponding friction coefficient. This acts as a threshold value: when reached, isolators start displacing under seismic action;

The friction coefficient μ is function of the acting vertical load according to the relationship shown before.

The acting vertical load N_{Sd} , used to model the behaviour of FPB under seismic action, usually corresponds to the quasi-permanent vertical load (i.e. the superstructure mass multiplied by the acceleration of gravity) which is the average vertical load acting on the isolator during the earthquake. Non-linear dynamic models can be used in order to take into account the variation of the vertical load during ground shaking.

$K_r = \frac{N_{Sd}}{R}$ elastic stiffness defined as the ratio between the acting vertical load and the equivalent radius of curvature R ;

The equivalent radius of curvature R , for the FIP series isolators, coincides with the geometric radius of curvature of the primary surface, while in the FIP-D series isolators, it is equal to twice the geometric radius of curvature of each of the two surfaces curves.

The stiffness-related period, associated to the isolator mode of vibration is determined, as pointed out at the beginning of the section, from the radius of curvature value:

$$T = 2\pi * \sqrt{\frac{R}{g}} \quad (3.5)$$

$F_{maximum} = F_0 + K_r * d = \mu * N_{Sd} + \frac{N_{Sd}}{R} * d$ is the horizontal maximum force developed by the isolator.

An additional thing has to be underlined; friction pendulum bearing starts sliding, displacing under the seismic action, when the F_0 value is overcome. Starting from the origin point, it should be kept in mind that an initial range, almost rigid, with an associated high stiffness K_1 of the isolator before its activation, is required. This demonstrates to be really important in the actual modelling part of the isolator with the software OpenSees that will be discussed in Chapter 4.

Friction pendulum bearing behaviour can, eventually, be modelled as equivalent linear if NTC18 requirements, presented in the previous section and that will be specified for these devices in the following one, are met. In this case, equivalent stiffness and equivalent viscous damping are determined as follows:

$$K_e = N_{Sd} * \left(\frac{1}{R} + \frac{\mu}{d} \right) \quad (3.6)$$

$$\xi_e = \frac{2}{\pi} * \frac{1}{\frac{d}{\mu R} + 1} \quad (3.7)$$

It is worth noting that both the equivalent stiffness and the equivalent viscous damping coefficient depend on the displacement. Consequently, even when it is allowed by the standards to model the isolation system as linear equivalent, an iterative procedure must be applied, until the difference between the displacement values in two successive steps becomes negligible. With the dependence of the equivalent stiffness on the vertical load, isolators plane centre of stiffness and the centre of gravity of the masses automatically coincide in plan. The corresponding equivalent period can be obtained:

$$T_e = 2\pi * \sqrt{\frac{1}{g * \left(\frac{1}{R} + \frac{\mu}{d}\right)}} \quad (3.8)$$

As for the elastic stiffness-related period T , also the equivalent one is not dependant on the involved structural mass but only on the isolator properties, namely the radius of curvature, the friction coefficient and the displacement d .

3.3.2. Friction pendulum bearings NTC18 requirements

As pointed out in the previous section, NTC18 prescribes different requirements to be met in order to model the isolator behaviour as equivalent linear and limit states checks to verify the isolators performance under seismic action. Herein, both of them are presented for the specific case of friction pendulum bearings, following what prescribed by NTC18 §7.10.5.2 and NTC18 §7.10.6.

For friction pendulum bearing case, NTC18 §7.10.5.2 requirements to be fulfilled for linear equivalent modelling are presented below:

- the equivalent stiffness of the isolation system is at least equal to 50% of the secant stiffness for cycles with displacement equal to 20% of the reference displacement; in practical terms:

$$\frac{0.1\Delta_{maximum}}{R} \geq 0.2\mu \quad (3.9)$$

- the equivalent linear damping, as defined above, is less than 30%:

$$\xi_e = \frac{2}{\pi} * \frac{1}{\frac{d}{\mu R} + 1} < 30\% \quad (3.10)$$

- the force-displacement characteristics of the system do not vary by more than 10% due to variations in the strain rate in a range of $\pm 30\%$ around the design value, and the vertical action on the devices, in the range of project variability: this requirement cannot be met since FPB behaviour is sensitive to axial load and velocity through friction coefficient μ .
- the increase in force in the isolation devices for displacements between $0.5d_c$ and d_{dc} , being d_{dc} the displacement of the centre of stiffness due to seismic action, is at least equal to 2.5% of the total weight of the superstructure; in practical terms:

$$\frac{0.5\Delta_{maximum}}{R} \geq 2.5 \% \quad (3.11)$$

Only one non-conformance is enough to prevent equivalent linear modelling: due to FPBs nature, third requirement can never be met, so a non-linear model is needed.

Isolator limit state checks, described in NTC18 §7.10.6, are presented herein for completeness reasons:

- Serviceability limit states:

For base isolated structures, no verifications are needed at the operational limit state (SLO).

Damage limit state requirements are, instead, defined as:

1. devices should not suffer any damage to compromise performance;
2. foundation performance to be verified; criteria 1 and 2 are satisfied if life safety limit state (SLV) checks are met.
3. superstructure drifts, θ , need to be checked as less than 2/3 of the limits for regular construction in both directions of response; drift limit is taken from NTC18 §7.3.6, in the case of “ductile partitions rigidly connected to the structure”:

$$\theta_{limit} = 0.0075 * h_s \quad (3.12)$$

with:

h_s considered inter-storey height;

4. residual displacements, Δ_r , to be checked not to impede functionality: an assumed threshold value is considered, for example 5 cm.

- Ultimate limit states:

Life safety limit state (SLV) checks are the following:

1. substructure needs to be evaluated with results from analysis or else by computing the maximum force transferred via the isolator system capacity;
2. superstructure to be designed for a behaviour factor $q \leq 1.5$; criteria 1 and 2 are assumed to be satisfied as the substructure and superstructure will be designed for appropriate level of force in order to render their behaviour linear elastic.
3. to avoid pounding, the gap between the isolation system and the surrounding substructure needs to be verified at the SLV limit state; this is checked by ensuring the maximum device displacement is less than the provided perimeter gap (assume a value).
4. device performance is to be verified; this is verified by ensuring the maximum displacement in any direction is less than the device's stated displacement capacity. In addition, the maximum axial force acting through the device during analysis is compared to the stated capacity by the manufacturer to ensure that all generated compressive forces may be transferred through the devices. The minimum axial force is also checked to ensure that the devices do not experience tension due to uplift.

At the collapse limit state (SLC), perimeter gap and displacement capacity have to be verified using the same checks employed for the life safety limit state.

All these verifications, have to be made performing non-linear analysis on the base isolated structural configuration, using a set of 7 ground motion records for each limit state, selected as compatible with the considered site seismic hazard, and their mean response over them has to be evaluated and checked as prescribed by NTC18.



4. CASE STUDY

In this chapter, the case study model, given by a bi-dimensional RC moment resisting frame, is presented together with the characterisation of the seismic hazard, for the selected location, representing the design seismic action. L'Aquila site is considered as one of the more seismic-prone sites in Italy and the required parameters to define the design spectrum are evaluated from the INGV model. Performance objectives in terms of expected loss ratio at three different limit states, with corresponding return periods, and expected annual loss target value, are set up. The CSD approach is exploited in order to show how a fixed-base traditional configuration for the presented model would not be expected to comply with the defined objectives at the serviceability limit state, since an initial feasible secant to yield period range cannot be found for the building. On the other hand, seismic isolation is demonstrated to be a feasible structural solution that can be adopted.

For the isolation system, as pointed out in Chapter 3.3, friction pendulum bearings are used and selected from an Italian producer's catalogue “FIP industriale”. To validate this conclusion, both model configurations, fixed base and base isolated one, are designed and verified with respect to corresponding NTC18 requirements. For the latter, both medium and low friction devices are used in order to subsequently evaluate the influence friction coefficient has on the structural response and performance.

4.1. PRESENTATION OF THE CASE STUDY BUILDING

The case study building examined is represented by a three-bay four-storey RC moment resisting frame, located in L'Aquila, to be designed for seismic action in agreement with NTC18 prescriptions. The front view of the frame is shown below: red and blue numbers, respectively, indicate column and beam elements, whereas the black ones, the nodes. This reference system will be used in the modelling process.

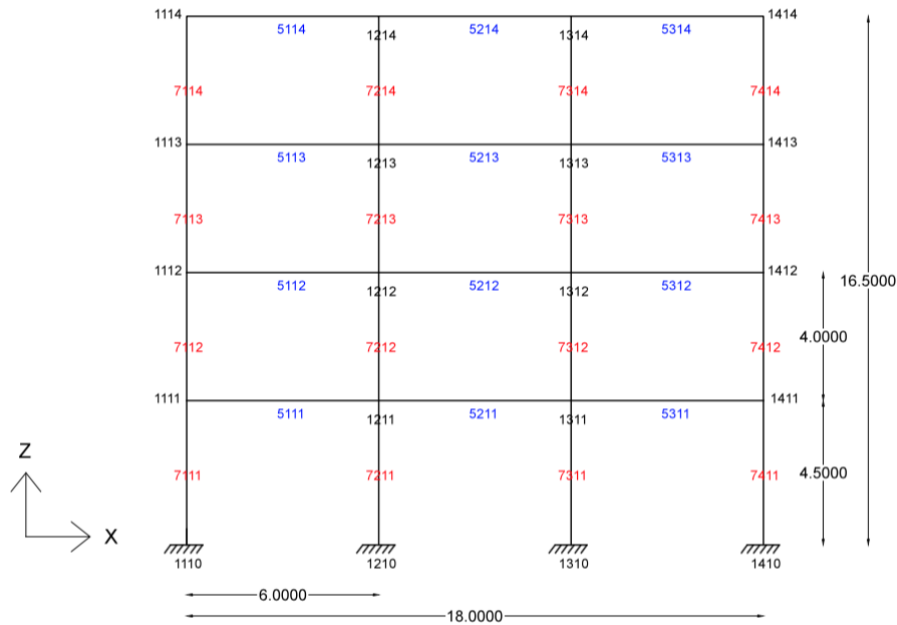


Figure 4.1: Front view of the case study building to be modelled

The first story height is set at 4.5 [m] while for the other levels, a typical value of 4 [m] is used. Each span in the longitudinal direction is 6 [m] wide, for a total width of 18 [m]. Office occupancy is selected and according to NTC18 §2.5.3 equation 2.5.7, seismic action effects have to be evaluated taking into account the below defined gravity loads-associated masses:

$$G_1 + G_2 + \sum_j \psi_j Q_j \quad (4.1)$$

where:

G_1 is the permanent structural gravity load;

G_2 is the permanent non-structural gravity load;

Q_j is the occupancy-dependant variable load and ψ_j the corresponding combination coefficient, selected from NTC18 §2.5.2 table 7.5.I.

In the examined case, typical floor and roof distributed gravity loads are considered as already combined:

Table 4.1: Distributed load values for typical floor and for the roof

Typical floor distributed load, q_{floor}	8 [kPa]
Roof level distributed load, q_{roof}	7 [kPa]

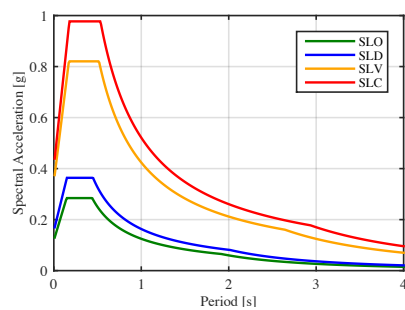
In order to estimate structural demands, these values will be evaluated together with the seismic induced lateral forces, according to the earthquake design combination: NTC18 §2.5.3 equation 2.5.5.

In order to define the design seismic action, L'Aquila site seismic hazard parameters, introduced in Section 2.1, corresponding to the four limit states defined by NTC18, are selected from the INGV model:

Table 4.2: Seismic hazard parameters for L'Aquila site, for each limit state, from INGV model

	SLO	SLD	SLV	SLC
$a_g [g]$	0.079	0.104	0.261	0.334
T_c^*	0.272	0.281	0.347	0.364
F_0	2.4	2.332	2.364	2.4

These coefficients are then used to obtain the associated design elastic response spectrum for all the limit states, according to the expressions presented in Section 2.1.

**Figure 4.2: Design elastic response spectra for NTC18 limit states referred to L'Aquila site**

The RC and steel reinforcement mechanical properties were assumed, together with starting geometrical dimensions of structural elements, as reported in Figure 20:

All floors	f_y [MPa]	γ_s	f_{yd} [MPa]	E_s [MPa]	$\varepsilon_{yd} / \varepsilon_y$	f_c [MPa]	γ_c	f_{cd} [MPa]	E_c [MPa]	b [mm]	h [mm]	c_v [mm]
Beams	413.69	1.15	359.73	200000	0.0018	34.47	1.5	22.98	26392	812.8	609.6	30
1st-2nd lateral Columns	413.69	1.15	359.73	200000	0.0018	48.26	1.5	32.17	29964	812.8	762	30
1st-2nd central Columns	413.69	1.15	359.73	200000	0.0018	48.26	1.5	32.17	29964	812.8	965.2	30
3rd-Top lateral Columns	413.69	1.15	359.73	200000	0.0018	34.47	1.5	22.98	26392	812.8	762	30
3rd-Top central Columns	413.69	1.15	359.73	200000	0.0018	34.47	1.5	22.98	26392	812.8	965.2	30

Figure 4.3: Beams and columns material and geometrical initial properties

where:

f_y is the steel reinforcement yield strength;

γ_s and γ_c are, respectively, the steel and concrete partial safety factor;

$\varepsilon_{y,d}$ is the design steel yield strain;

f_c is the concrete compressive strength;

$f_{c,d}$ is the design concrete compressive strength;

E_s and E_c are, respectively, the steel and concrete Young modulus;

b and h are, respectively, the cross section width and height;

c_v is the assumed concrete cover;

Examining these values, it is possible to notice how the first two floor columns are stronger, in terms of cylindrical concrete compressive strength, than last two ones: this is due to the fact that soft-storey mechanisms are more likely to characterize first structural levels rather than higher ones. Moreover, for all floors, central columns are bigger than lateral ones since, from tributary area considerations, they must sustain a doubled mass and consequently associated gravity load.

4.1.1. Fixed-base configuration modelling

The case study building presented previously is modelled using the software OpenSees in order to assess its structural response and seismic performance according to the different

types of analysis presented in the following chapter. Some initial modelling assumptions have to be specified:

- the case study building is modelled with a bi-dimensional RC frame mainly resisting in its longitudinal direction. For each node, six degrees of freedom are considered: the in-plane horizontal translation along X direction, the vertical one (Z axis) and the out of plane one, associated to Y direction; the corresponding rotations are also evaluated. In order to comply with the bi-dimensional frame assumption, expect for the base nodes that are considered as completely restrained, for all the others, only the out of plane translation is avoided.
- the structural mass and consequently associated gravity loads are determined, for each column, according to tributary area considerations: as anticipated before, central columns sustain more mass with respect to lateral ones. Moreover, a mass amplification factor equal to 4.0 is considered to account for additional tributary mass coming from the gravity loads resisting system present in the transverse direction. This is done to better comply with real resisting mechanism of perimeter RC frame systems, reason for which a 6 [m] out of plane width is defined. Ideally, this additional mass should be considered in a P-delta column but, since the present element formulation is not sensitive to axial load, these can be directly considered by simply amplifying the present ones;

Lateral columns associated masses:

$$m_{l,f} = \frac{\frac{1}{6} * q_{floor} * B_{oop} * B_{tot}}{g} = 14,68 \text{ [tons]} \text{ typical floor lateral columns mass}$$

$$m_{l,r} = \frac{\frac{1}{6} * q_{roof} * B_{oop} * B_{tot}}{g} = 12.84 \text{ [tons]} \text{ roof level lateral columns mass}$$

Central columns associated masses:

$$m_{c,f} = \frac{\frac{1}{3} * q_{floor} * B_{oop} * B_{tot}}{g} = 29.36 \text{ [tons]} \text{ typical floor central columns mass}$$

$$m_{c,r} = \frac{\frac{1}{3} * q_{roof} * B_{oop} * B_{tot}}{g} = 25.68 \text{ [tons]} \text{ roof level central columns mass}$$

These non-amplified values will be used to compute the axial load for element modelling that will be presented in the following section.

Total floor amplified masses:

$$m_{floor} = \frac{q_{floor} * B_{tot} * B_{oop} * m_{amp}}{g} \approx 352 \text{ [tons]} \text{ typical floor amplified mass}$$

$$m_{roof} = \frac{q_{roof} * B_{tot} * B_{oop} * m_{amp}}{g} \approx 308 \text{ [tons]} \text{ roof level amplified mass}$$

$$M_{tot} = 3 * m_{floor} + m_{roof} \approx 1365 \text{ [tons]} \text{ total building amplified mass}$$

- structural members (i.e. beams and columns) are modelled as elastic element with plastic hinges at the ends: they are considered to be internally elastic allowing the formation of plastic hinges to dissipate energy only at the ends and for a certain length termed plastic hinge length L_p : this defines the so-called dissipative zones.

Regarding the non-linear behaviour in the structural modelling, reference is made to (Curt B. Haselton, 2016), which describes the calibration of a phenomenological hinge model to simulate the non-linear hysteretic response of RC beams and columns, under seismically induced large deformations via experimental testing, from the initiation of damage to the onset of lateral collapse. Monotonic backbone curve and hysteretic degradation rules are defined to capture post-peak in-cycle softening, combined with cyclic deterioration, which are associated with concrete crushing and reinforcing bar buckling at large cyclic deformations. Model calibration is based on experimental data for a set of rectangular RC columns with widely varying seismic design and detailing characteristics. For each test, the element model parameters, including initial stiffness, inelastic rotation limits, and cyclic energy dissipation capacity, are systematically calibrated to laboratory test data. Regression analyses are then used to develop semi-empirical equations to calculate the model parameters, as function of the column design parameters, that will be used for the modelling of the case study building.

In order to simulate structural response up to collapse, analysis models must capture the full range of behaviour from flexural yielding to post-peak cyclic degradation in strength and stiffness ((Ibarra, et al., 2005); (Haselton, 2007)). In flexure-controlled RC beam-columns, post-peak softening is usually associated with the physical phenomena of concrete crushing, reinforcing bar buckling and fracture, or also bond failure. Two curves are commonly used to describe component response: a monotonic loading curve and a cyclic envelope curve. The differences between these curves are illustrated in Figure 4.4:

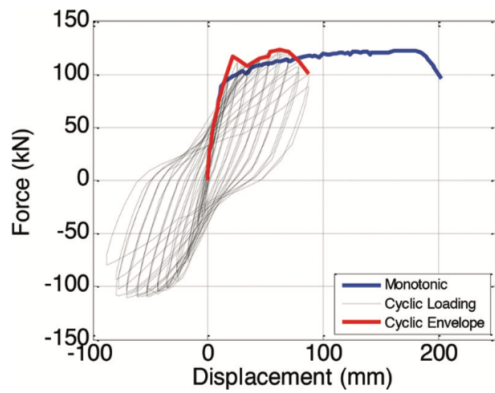


Figure 4.4: Experimental data from cyclic and monotonic tests of two identical RC columns

In this study, a model formulation proposed by (Ibarra, et al., 2005) is followed, whereby a backbone curve that reflects the response under monotonic loading is combined with hysteretic response parameters that can represent the backbone curve degradation under cyclic loading, defining so a certain energy dissipation capacity. This model has the advantage of separating the two distinct modes of deterioration: (i) cyclic strength deterioration due to strength loss occurring between subsequent cycles of loading, wherein the model maintains a positive tangent stiffness in each cycle and, in contrast, (ii) in-cycle strength deterioration due to strength loss occurring during a single cycle of loading, in which force-deformation response develops a negative tangent stiffness, pointed out as strain softening response. In-cycle strength deterioration is indeed modelled through a negative slope in the monotonic loading curve. In order to calibrate the model parameters, each experimental test is defined as a cantilever column (i.e. an elastic element with a zero-length moment-rotation hinge) as shown in Figure 4.5:

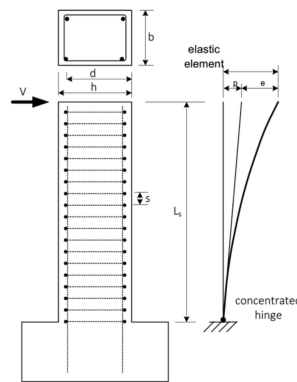


Figure 4.5: Assumed cantilever model of RC beam and column experimental tests

The moment-rotation hinge is modelled using the (Ibarra, et al., 2005) hysteretic material present in OpenSees (2014). Plastic hinge is assigned a high elastic (pre-yield) stiffness, and the stiffness of the elastic element is adjusted (increased) accordingly, such that the resulting column assembly has an effective elastic stiffness consistent with a fix-ended cantilever. The idealized model is characterized in terms of the maximum end moment for the equivalent cantilever column, M , and chord rotation, ϑ , computed as the lateral tip displacement δ divided by the member length, L_s , termed as shear span. Total chord rotation includes contributions that result from elastic deformations along the member length δ_e and the plastic hinge rotation δ_p .

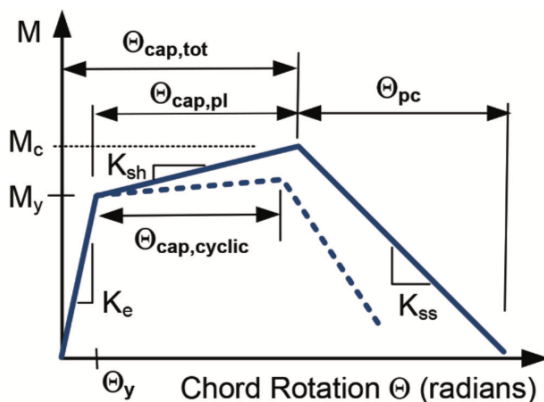


Figure 4.6: Idealized tri-linear end moment versus chord rotation constitutive law

As shown in Figure 4.6, the monotonic loading curve is described by a trilinear idealization of the moment versus chord rotation, defined by five parameters: yielding moment M_y , elastic stiffness K_e , capping or maximum moment M_c , hardening ratio M_c/M_y , capping plastic chord rotation $\vartheta_{cap,pl}$ and post-capping chord rotation ϑ_{pc} . From these, it is possible to determine the yield rotation ϑ_y , the inelastic strain hardening K_{sh} and the post peak strain-softening, given by the negative strain-softening slope K_{ss} , essential to capture the in-cycle strength deterioration. Moreover, the residual strength at large rotations is assumed to be negligible and it is not quantified due to insufficient test data. The lower dashed curve represents a cyclic envelope, which would be obtained as previously specified by a curve that envelopes the response curves from a cyclically loaded member. As can be seen, cyclic loading affects inelastic rotation capacity, peak strength, but also the hardening and softening stiffness: the first one decreases while the latter increases, in terms of slope.

In order to complete the model, cyclic strength deterioration needs to be evaluated: it requires an appropriate set of hysteretic rules, many varieties of which can be found in the literature. While in concept it is desirable to define hinge parameters that are independent of the rules of the specific hysteretic model employed, some of the parameters are inextricably linked to the hysteretic model formulation. In the Ibarra et al. (2005) model, the monotonic backbone envelope is degraded by the ratio of the total energy dissipated by the plastic hinge $\sum E_i$ to the total energy dissipation capacity E_t , which is defined as:

$$E_t = \gamma M_y \vartheta_y \quad (4.2)$$

or

$$E_t = \lambda' M_y \vartheta_{cap,pl} \quad (4.3)$$

In (Curt B. Haselton, 2016), based on (Ibarra, et al., 2005) hinge model, determination of the dissipation capacity parameters, γ and λ' , through empirical equations, is included.

Starting from these specific considerations, an OpenSees procedure is developed in order to model structural members as described above, coming up with the tri-linear monotonic backbone curve and degradation coefficients. This procedure requires the definition of certain input parameters for all beams and columns:

- concrete compressive strength, steel yield one and corresponding Young modulus as reported in Figure 4.4;
- cross section geometrical dimensions and assumed concrete cover;
- assumed longitudinal reinforcement diameter, stirrups diameter and associated spacing;
- confinement strength ratio k for which:

$$f'_{cc} = k * f_c \quad (4.4)$$

k , in the considered model is set equal to 1.4 for all beams and columns for simplicity;

- bond slip parameter α_{sl} , now equal to 0 meaning that this phenomenon is not anticipated here;

- acting axial load on the element and shear span L_s ; the latter is computed as 0.5 times the single bay width for beams while as 0.5 times the floor height for columns;
- top, middle and bottom longitudinal reinforcement ratios ρ , in both element end sections with respect to both Y and Z axis, and shear reinforcement ratio ρ_{shr} . In the examined case, mid reinforcement is assumed to not be present.

Referring to (Curt B. Haselton, 2016), the tri-linear monotonic curve relevant terms are determined using the following empirical equations:

M_y yielding moment, coming from a moment-curvature analysis with OpenSees;

$$\phi_Y = 2.1 * \frac{f_y}{E_s * h} \quad (4.5)$$

yielding curvature according to (T.J. Sullivan, 2012), computed in this case with respect to local z-z axis. Corresponding yielding chord rotation, which actually comes into play in the tri-linear model, can be obtained multiplying the curvature by the involved geometrical dimension;

$$K_e = M_y / \phi_Y \quad (4.6)$$

initial cracked section stiffness characterizing the first range of the monotonic curve;

$$M_{capping} = 1.25 * 0.89^\nu * 0.91^{0.01f_c} * M_y \quad (4.7)$$

capping moment, function of the normalized axial load ratio ν computed as the acting axial load P divided by gross section area and concrete compressive strength;

$$M_{ultimate} = 0.1 * M_y \quad (4.8)$$

ultimate moment: the residual strength at large rotations is assumed to be negligible and it is not quantified.

$$\vartheta_{cap,pl} = 0.12 * (1 + \alpha_{sl} 0.55) * 0.16^\nu * 0.22 + 40 \rho_{shr}^{0.43} * 0.54^{0.01f_c} * 0.66^{0.1s_n} * 2.27^{10\rho_l} \quad (4.9)$$

capping plastic chord rotation, with:

$$s_n = \frac{s}{\phi_l} * (0.01f_y)^{0.5} \quad \text{reinforcing bar slenderness ratio of stirrups spacing to longitudinal bar diameter.}$$

$$\phi_{cap} = \frac{\vartheta_{cap,pl}}{L_p} + \phi_Y \quad \text{corresponding capping curvature where:}$$

$$L_p = 0.08L_s + 0.022f_y\phi_l \quad \text{plastic hinge length expression coming from (T. Paulay, 1992)}$$

$$\vartheta_{post,cap} = 0.76 * 0.031^\nu * (0.02 + 40\rho_{shr})^{1.02} \leq 0.1 \quad (4.10)$$

post-capping chord rotation with:

$$\phi_{ult} = \phi_{cap} + \frac{\vartheta_{post,cap}}{L_p} \quad \text{corresponding curvature.}$$

The last two involved terms are, firstly, the hardening ratio, representing the slope of the monotonic curve second range, and, then, the stiffness deterioration coefficient, which describes the cyclic energy dissipation capacity, to be combined with the before represented constitutive law:

$$K = \frac{\frac{M_{capping}-M_y}{\phi_{cap}-\phi_Y}}{M_y*\phi_Y} \quad (4.11)$$

and

$$\lambda = 170.7 * 0.27^\nu * 0.1^{\frac{s}{d}} \quad (4.12)$$

with:

d RC cross section's effective depth.

Using all these values, the actual non-linear behaviour is built up for the flexural hinge at member ends. The two flexural plastic hinges are then aggregated with the one referred to the axial behaviour so that the plastic hinge modelling is now completed. However, it is also necessary to define a material model for the internal structural member elastic

behaviour in order to obtain a model of the whole considered frame element. The last step of the whole element creation is performed using the “forceBeamColumn” element command, available in OpenSees, which creates the member, putting together the plastic hinge behaviour with the elastic one through a force-based formulation using one integration method among all the possible that are available; in this case the Hinge Radau one is employed.

4.1.2. Friction pendulum bearings modelling

Seismic isolation system needs to be added at the just described structural model: friction pendulum bearings are used and selected from the Italian catalogue “FIP Industriale”. As the conceptual design represents an initial step of the design process, the frame has not been designed yet and only geometrical dimensions and material properties are set; for these reasons, isolator selection process is driven by a demand-capacity comparison: the design axial capacity of the devices must be enough to sustain the vertical acting load in compression or possible tension from the superstructure, present above the isolation plane. Due to the fact that central columns carry twice the gravity load with respect to lateral ones, isolators with different vertical capacity are required.

$N_{sd,l} = m_{amp} * (3 * m_{l,f} + m_{l,r}) * 9.81 = 2304 [kN]$ acting vertical load on lateral columns, obtained considering the amplified mass coming from the superstructure; $m_{l,f}$ and $m_{l,r}$ are the masses due to tributary area computed in Section 4.1.

$N_{sd,c} = m_{amp} * (3 * m_{c,f} + m_{c,r}) * 9.81 = 4608 [kN]$ acting vertical load on central columns, obtained considering the amplified mass coming from the superstructure; $m_{c,f}$ and $m_{c,r}$ are the masses due to tributary area computed in Section 4.1.

The catalogue table from which they are selected is reported in Figure 4.7: both medium and low friction devices are examined with the associated mechanical parameters:

Attrito minimo		Attrito medio		SPOSTAMENTO ± 200 mm						
Sigla isolatore	N_{sd} kN	Sigla isolatore	N_{sd} kN	D	V	Z	H	n	W	
FIP-D 2.280400 (3100)	1000			480	570	480	108	4	85	
FIP-D 1.370400 (3100)	1500			490	600	490	114	4	110	
FIP-D 1.470400 (3100)	2000			520	690	520	109	4	130	
FIP-D 1.550400 (3100)	2500			540	710	540	106	4	140	
FIP-D 1.630400 (3100)	3000			560	730	560	125	4	170	
FIP-D 1.720400 (3100)	3500			580	750	580	121	4	180	
FIP-D 1.810400 (3100)	4000			600	770	600	128	4	210	
FIP-D 1.1050400 (3100)	5000			640	890	690	152	4	290	
FIP-D 1.1150400 (3100)	6000			670	920	710	146	4	310	
FIP-D 1.1250400 (3100)	7000			6850	750	950	730	150	4	360
FIP-D 1.1450400 (3100)	8000			6900	870	740	176	4	420	
FIP-D 1.1650400 (3100)	9000			6600	750	1000	770	169	4	460
FIP-D 1.1800400 (3100)	10000			7250	770	1100	850	175	4	550
FIP-D 1.2200400 (3100)	12500			9350	820	1150	890	214	4	710
FIP-D 1.2600400 (3100)	15000			11500	870	1110	1010	220	8	860
FIP-D 1.3050400 (3100)	17500			14000	920	1180	1040	235	8	1100
FIP-D 1.3450400 (3100)	20000			16250	980	1240	1140	285	8	1300
FIP-D 1.4300400 (3100)	25000			21000	1040	1320	1370	280	12	1800
FIP-D 1.5100400 (3100)	30000			25500	1110	1390	1420	381	12	2450
FIP-D 1.6500400 (3100)	40000			34500	1230	1510	1670	397	16	3200
FIP-D 1.8200400 (3100)	50000			44000	1340	1620	1920	429	20	4600
FIP-D 1.9800400 (3100)	60000			53500	1440	1720	2160	426	24	5600

Figure 4.7: Selected low and medium friction pendulum bearings from FIP catalogue with a displacement capacity of 200mm

Low friction isolators: FIP-D L 630/400 3100 & FIP-D L 1000/400 3100

- $R_{eff} = 3.1 [m]$ radius of curvature;
- $\mu_{lateral} = 3.2\%$ lateral isolator friction coefficient;
- $N_{Ed,l} = 3000 [kN]$ lateral isolator vertical capacity;
- $\mu_{central} = 2.68\%$ central isolator friction coefficient;
- $N_{Ed,c} = 5000 [kN]$ central isolator vertical capacity;
- $\Delta_d = \pm 200 [mm]$ design displacement capacity in both horizontal directions;

Medium friction isolators: FIP-D M 1000/400 3100 & FIP-D M 1350/400 3100

- $R_{eff} = 3.1 [m]$ radius of curvature;
- $\mu_{lateral} = 6.5\%$ lateral isolator friction coefficient;
- $N_{Ed,l} = 3100 [kN]$ lateral isolator vertical capacity;
- $\mu_{central} = 5.66\%$ central isolator friction coefficient;
- $N_{Ed,c} = 4850 [kN]$ central isolator vertical capacity;
- $\Delta_d = \pm 200 [mm]$ design displacement capacity in both horizontal directions;

Isolators with the same radius of curvature and design displacement capacity are selected in both medium and low friction configurations. In order to model them with OpenSees, the “FPBearing” element command is employed. Isolator element is defined by two nodes: the first one represents the concave sliding surface while the second represents the articulated slider. The element can have zero length or the appropriate bearing height, in this case the isolator height, taken from the catalogue, is considered. The bearing can have unidirectional (2D) or coupled (3D) friction properties (with post-yield stiffening due to the concave sliding surface) for the shear deformations, while force-deformation behaviours defined by Uniaxial-Materials command in the remaining two (2D) or four (3D) directions. To capture the uplift behaviour of the bearing, the designer-specified Uniaxial-Material in the axial direction is modified for no-tension development. To avoid the introduction of artificial viscous damping in the isolation system (referred to as

"damping leakage in the isolation system"), the bearing element does not contribute to the Rayleigh damping model defined for the superstructure by default.

Moreover, a friction material model needs to be defined: due to the fact that, in the range of seismic induced velocities, friction coefficient can be assumed as velocity independent, the Coulomb model is simply used for the isolation system:

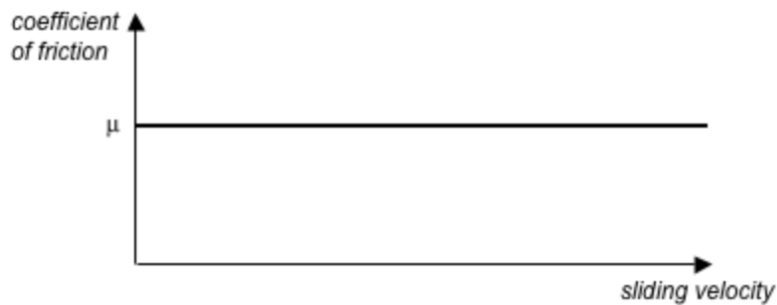


Figure 4.8: Coulomb friction model selected for the isolators due to friction coefficient velocity independence

Friction coefficient, in medium and low friction case is computed as a function of the axial load ratio (demand over capacity), reason for which, central and lateral isolators are characterized by different values:

$$\mu_{medium} = 0.01 * 5.5 * \left(\frac{N_{sd}}{N_{Ed}} \right)^{-0.563} \quad (4.13)$$

and

$$\mu_{low} = 0.01 * 2.5 * \left(\frac{N_{sd}}{N_{Ed}} \right)^{-0.834} \quad (4.14)$$

The above-mentioned command requires also the isolator stiffness definition: the one to be used, as pointed out in Section 3.2, is not the elastic one. Instead a designer-based high value has to be set in order to represent the stiff behaviour of the isolator before the activation, and so before it actually starts displacing under ground shaking:

$K_R = 5 * 10^4$ [kN/m] is the considered value to represent this rigid behaviour for both central and lateral devices, and both medium and low friction configurations.

Models for fixed base and base isolated configurations are set up, only at an initial design stage which is enough to deal with conceptual seismic design approach consideration in

order to identify which of the two can be considered as a feasible solution to comply with defined performance objectives.

4.2. CSD APPROACH APPLICATION

Once the model has been completely set up, conceptual seismic design comes into play in order to show how, given the frame in its initial configuration (where only geometrical dimensions, material properties and structural member cross sections are given) but not yet designed, a traditional fixed-base configuration will not be suitable in order to comply with a set of designers-established performance objectives at the serviceability limit state. A base isolation system is introduced as a possible alternative structural solution, selecting friction pendulum bearings to be placed under the four present first floor columns, so that their vertical load capacity is enough to sustain the acting vertical loads, coming from the superstructure amplified mass. Repeating the same steps as done for the fixed-base case, a feasible initial period range can now be found proving how seismic isolation is a structural solution able to comply with SLS defined performance objectives.

4.2.1. Performance objectives definition

The case study building is located at L'Aquila, chosen as one of the highest-risk cities in Italy, and it is used to represent the seismic hazard considered in the analysis. The hazard is represented by the intensity measure peak ground acceleration (PGA) and the corresponding hazard curve is obtained from the INGV model, where PGA values are given for different return period values T_r . Actually, to come up with the rigorous hazard curve, the mean annual frequency of exceedance H is determined with the following expression:

$$H = \frac{1}{T_r} \quad (4.15)$$

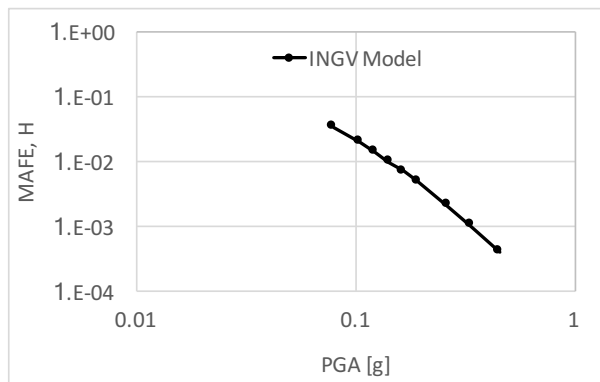


Figure 4.9: L'Aquila INGV model hazard curve in terms of PGA

In order to determine the performance objectives to be respected in terms of loss to be used within the CSD framework, some assumption based on engineering judgement must be followed since no precise prescriptions or indications, starting, for example, from the structural model and its occupancy, are present in existing codes. For the case study building, an EAL limit is set at 0.07% at the start of design. Expected loss ratios, representing the expected value of seismic induced direct monetary loss coming from building damage and normalized by its replacement cost at different limit states are also defined, together with the associated mean annual frequency of exceedance;

- Operational limit state (OLS): $\lambda_{OLS} = 0.10$ and $y_{OLS} = 0.1\%$; these values seem to be reasonable since operational limit state point is considered as the starting one of direct monetary loss accumulation due to building damage.
- Ultimate limit state (ULS): $\lambda_{ULS} = 10^{-4}$ and $y_{ULS} = 100\%$; it is considered as the limit state where expected loss ratio saturates at the building replacement cost. Direct economic losses may no longer increase, only indirect ones can be present but their estimation goes beyond the scope of this work and could be the subject of possible future developments.
- Serviceability limit state (SLS): $y_{SLS} = 4\%$; an intermediate value is selected to represent an initial accumulation of damage, still not so much relevant to induce the development of a collapse mechanism .

The serviceability limit state mean annual frequency of exceedance is determined with a trial-and-error iterative procedure so that the final obtained value is the one allowing the definition of a loss curve whose enclosed area, namely the EAL, is equal to the limiting one of 0.07% defined before.

In order to come up with a reasonable EAL estimation, the area is not evaluated as the one beneath the approximated curve, simply given by the three limit state points with corresponding mean annual frequency of exceedance, but as the one under the refined curve.

$$\lambda = c_0 e^{(-c_1 \ln y - c_2 \ln y^2)} \quad (4.16)$$

where c_0 , c_1 and c_2 are coefficients fitted to pass through the three limit state points. Integrating with the trapezoidal rule the expression, serviceability limit state mean annual frequency of exceedance is found equal to $\lambda_{SLS} = 3.18 * 10^{-3}$, in order to satisfy the EAL requirement. Figure 4.10, reported below, provides the comparison between the approximated and refined loss curves showing how, considering only the three limit state points, the area enclosed by the first one is significantly larger than the area enclosed

by the more refined curve meaning that an EAL overestimation is present. For these reasons, the definition of a more precise loss curve is required.

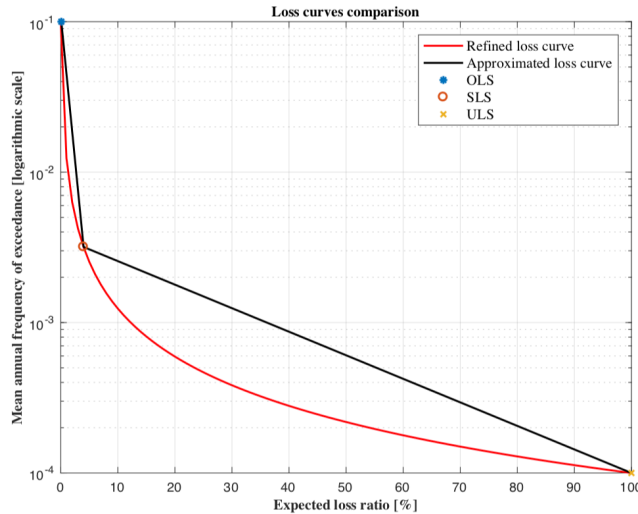


Figure 4.10: Approximated and refined loss curve comparison

This value has now to be related with the SLS ground shaking mean annual frequency of exceedance so that the corresponding period and PGA values from the INGV model can be determined. In the past, limit state MAPE has typically been assumed equal to the ground shaking one in a deterministic fashion, but looking for a more risk-consistent approach, which considers an intrinsic variability at each stage of the PEER PBEE integral, the relationship below is used to obtain SLS ground shaking MAPE:

$$H_{SLS} = \frac{\lambda_{SLS}}{e^{0.5k_1\beta^2}} = 2.80 * 10^{-3} \quad (4.17)$$

with the first-order site hazard polynomial coefficient $k_1 = 6.41 * 10^{-5}$ fitted to the hazard curve and SLS dispersion $\beta = 0.2$. Taking the inverse of the just obtained value, the SLS return period results as:

$$TR_{SLS} = \frac{1}{H_{SLS}} = 358 \text{ [yrs]} \quad (4.18)$$

Entering the INGV model data, the serviceability limit state peak ground acceleration is determined as $PGA_{SLS} = 0.23 \text{ [g]}$.

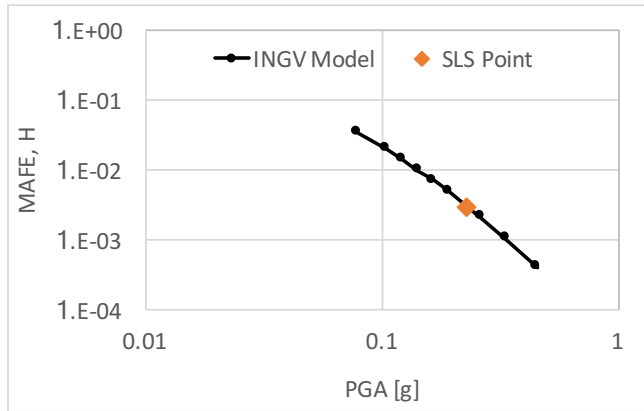


Figure 4.11: SLS point identification on the hazard curve coming from INGV model

As can be seen, the present serviceability limit state return period does not coincide with any of the NTC18 values. For this reason, in order to obtain the corresponding design spectrum, the required parameters that comes into play in the equations are extrapolated from the INGV model ones:

Table 4.3: Design spectral parameters from INGV model, corresponding to the SLS return period

T_c^*	0.3
F_0	2.2

Now having all the needed values, the SLS response spectrum to be used in CSD is determined:

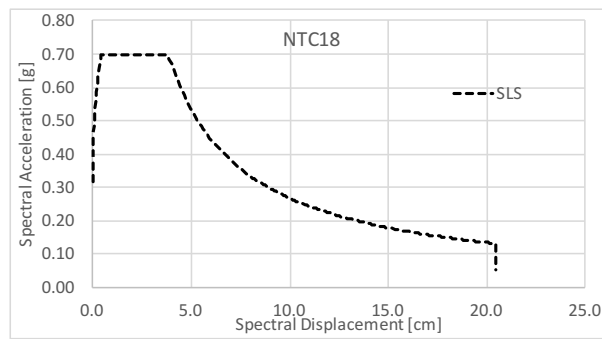


Figure 4.12: NTC18 SLS elastic design response spectrum

Once performance objectives are established, it is necessary to come up with the associated maximum allowable engineering demand parameters, such as maximum peak inter-storey drift ratio and maximum peak floor acceleration, characterising the structural response at the SLS hazard level. To do this, (Ramirez, 2009) storey loss functions for low-rise (1 to 5 stories), ductile RC perimeter moment frames with office occupancy are used. Actually, according to the storey-based building-specific loss estimation procedure, these are developed for the different building floor level, i.e. (i) first floor, (ii) typical floor and (iii) roof level. Herein, typical floor ones are used as representative of the global structural response since expected loss ratios have been defined as referred to the whole structure and not specified for a precise level of the building.

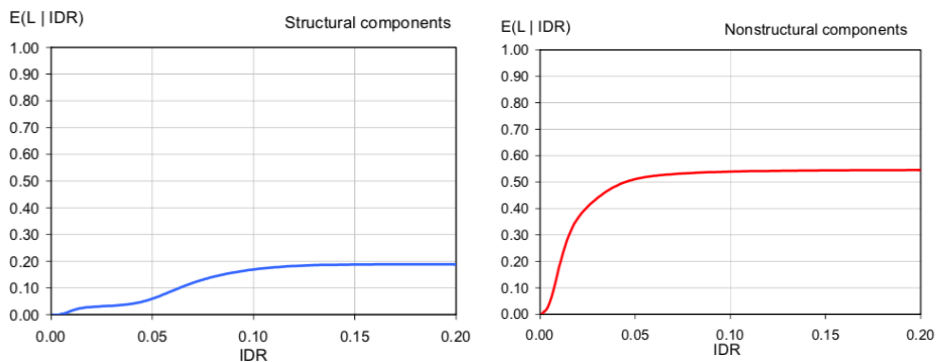


Figure 4.13: Structural drift sensitive and non-structural drift sensitive components loss curves

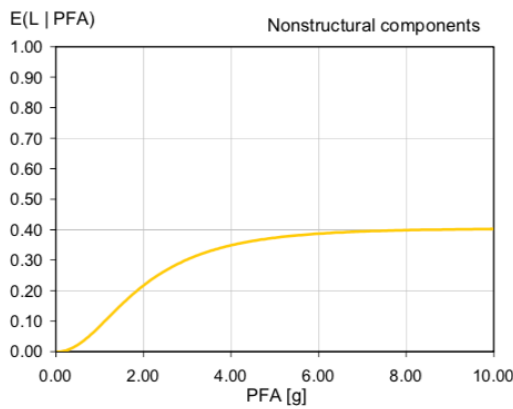


Figure 4.14: Non-structural acceleration sensitive components loss curve

Three damageable components are assumed to contribute to the seismic induced direct monetary loss, such as drift sensitive structural components, drift sensitive non-structural ones and acceleration sensitive elements. For each of them the corresponding loss curves are shown in Figure 4.13 and Figure 4.14. Moreover, associated weighting coefficients, whose sum has to be equal to 1, are set. The expected loss ratio for each component, starting from the SLS value, can be obtained:

$$y_{component} = y_{SLS} * Y_{component} \quad (4.19)$$

where:

$y_{component}$ is the component expected loss ratio;

y_{SLS} is the SLS expected loss ratio, previously assumed as 4%;

$Y_{component}$ is the component weighting coefficient;

the resulting values are reported in Table 4.4:

Table 4.4: Weighting coefficients and consequently obtained expected loss ratio for the three damageable components

Structural drift sensitive	$Y_{S,PSD} = 0.20$	$y_{S,PSD} = 0.80\%$
NS drift sensitive	$Y_{NS,PSD} = 0.40$	$y_{NS,PSD} = 1.60\%$
NS acceleration sensitive	$Y_{NS,PFA} = 0.40$	$y_{NS,PFA} = 1.60\%$

The typical floor corresponding loss curves must be entered with these expected loss ratios obtaining the following maximum allowable engineering demand parameter for each component:

$\theta_{m,S,PSD} = 0.80\%$ maximum peak storey drift for structural elements;

$\theta_{m,NS,PSD} = 0.40\%$ maximum peak storey drift for non-structural elements;

$a_{m,NS,PFA} = 0.42 [g]$ maximum peak floor acceleration for non-structural elements;

The minimum between the two drift values is taken as the SLS design parameter, i.e. the one referred to non-structural elements.

4.2.2. SLS requirements

From the imposed performance objectives, the maximum allowable peak storey drift and peak floor acceleration are obtained. These have now to be converted into SLS spectral values of displacement and acceleration, respectively, so that the acceleration-displacement response spectrum at SLS is entered and, if it should exist, the associated feasible initial secant to yield period range is determined. It is important to underline how all the performed steps, up to now, do not strictly depend on the adopted structural solution but are only function of the considered building geometry and occupancy, factors that are maintained whatever structural solution, such as fixed-base or base-isolated, for example, is selected given the performance objectives.

Spectral displacement is computed from maximum peak storey drift assuming that the considered RC frame response will be a first mode dominated one, as done in direct displacement-based design, so that the SLS design displacement is obtained from the displaced shape, function only of the structural configuration. For RC buildings, the expression to be used is the following:

$$\Delta_i = \omega_\theta * PSD * H_i * \frac{4*H_n - H_i}{4*H_n - H_1} \quad (4.20)$$

where the reduction factor included for possible storey drift amplification due to higher mode effects ω_θ is set equal to 1. The results are shown in Figure 4.15 and 4.16:

Floor	H_i [m]	m [kN]
4	16.5	756
3	12.5	864
2	8.5	864
1	4.5	864
0	0	

Figure 4.15: Displaced shape values for the examined RC frame

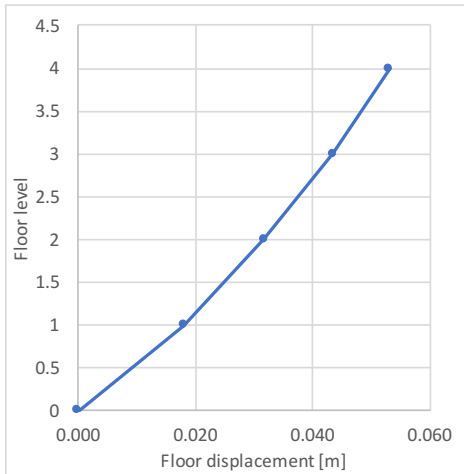


Figure 4.16: Displaced shape plot for the examined RC frame

SLS design displacement is obtained:

$$\Delta d_{SLS} = \frac{\sum m_i * \Delta_i^2}{\sum m_i * \Delta_i} = 0.041 \text{ [m]} \quad (4.21)$$

On the other hand, for the spectral acceleration, the conversion is not as simple as it was for the displacement, since the maximum peak floor acceleration cannot be assumed as being first-mode dominated. However, as pointed out in Section 2.2, it is possible to use an approximate expression relating spectral acceleration with maximum allowable PFA, found from the defined performance objectives, through a coefficient γ equal to 0.60 for RC frames, so that the SLS spectral acceleration can be computed:

$$\alpha_{SLS} \sim \gamma * PFA = 0.25 \text{ [g]} \quad (4.22)$$

Spectral values have been determined and the ADRS must be entered in order to look for the feasible initial period range for the fixed-base configuration. This consists in an upper and lower first period values to be looked for, whose range identifies an associated space of feasible structural solutions. As can be seen from the results reported in Table 4.5, the direct implementation of the CSD approach assuming a fixed-base configuration does not lead to a realistic range of allowable initial periods, compatible with the SLS design response spectrum:

Table 4.5: Fixed-base period range values corresponding to the spectral displacement and acceleration, used to enter the ADRS

$\Delta d_{SLS} = 4.1 \text{ [cm]}$	$T_{upper} = 0.50 \text{ [s]}$	$S_{a,\Delta d_{SLS}} = 0.65 \text{ [g]}$
$\alpha_{SLS} = 0.25 \text{ [g]}$	$T_{lower} = 1.30 \text{ [s]}$	$S_{d,\alpha_{SLS}} = 10.58 \text{ [cm]}$

Consequently, as illustrated in Figure 4.17, the corresponding space of possible solutions cannot be found. This means that a fixed-base structural system which complies with the SLS performance requirements cannot be obtained.

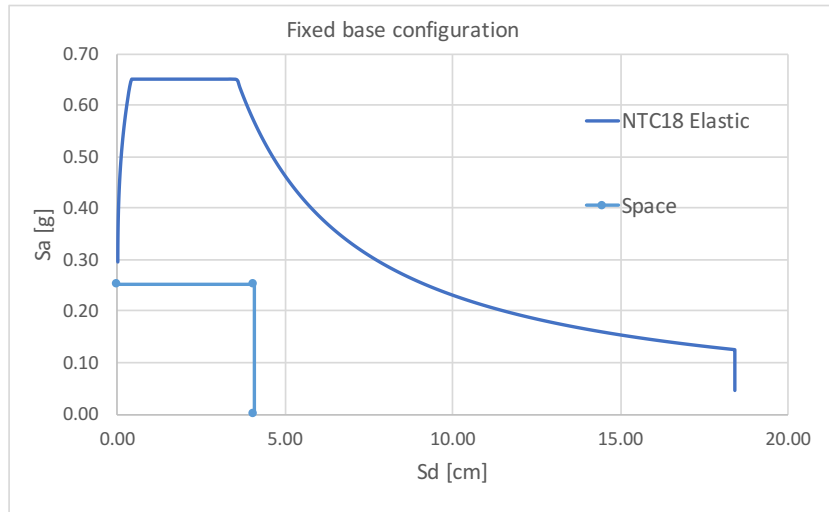


Figure 4.17: A feasible and spectrum compatible solution space for fixed-base configuration cannot be determined

Herein, base isolation comes into play as an alternative structural solution so that a feasible space and period range can be obtained; meaning that, SLS performance objectives initially specified in terms of EAL, are fulfilled. Among all possible devices, friction pendulum bearings are selected following the criterion of maximum design vertical load capacity high enough to sustain the loads coming from the superstructure. It is important to remark how this represents only a preliminary step in the design, reason for which selection process is driven by the demand-capacity comparison principle. In the following section, the design of isolators will be performed according to NTC18 requirements, assessing their structural response at the different limit states.

The introduction of an isolation system provides a reduction of the SLS seismic demand due to the associated equivalent viscous damping which represents the dissipative capacity of the devices to attenuate seismic action. This is modelled through the definition of a coefficient ξ_e , namely the equivalent viscous damping parameter, computed as a function of the isolator properties (i.e. the friction coefficient, the radius of curvature and the ultimate displacement capacity). Changing the device typology will also change the permissible energy dissipation and therefore seismic demand reduction. The ultimate displacement capacity is considered since the coefficient is defined as an equivalent one, modelling the amount of dissipation for an equivalent linear system, whose associated stiffness is taken as the secant one, corresponding to the isolator displacement capacity.

The two types of configurations, medium and low friction, with corresponding mechanical parameters, selected in Section 4.1.2, are now employed, both with the same radius of curvature $R = 3.1 [m]$ and ultimate displacement capacity $d = 200 [mm]$. In order to estimate the provided spectral reduction and adapting a conservative approach, on the safe side, a maximum allowable horizontal displacement of 120mm is considered for the isolators, hence expecting something lower than this threshold when NTC18 limit state checks will be performed in Section 4.4 for base-isolated configurations. Moreover, two friction coefficients μ are examined, also within the selected typology due to the different load acting on central and lateral columns as already pointed out. In both cases, the one referred to lateral devices is used to compute the equivalent damping coefficient, with the following expressions, respectively for medium and low friction configuration:

$$\xi_{e_m} = \frac{2}{\pi} * \frac{1}{\frac{d}{\mu R} + 1} = 0.38 \quad (4.23)$$

and

$$\xi_{e_l} = \frac{2}{\pi} * \frac{1}{\frac{d}{\mu R} + 1} = 0.29 \quad (4.24)$$

From the design point of view, starting from these values, a seismic demand reduction is provided through the definition of a spectrum reduction factor, computed as a function of the equivalent viscous damping, which allow the definition of an “overdamped” design spectrum at serviceability limit state:

$$\eta = \sqrt{\frac{0.1}{0.05 + \xi_e}} \geq 0.55 \quad (4.25)$$

In both medium and low friction cases, the provided spectral reduction factor is lower than the NTC18 imposed threshold of 0.55: consequently, SLS design seismic action is reduced of the same amount ($\eta = 0.55$) independently on the selected isolator typology.

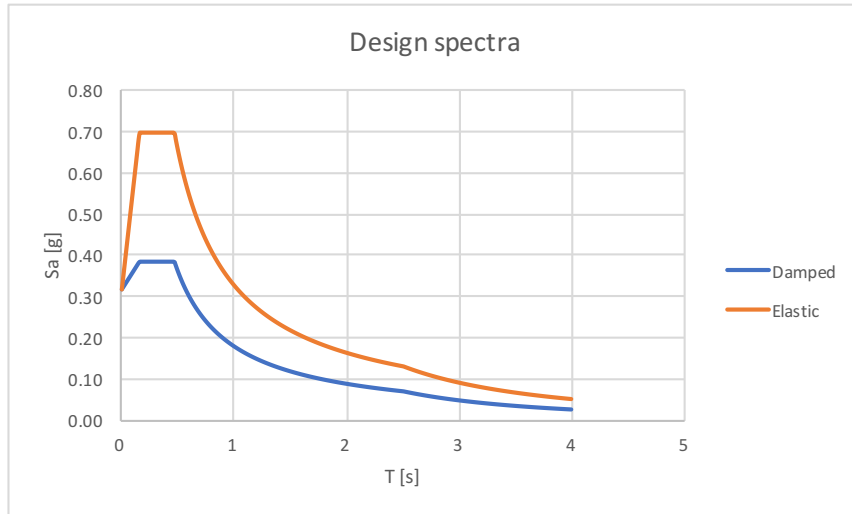


Figure 4.18: Elastic and overdamped design response spectra comparison

This also means that, due to the isolator axial load ratio (vertical capacity over acting load) which mainly influences the friction coefficient definition, moving from medium to low friction pendulum bearings, does not have an effect on the amount of permissible seismic demand reduction, according to the expressions utilised by the design code.

The overdamped design spectra, in terms of spectral acceleration and displacement, can now be entered with the maximum allowable peak inter-storey drift and peak floor acceleration previously identified, independently of the selected structural system, from the imposed performance objectives. In this case, the identified period range, shown in Table 4.6, makes sense, whereas for the fixed-base structural solution it did not.

Table 4.6: Base-isolated period range values corresponding to the spectral displacement and acceleration, used to enter the ADRS

$\Delta d_{SLS} = 4.1 \text{ [cm]}$	$T_{upper} = 0.91 \text{ [s]}$	$S_{a,\Delta d_{SLS}} = 0.20 \text{ [g]}$
$a_{SLS} = 0.25 \text{ [g]}$	$T_{lower} = 0.71 \text{ [s]}$	$S_{d,a_{SLS}} = 3.20 \text{ [cm]}$

The spectral displacement corresponding period value stands for the upper period limit while the spectral acceleration one stands for the feasible range lower bound and differently from the fixed base case a feasible range period can be identified since upper and lower limits are correctly defined. This is illustrated in Figure 4.19:

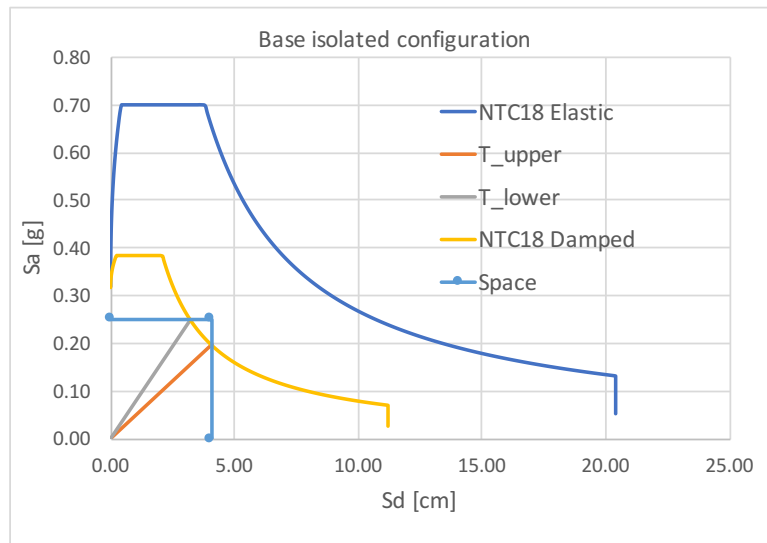


Figure 4.19: Feasible solution space and feasible initial period range determined thanks to seismic isolation

The space defined by the two lines, corresponding to the feasible initial period range, compatible with the overdamped SLS design response spectrum, represents an area of possible structural solutions that, thanks to seismic isolation, are able to comply with the performance objectives at serviceability limit state, initially defined utilising the CSD framework.

Conceptual seismic design approach is used here, not with the aim of directly designing the structure, but as an instrument to help designers in selecting suitable structural solutions, able to comply with limit state defined performance objectives. Indeed, in the examined case, a traditional fixed-base solution is shown not able to do that, since a feasible solution space cannot be determined, while with the use of seismic isolation this can be obtained together with a feasible initial period range, coming up with a structural solution that complies with the SLS performance objectives.

In order to validate these conclusions, both fixed-base and isolated configurations are designed in the following section with respect to NTC18 requirements. NRHA are then performed to assess their seismic performance in terms of provided expected annual loss (EAL) to be compared with the defined target value of 0.07%.

4.3. NTC18 FIXED-BASE CONFIGURATION DESIGN

The conceptual seismic design approach has been used as a discriminant method between feasible and not feasible structural solutions in order to comply with the defined performance objectives. The fixed-base configuration resulted as not able to fulfil these requirements at an initial design stage. It will now be designed according to NTC18 to validate the conclusions driven by the CSD approach.

Seismic action, described by the L'Aquila site design response spectra at different limit states as outlined in Section 4.1, has to be combined with the distributed floor loads so that the induced demands on structural members are evaluated and the cross section members design performed with respect to them, and in agreement with NTC18 requirements. The actions combination to be considered in presence of earthquake one, is described by equation 2.5.5 of NTC18 §2.5.3:

$$E + G_1 + G_2 + P + \psi_j Q_j \quad (4.26)$$

where:

E denotes the seismic action, considered suitably according to the performed method of structural analysis;

G_1, G_2, P, Q_j respectively are the permanent structural loads, permanent non-structural loads, pre-compression loads (assumed to be absent in the case study) and the occupancy dependant distributed loads to be multiplied by the corresponding combination coefficients ψ_j . All of them are assumed to be already combined in the floor load values defined in Section 3.1:

$q_{floor} = 8 [kPa]$ typical floor load;

$q_{roof} = 7 [kPa]$ roof load;

Seismic action is accounted for, starting from the corresponding limit state design spectrum for L'Aquila site, with a set of concentrated lateral forces acting at each floor level, according to the so-called equivalent lateral load method, compatibly with the linear static analysis outlined in NTC18 §7.3.2.2.

This type of analysis is performed for the sake of simplicity; the actual non-linear structural behaviour is evaluated by means of the definition of the so-called behaviour factor q , presented in Section 2.1. It allows designers to obtain a reduced inelastic design response spectrum, due to the dissipative capacity structural members are actually

characterized by. Mainly, it depends on the selected structural typology and followed design criteria but also on the material dissipative capacity through the definition of a design ductility class, see Section 2.1, in which the building must fall if some detailing requirements are met. Following NTC18 §7.3.1 it is thus computed:

$$q_l = q_0 * K_R \quad (4.27)$$

where:

q_0 is the life-safety limit state basic behaviour factor value, whose upper limits are reported in table 7.3.II of NTC18, depending on selected ductility class, structural typology and α_u/α_1 ratio, between the seismic action level causing the development of a collapse mechanism and the one which provides yielding and thus the opening of the first plastic hinge. The examined case study is constituted by a RC frame to be designed with respect to medium-level ductility class: corresponding behaviour factor is determined below, selecting the first row of frame structural typology and then, class CD “B”:

Tab. 7.3.II – Valori massimi del valore di base q_0 del fattore di comportamento allo SLV per diverse tecniche costruttive ed in funzione della tipologia strutturale e della classe di duttilità CD

Tipologia strutturale	q_0	
	CD''A''	CD''B''
Costruzioni di calcestruzzo (§ 7.4.3.2)		
Strutture a telaio, a pareti accoppiate, miste (v. § 7.4.3.1)	4,5 α_u/α_1	3,0 α_u/α_1
Strutture a pareti non accoppiate (v. § 7.4.3.1)	4,0 α_u/α_1	3,0
Strutture deformabili torsionalmente (v. § 7.4.3.1)	3,0	2,0
Strutture a pendolo inverso (v. § 7.4.3.1)	2,0	1,5
Strutture a pendolo inverso intelaiate monopiano (v. § 7.4.3.1)	3,5	2,5
Costruzioni con struttura prefabbricata (§ 7.4.5.1)		
Strutture a pannelli	4,0 α_u/α_1	3,0
Strutture monolitiche a cella	3,0	2,0
Strutture con pilastri incastri orizzontamenti incimerati	3,5	2,5

Figure 4.20: NTC18 Table 7.3.II for basic behaviour factor estimation

The ratio α_u/α_1 is obtained following NTC18§7.4.3.2 as equal to 1.3, for frame structures with more than one bay and storey.

K_R is the factor depending on the in-height structural characteristics: if regularity is present, as in the case study building, it is set equal to 1.

A behaviour factor equal to $q_l = 3.9$ has to be used in the inelastic design response spectrum; in order to be determined, the coefficient η must be replaced by $1/q$ in the corresponding equations outlined in Section 2.1. Since the basic behaviour factor is defined at the life safety limit state, the associated design spectrum is the one to be reduced to account for inelastic behaviour.

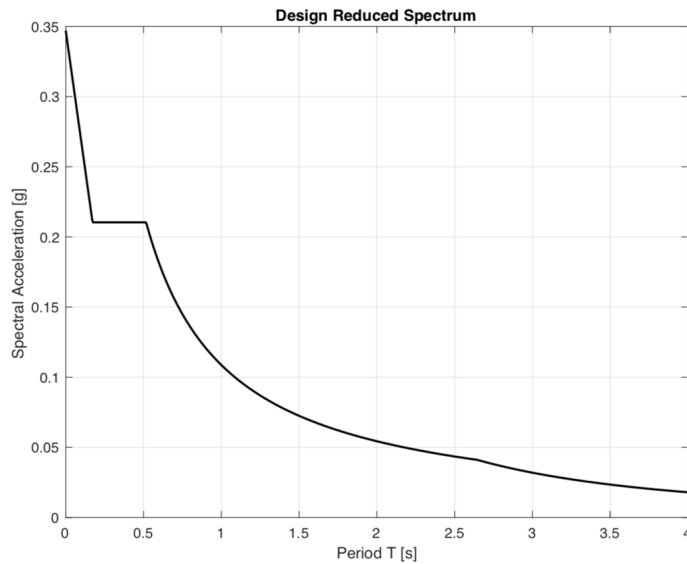


Figure 4.21: L'Aquila life safety reduced design spectrum

The idea of the equivalent lateral load method is to determine the inelastic reduced spectral acceleration, evaluated at the structural fundamental period T_1 , from the response spectrum shown in Figure 4.21. This is then multiplied by the total amplified structural mass and a coefficient λ in order to compute the total base shear, divided into concentrated lateral forces, to be applied at each floor level, representing the present seismic action.

Following NTC18 §7.3.2.2 requirements, first structure's fundamental period, for civil or industrial constructions that do not exceed 40 m in height and whose mass is distributed approximately uniformly along the height, can be estimated, in the absence of more detailed calculations, using the following formula:

$$T_1 = 2\sqrt{d} \quad (4.28)$$

where:

d is the structural elastic top floor lateral displacement due to the load combination computed with the 2.5.7 NTC18 equation, i.e. the one combining the permanent structural and non-structural gravity loads with the occupancy dependant live one applied horizontally. In the case study model, floor loads are already defined, as combined, equal to the values of q_{floor} and q_{roof} , outlined in section 4.1.1: these are then multiplied by

the out of plane width to obtain longitudinally distributed loads $q_f = 48 [kPa]$ and $q_r = 42 [kPa]$, which are then transformed in concentrated forces to be laterally applied. Using software FTool, the elastic top displacement is determined as:

$$d \approx 0.5 [m]$$

First structural period $T_1 = 1.4 [s]$ is used to read the corresponding inelastic spectral acceleration:

$$S_a(T_1 = 1.4s) = 0.09 [g]$$

The total base shear is obtained multiplying the latter with the total amplified structural mass and the λ coefficient, equal to 1 in the examined case, since first period T_1 is lower than $2 * T_C$, where T_C is the life-safety limit state corner period, from L'Aquila site, defined in Section 3.1.1.1. It is equal to:

$$V_b = 1213 [kN]$$

and has to be divided in floor levels acting lateral forces, with the following relationship:

$$F_{l,i} = V_b * \frac{m_i * h_i}{\sum_i m_i h_i} \quad (4.29)$$

where:

m_i and h_i , respectively are, the masses floor vector and increasing floor height one.

The obtained forces result as:

$$F_{l,i} = [136 \ 258 \ 379 \ 438] [kN]$$

The fixed base structural model is then implemented in the software “FTool” in order to perform structural analysis under, firstly, vertical distributed loads q_f and q_r and then under the lateral forces just determined representing the seismic actions. Induced axial, shear and flexure demands in beams and columns are evaluated in the relevant cross section (the two at the ends of the considered element with also the middle one) and combined using NTC18 equation 2.5.7, standing for the earthquake load design combination.

All the obtained structural demands are reported in Appendix A.

4.3.1. NTC18 capacity design requirements

Starting from the available resulting structural demands, beam and column frame elements must be designed in order to comply with general requirements and, additionally, the capacity design one, outlined in NTC18.

Starting from beam elements, for each floor level, they are first designed with respect to maximum positive and maximum negative bending moments; the obtained cross sections, given the defined geometrical dimensions and determined amount of reinforcement, have to be verified computing their resistance, with respect to both positive and negative moment, to be compared with the maximum acting demand. Note that, during this verification process, the interaction between flexural demand and present axial load in the corresponding cross section, is accounted for. Moreover, as specified in the modelling part in Section 4.1.1., reinforcement is placed at the top or at the bottom of the element cross section; no middle reinforcement is considered. Once the obtained cross section is verified, additional capacity design requirements must be checked, in terms of placed reinforcement amount in order to ensure an enough ductile structural behaviour. From NTC18 §7.4.6.2.1 they result in:

- at least 2 ϕ_{14} longitudinal bars must be present both at top and bottom for the whole beam length;
- in each section of the beam, unless there are justifications showing that the collapse modes of the section are consistent with the ductility class adopted, the geometric ratio relating to the tension reinforcement, regardless of whether the tension reinforcement is that at the upper edge of the section or that at the lower edge of section, must be included within the following limits:

$$\frac{1.4}{f_{yk}} \leq \rho \leq \rho_{compr} + 3.5/f_{yk} \quad (4.30)$$

where:

$f_{yk} = 413.69 \text{ [MPa]}$ is the steel yield strength characteristic value;

ρ is the tension reinforcement ratio, computed as the ratio between the tension reinforcement area and the concrete cross section one;

ρ_{compr} is the compression reinforcement ratio, computed as the ratio between the compression reinforcement area and the concrete cross section one;

After that, capacity design with respect to shear is performed: the basic idea of this approach is to provide enough ductility to structural response in order to avoid brittle failure and collapse mechanisms: for these reasons, flexure is looked for rather than

shear, since the first is ductile. To ensure this mechanism develops, acting shear must be computed assuming that plastic hinges are formed at beam end cross sections, and so plastic moment is developed, according to a strong column weak beam mechanism, and amplifying this associated shear, summed with the one coming from distributed floor loads, by an over-strength factor γ_{Rd} , according to this expression:

$$V_{Ed} = \left(V_{floor} + \left(\frac{M_{pl,Rd}^+ + M_{pl,Rd}^-}{L_c} \right) \right) * \gamma_{Rd} \quad (4.31)$$

where:

V_{Ed} is the total acting shear along the beam element;

V_{floor} is the distributed floor loads induced shear;

$M_{pl,Rd}$ are the resisting positive plastic moment assumed to be reached at beam end cross sections, corresponding to plastic hinge opening;

L_c is the beam clear length given by the beam element total span from which the two plastic hinge length L_p , defined in the modelling Section 4.1.1, are subtracted.

γ_{Rd} is the over-strength factor, function of the selected ductility class, obtained according to NTC18 Table 7.2.II. For middle ductility level, i.e. class CD “B”, it is set equal to 1.1.

ϕ_{10} stirrups are used, corresponding maximum allowable spacing is determined from NTC18 § 7.5.6.2.1

$$s_M = \min \left(\frac{As_w * 1000}{b * 1.5}; 0.25d_b; 225 \text{ [mm]}; 6\phi_l; 24\phi_s \right) \quad (4.32)$$

where:

As_w is the shear reinforcement area based on how many stirrups are present each cross section;

$\phi_l = 24 \text{ [mm]}$ is the assumed diameter for longitudinal reinforcement;

$\phi_s = 10 \text{ [mm]}$ is the stirrups assumed diameter, i.e. transverse reinforcement;

$d_b = h_b - \left(c_v + \frac{\phi_l}{2} + \phi_s \right)$ is the beam effective height to be used in the design;

Having assumed the stirrup diameter and determined the maximum allowable spacing s_M ; the cross section shear resistance must be computed and compared with the acting shear coming from capacity design. According to NTC18 § 4.1.2.3.5.2, the shear resistance of an element cross section, in presence of shear reinforcement, is evaluated as the minimum between the compressed concrete contribution and the reinforcement steel one, as follows:

$$V_{R,sd} = 0.9 * d * \frac{A_{sw}}{s} * f_{y,d} * (\cotg(\alpha) + tg(\alpha)) * \sin(\alpha) \quad (4.33)$$

$$V_{R,cd} = 0.9 * d * b_w * \alpha_c * \nu * f_{cd} * \frac{\cotg(\alpha) + \cotg(\vartheta)}{1 + \cotg(\vartheta)^2} \quad (4.34)$$

where:

$\alpha = 90$ [deg] is the assumed angle of inclination for the vertical stirrups, assuming a strut and tie model in order to evaluate cross section shear resistance;

$\nu = 0.5$ coefficient defining the reduced concrete design compressive;

$f_{y,d}$ and $f_{c,d}$, respectively, are the design values of the steel yield and concrete compressive strength outlined in section 4.1.1;

$\alpha_c = 1$ since axial force is not considered;

ϑ is the concrete compressive strut angle of inclination so that:

$$\cotg(\vartheta) = \sqrt{\frac{\nu * \alpha_c}{\omega_{sw} * \sin(\alpha)} - 1} \quad (4.35)$$

where:

$\omega_{sw} = \frac{A_{sw} * f_{yd}}{b * s * f_{cd}}$ is the mechanical shear reinforcement ratio;

$\cotg(\vartheta)$ must be between 1 and 2.5 for compatibility reason with the assumed strut and tie shear resisting model.

This procedure has to be repeated for beam elements at all floor levels; the designed beam cross section properties are reported in Appendix B.

Once beam cross sections have been designed, column elements are considered and as first thing, the limit for normalized acting axial force is checked, according to NTC18 §7.4.4.2.1:

$$\mu_{Ed} = \frac{N_{Ed}}{b_c h_c f_{cd}} \leq 0.65 \quad (4.36)$$

where:

N_{Ed} is the maximum acting load;

b_c and h_c are the examined column cross section geometrical dimensions;

f_{cd} is the design concrete compressive strength value;

Moreover, the minimum eccentricity between acting moment and axial load could be verified:

$$\frac{M_{Ed}}{N_{Ed}} > e_m = \min (20 [mm]; 0.05 h_c) \quad (4.37)$$

Column flexural design considering bending moment and axial load interaction has to be performed. In order to determine the amount of required longitudinal reinforcement, that usually it is assumed as symmetrically placed in column cross sections, to give them more stability with respect to bending moment in both directions, normalized axial load and bending moment demand must be computed and used to enter a selected interaction diagram, function of the column cross section dimension and material properties. The design capacity curve, described by the associated mechanical reinforcement ratio w , is identified as the first one under which the design point (normalized axial load, normalized bending moment), is contained.

Normalized axial load and bending moment are, respectively, as follows:

$$v_{Ed} = \frac{N_{Ed}}{b_c h_c} \quad (4.38)$$

$$\mu_{Ed} = \frac{M_{Ed}}{A_c h_c} \quad (4.39)$$

A_c is the column cross section area.

From column cross section dimensions and material properties shown in Figure 4.3, the bending moment-axial load interaction diagram illustrated in Figure 4.22, is employed:

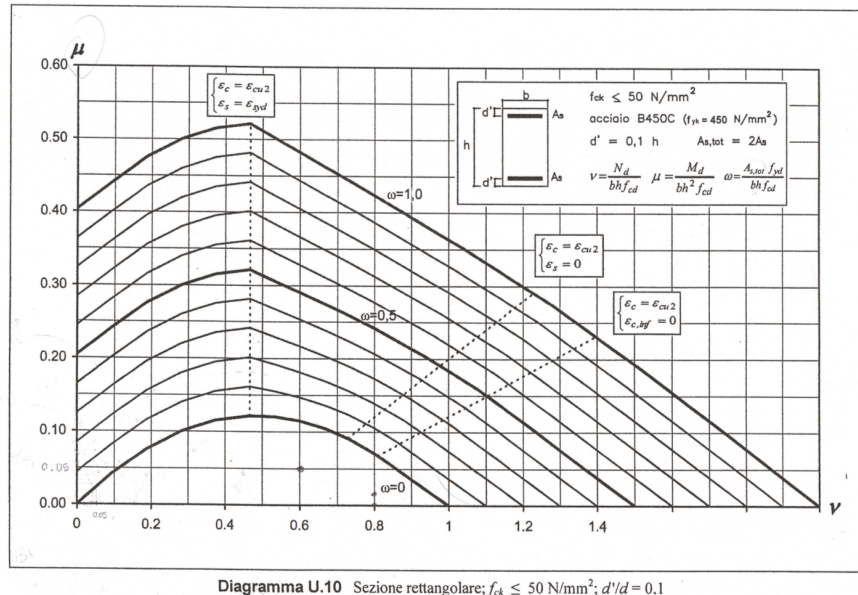


Figure 4.22: Bending moment-axial load interaction diagram

The design points are identified and consequently a suitable capacity curve (beneath which the design point must be contained) and corresponding mechanical reinforcement ratio w , are determined. From this value, the amount of longitudinal reinforcement to be symmetrically placed is obtained and checked according to NTC18 capacity design requirements, that can be found looking at NTC18 § 7.4.6.2.2.

$$1\% \leq \rho_l \leq 4\% \quad (4.40)$$

Longitudinal reinforcement ratio must fall between these limit values in order to ensure an enough ductile structural behaviour. As for the beams, $\phi 24$ bars are assumed to be used.

After that, capacity design with respect to shear has to be performed determining the acting shear along the column which is computed in terms of this bending moment value:

$$M_{i,d} = M_{c,Rd} * \min \left(1, \frac{\sum M_{b,Rd}}{\sum M_{c,Rd}} \right) \quad (4.41)$$

where:

$M_{c,Rd}$ is the column plastic moment capacity in the end cross section;

$M_{b,Rd}$ is the below or above present plastic moment developed due to plastic hinge opening in beam end cross section;

The resulting shear is:

$$V_{Ed} = \gamma_{Rd} * \frac{M_{i,d} + M_{i,d}}{l_p} \quad (4.42)$$

where:

γ_{Rd} is the over-strength factor previously defined for the beam capacity design with respect to shear;

l_p is the length of the considered column, namely the corresponding storey height;

Also for the columns, ϕ_{10} stirrups are used and the maximum allowable spacing is evaluated according to NTC18 §7.4.6.2.2.

$$s_M = \min(0.33 * \min(b_c, h_c); 125 [mm]; 8\phi_l) \quad (4.43)$$

Column cross section shear resistance is determined, as did for the beams, comparing the compressed concrete contribution with the reinforcement steel one, and selecting the minimum. Once shear capacity has been verified, an additional shear reinforcement capacity design requirement is evaluated, following NTC18 §7.4.6.2.2.

$$\alpha * \omega_{wd} \geq 30\mu_\phi * v_{Ed} * \varepsilon_{s,yd} * \frac{b_c}{b_0} + 0.0035 \quad (4.44)$$

where:

ω_{wd} is the shear mechanical reinforcement ratio inside the dissipative zone, computed with NTC18 7.4.30 equation;

μ_ϕ is the collapse limit state ductility demand;

v_{Ed} is the acting normalized axial load;

$\varepsilon_{s,yd}$ is the design value of the steel yield strain, taken as the ratio between the design steel yield strength and the steel Young modulus;

b_c is the minimum gross section width;

$$b_0 = b_c$$

and $\alpha = \alpha_s * \alpha_n$ is the confinement efficiency coefficient computed with NTC18 7.4.31a and 7.4.31b equations.

This procedure has to be repeated for column elements at all floor levels and the designed column cross section properties are reported in Appendix B.

Moreover, as last capacity design requirements to be verified, according to NTC18 §7.4.4.2.1, for each direction of application of the seismic actions, for each beam-column node (with the exception of the top floor nodes), the total bending capacity of the columns must be greater than the overall bending capacity of the beams amplified by the over-strength coefficient γ_{Rd} , in accordance with the formula:

$$\sum M_{c,Rd} \geq \gamma_{Rd} * \sum M_{b,Rd} \quad (4.45)$$

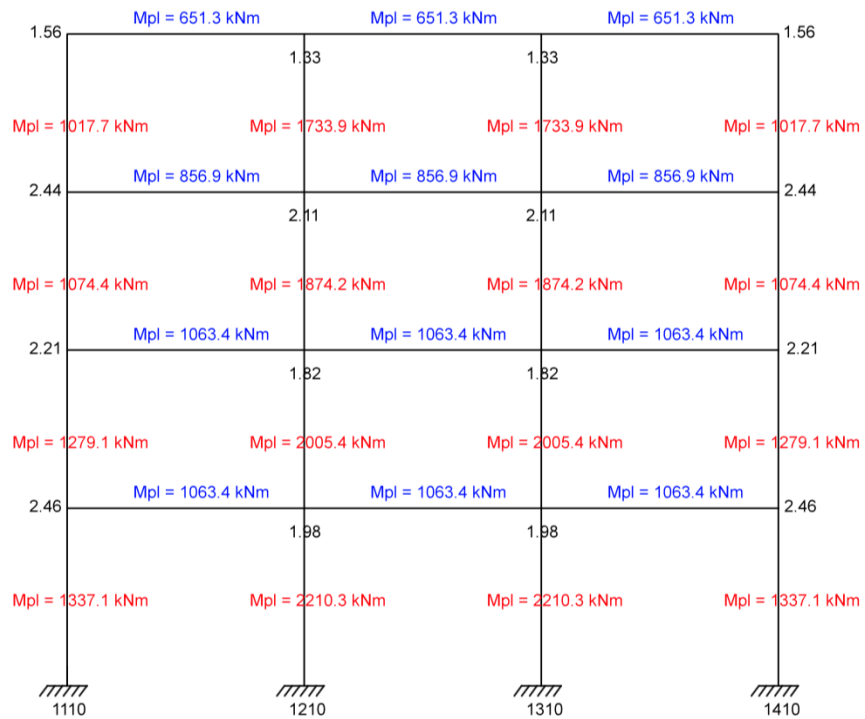


Figure 4.23: Capacity design nodal check

In Figure 4.23, for each node (also the top floor ones even if it is not directly required), the ratio between the sum of the nodal converging columns plastic moment and the sum of the nodal converging beams plastic moment, is computed and checked to be larger than the selected over-strength factor, hence ensuring capacity design has been followed. For all the nodes this requirement is satisfied.

As outlined, in Section 4.1.1, for the element modelling proposed formulation, the reinforcement ratios, both longitudinal and transverse, together with stirrups spacing are the most relevant parameters obtained from performed seismic design according to NTC18 capacity design requirements. In terms of designed cross sections, some of them are repeated over different floor levels due to the similarity in the induced demand and in order to achieve a better regularity over the whole structural system.

4.4. NTC18 BASE ISOLATED CONFIGURATION DESIGN

Friction pendulum bearings are first selected following an axial load capacity-demand comparison as outlined in Section 4.1.2; for both medium friction and low friction case, two different typologies of devices are considered due to different acting vertical load on central and lateral columns. They are recalled just below:

Low friction case: FIP-D L 630/400 3100 & FIP-D L 1000/400 3100

Medium friction case: FIP-D M 1000/400 3100 & FIP-D M 1350/400 3100

The first number in the isolator acronym is randomly defined by the producer, while the second one stands for the total allowable displacement in both horizontal direction, which in this case is ± 200 mm. The latter is the associated radius of curvature, also expressed in mm.

Since modelling part has already been described in Section 4.1.2, base isolated configurations, both in low friction and medium friction case, have to be designed according to NTC18 requirements: non-linear response history analysis must be performed meaning that isolators, both in medium friction and low friction case, are modelled as non-linear. This is done in agreement with the modelling checks, outlined in Section 3.3.2, that, if respected, would allow the use of an equivalent linear model for the isolation devices. As an example, the verifications are reported for the medium friction case. Lateral isolators are considered:

- the equivalent stiffness of the isolation system is at least equal to 50% of the secant stiffness for cycles with displacement equal to 20% of the reference displacement.

$$\frac{0.1\Delta_{maximum}}{R} \geq 0.2\mu = 0.0065 \geq 0.0130$$

- the equivalent linear damping, as defined above, is less than 30%:

$$\xi_e = \frac{2}{\pi} * \frac{1}{\frac{d}{\mu R} + 1} < 30\% = 31.9\% < 30\%$$

- the force-displacement characteristics of the system do not vary by more than 10% due to variations in the strain rate in a range of $\pm 30\%$ around the design value, and the vertical action on the devices, in the range of project variability: this requirement cannot be met since FPB behaviour is sensitive to axial load and velocity through friction coefficient μ .
- the increase in force in the isolation devices for displacements between $0.5d_c$ and d_{dc} , being d_{dc} the displacement of the centre of stiffness due to

seismic action, is at least equal to 2.5% of the total weight of the superstructure; in practical terms:

$$\frac{0.5\Delta_{maximum}}{R} \geq 2.5 \% = 0.03 \geq 0.025$$

The equivalent stiffness and damping checks together with the third one are not satisfied for medium friction lateral isolators. This means that an equivalent linear model cannot be defined but the actual non-linear behaviour of all isolators, also the central ones, must be accounted for. For compatibility reason, same conclusions are taken as valid for the low friction case.

In order to perform NRHA, different sets of selected ground motion records, for each limit state are used. Then, structural response is checked to comply with the NTC18 limit state verifications, as outlined in Section 3.3.2. The ground motion records to be used must be determined so that the limit-state average response spectrum of the selected records response spectra is compatible with the corresponding limit state L'Aquila-site elastic design response one. NTC18 §3.2.3.6 explains how this can be verified, outlined below.

The compatibility with the elastic response spectrum is to be verified on the basis of spectral ordinates average, obtained from the different ground motion records, for an equivalent viscous damping coefficient of 5%, namely in the elastic range. The average spectral ordinate must not have a deviation, in defect, greater than 10%, with respect to the corresponding component of the elastic spectrum, at any point of the greater between the intervals $0.15s \div 2.0s$ and $0.15s \div 2T$, in which T is the vibration period of the structure in the elastic range, for the verifications at the ultimate limit states, and $0.15s \div 1.5T$, for the verifications at the service limit states. In the case of constructions with seismic isolation, the upper limit of the coherence interval is assumed to be equal to $1.2T_{is}$, being T_{is} the equivalent period of the isolated structure, evaluated for the displacements of the isolation system produced by the limit state in exam. If these requirements cannot be satisfied, ground motions have to be scaled, in the considered range, with some factors to allow them complying with these prescriptions.

The used set of records, for each limit state, are reported in Appendix C. Figures from 4.24 to 4.27 illustrate the average response spectrum compared with the elastic design one, defined for L'Aquila site, for each limit state.

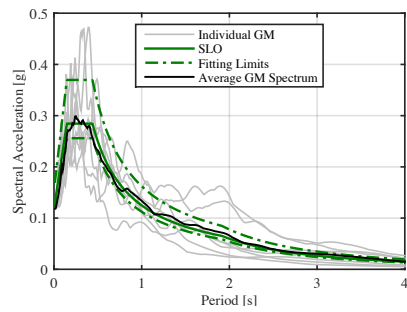


Figure 4.24: SLO average response spectrum to be compared with the L'Aquila-site limit-state corresponding one

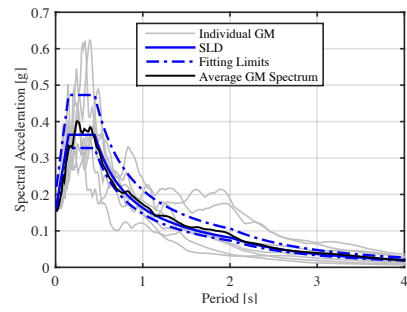


Figure 4.25: SLD average response spectrum to be compared with the L'Aquila-site limit-state corresponding one

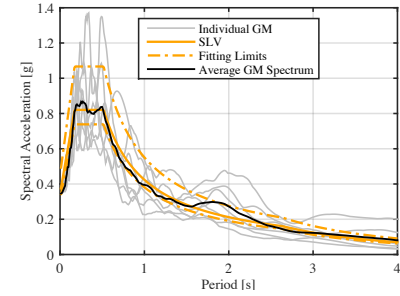


Figure 4.26: SLV average response spectrum to be compared with the L'Aquila-site limit-state corresponding one

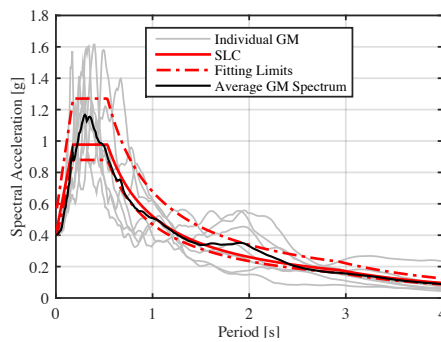


Figure 4.27: SLC average response spectrum to be compared with the L'Aquila-site limit-state corresponding one

Once the record selection process has been completed using the software REXEL, NRHA are performed using the selected records, for both medium friction and low friction base-isolated configurations. The mean response over all the surviving ground motions (i.e. the ones which do not cause structural collapse) is evaluated, in terms of different engineering demand parameters, depending on the considered limit state. For those, a lognormal distribution is assumed over the whole set of records. Structural collapse is assumed to be developed when one of the peak inter-storey drift ratios surpasses the threshold value of 5%, the analysis is stopped and the record is identified as a collapse one, not to be considered in the mean response evaluation. For the operational limit state (SLO) no requirements are defined while at the damage limit state (SLD), peak inter-story drift ratios must be compared with the limiting values outlined in Section 3.3.2, and also the isolator residual displacement value must be checked with respect to a defined threshold. At both life safety (SLV) and collapse (SLC) limit states, the mean value of the peak isolator horizontal displacement is compared with the corresponding capacity; moreover, also the residual displacement has to be verified. Additional detailing about these structural response checks can be found in Section 3.3.2.

Herein, there are the most relevant results for medium and low friction cases:

Low friction				Medium friction			
		SLD	Mean	SLD	Mean	Limit	Limit
[%]	1st drift	0.52	2.25	[%]	1st drift	0.77	2.25
[%]	2nd drift	0.26	2.00	[%]	2nd drift	0.38	2.00
[%]	3rd drift	0.21	2.00	[%]	3rd drift	0.27	2.00
[%]	Top drift	0.17	2.00	[%]	Top drift	0.22	2.00
[mm]	Res disp	2.43	50	[mm]	Res disp	2.75	50
		SLV	Mean	SLV	Mean	Limit	Limit
[mm]	Peak disp	99.45	250	[mm]	Peak disp	69.28	250
[mm]	Res disp	6.20	50	[mm]	Res disp	3.23	50
		SLC	Mean	NO GM_14	SLC	Mean	Limit
[mm]	Peak disp	112.87	250	[mm]	Peak disp	79.16	250
[mm]	Res disp	5.57	50	[mm]	Res disp	4.29	50

Figure 4.28: NTC18 limit state checks for both medium and low friction cases

In both configurations, all the NTC18 limit state verifications are satisfied, meaning that the friction pendulum bearings have been suitably selected and designed with respect to the above shown prescriptions. From the results, it can be seen how, at damage limit state, medium friction isolators provide higher peak drift ratios, especially at the first floor where the value could be affected by the high displacement value at the isolator node. Indeed, the first drift is computed with respect to first floor level node and isolator one horizontal displacements. Moreover, the assumed allowable displacement capacity of 120mm in Section 4.2.2, used to determine the over-damped response spectrum for CSD considerations at SLS, reduced with respect to ultimate capacity of 200mm taken from the isolators' catalogue, is enough to comply with the highest horizontal displacement demand at the isolator level for the SLC equal to 122.87mm, from Figure 4.28. This demonstrates how the above provided assumptions was reasonable. Actually, these are structural response checks performed to verify the FPBs design suitability. The following section addresses the influence and the impact friction coefficient has on structural response.



5. SEISMIC PERFORMANCE ASSESSMENT

In this chapter, the structural response and seismic performance of both fixed-base and base-isolated case study configurations, designed in agreement with the NTC18 requirements, are assessed. Moreover, a comparison between low and medium friction cases is also provided in order to evaluate the impact that the friction coefficient has on structural response. Firstly, the fundamental structural period T_1 of all structural solutions is reported; then static pushover analysis (SPO), with obtained capacity curves, and non-linear time history responses (NRHA) are performed for all of them. For the latter, 11 increasing intensity measure (IM) levels are considered, expressed in terms of spectral acceleration evaluated at the structural fundamental period $S_A(T_1)$, referred to a certain probability of exceedance, and corresponding return period, in the seismic action reference period V_R of 50 years. Each level is characterized by a set of 40 ground motion records, selected with the conditional mean spectrum method: according to this, they are scaled up by a factor to enforce all the corresponding response spectra having the same spectral acceleration at the structural configuration-fundamental period value and respect the conditional distribution of spectral acceleration values at other periods of vibration.

Seismic response is evaluated in terms of selected engineering demand parameters (EDP) such as peak inter-storey drift ratio, peak floor acceleration, velocity and displacement. The median value of all EDPs is considered over all the survived records among the whole considered set (i.e. the ones that do not cause structural collapse) assuming a lognormal distribution and fitting. After that, post processing of the data is performed to deal with the before mentioned comparisons.

Starting from the fixed base structural solution the fundamental period, from performed modal analysis, is found:

$$T_{Fb} = 1.26 \text{ [s]}$$

It is possible to observe how this is really closed to the estimated one, $T_1 = 1.4s$, in Section 4.1.1, when equivalent lateral force method has been employed to come up with the distribution of lateral concentrated forces, representing the seismic action, at the design process onset.

For base isolated configurations, a higher value is expected from modal analysis due to the improvement in flexibility provided by the introduction of the isolation system; it results as:

$$T_{is} = 2.02 [s]$$

Actually, it is important to underline how this first period is provided in agreement with the considered isolator elements modelling; as pointed out in Section 4.1.2. The catalogue-defined constitutive law, indeed, has been defined with a high initial stiffness in order to represent the before-activation isolators behaviour, in both medium and low friction case. Once activated, the isolator properties-related fundamental period is computed as a function of the effective radius of curvature, set equal to 3.1 m for both medium and low friction devices, according to the expression below:

$$T_{is} = 2\pi \sqrt{\frac{R}{g}} = 3.53 [s] \quad (5.1)$$

This is the period that will be used for the ground motion records selection, presented in Section 5.2.1.

5.1. STATIC PUSHOVER ANALYSIS

As mentioned in the introduction of this chapter, static pushover analysis is firstly performed using, in the examined case, a monotonically increasing uniform load distribution, over all structural levels. For the fixed base solution, it provides the reported capacity curve, evaluated in terms of top displacement along the horizontal axis, versus total base shear along the vertical one:

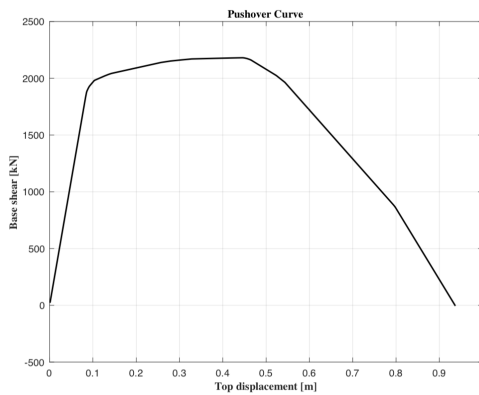


Figure 5.1: Capacity curve obtained from pushover analysis for the fixed base configuration

Looking at Figure 5.1, it is possible to notice how the fixed-base configuration is characterized by a quite high initial stiffness in the elastic domain, up to the point where yielding is developed, for a top displacement of 0.091 [m] and a base shear of 1924 [kN]. The corresponding elastic stiffness can be estimated equal to:

$$K_e = \frac{V_b}{d_{top}} = \frac{1924}{0.091} = 21142.86 \left[\frac{kN}{m} \right] \quad (5.2)$$

After that, the structure starts behaving in the plastic domain, with a certain strain hardening, till the maximum base shear value is reached:

$$V_{FB} = 2180.7 \text{ [kN]}$$

The ratio between this value and the total base shear obtained from the summation of the concentrated lateral forces representing the seismic action when equivalent lateral force method has been performed, in Section 4.3.1, is computed in order to evaluate the overstrength provided by the designed fixed-base structure in terms of base shear capacity with respect to the base shear seismic demand:

$$\frac{V_{FB}}{V_{Ed}} = \frac{2180.7}{1213} = 1.80$$

This means that the designed configuration is able to sustain almost twice the seismically induced base shear demand.

Maximum base shear resistance corresponds to a top displacement around 0.45 [m]. From this point on, the capacity curve is characterized by a negative slope and associated stiffness, representing the strain softening phenomenon, related to the development of a collapse mechanism due to spreading of plastic hinges opening at all frame levels, up to the final top displacement value around 0.92 m. Base shear is then equal to zero and the analysis stops.

In order to better describe structural response during pushover analysis, the envelope of peak inter-story drifts and the structural profile, namely the envelope of peak displacements at each floor level, are reported in Figure 5.2 and 5.3, at the end of analysis when collapse is reached:

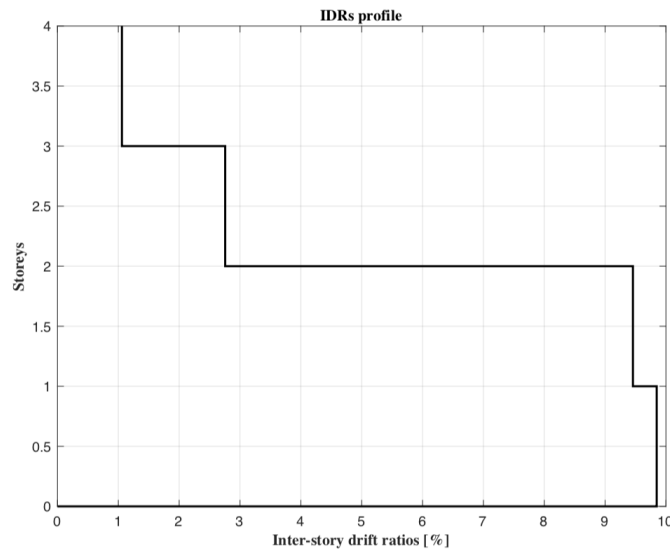


Figure 5.2: Inter-storey drift envelope for fixed base configuration, from pushover analysis

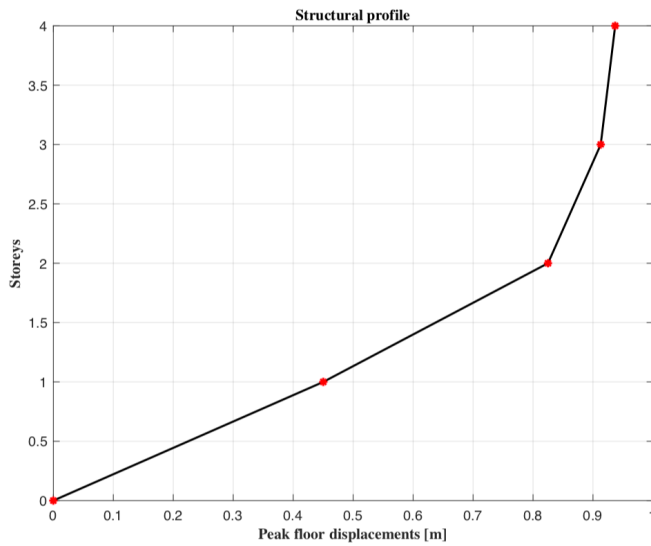


Figure 5.3: Structural profile for the fixed base configuration, from pushover analysis

From Figure 5.2, it is possible to notice how, at first two floor levels, high values of inter-storey drift ratios are reached, respectively about 10% and 9.5%, which clearly indicate the development of a collapse mechanism if compared with the assumed drift capacity, equal to 5%. This value has been proved to be a quite reasonable assumption since,

taking the maximum top displacement from the capacity curve above, before frame collapse, and dividing it by the total building height, i.e. 16.5 m, a value around 5% is obtained. Looking also at Figure 5.3, in agreement with the high first floors inter-storey drift ratios, it can be noticed how the large amount of structural displacements are concentrated at these two levels while, from third one to the top, a more regular displaced shape is present with less increase of lateral displacement; this is also proved by the reduction observed in the drift envelope.

These two envelopes are also shown at the point in which maximum base shear is provided:

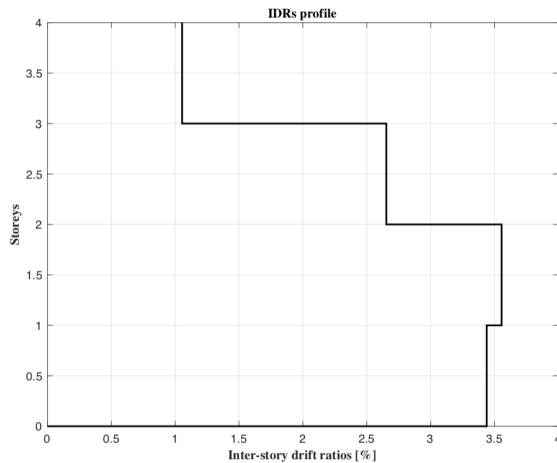


Figure 5.4: Inter-storey drift envelope for fixed base configuration, when maximum base shear is reached

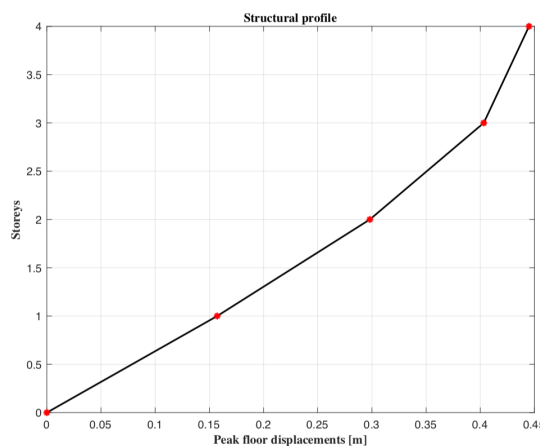


Figure 5.5: Structural profile for the fixed base configuration, when maximum base shear is reached

The inter-storey drift envelope, from Figure 5.4, appears more irregular along building height if compared with collapse one, reported in Figure 5.2. Differently, the structural profile, shown in Figure 5.5, has a similar trend with respect to the collapse profile, with obviously, lower values in this case.

Regarding the base isolated configuration, the same analysis is performed, in both medium and low friction cases, even if it does not have a paramount importance meaning, as for fixed base structure, due to the introduction of isolation devices which allow the building to move horizontally under earthquake action in order to reduce the amount of displacement transmitted the superstructure above the isolation plane, i.e. protected by consequently induced damage. This can be better seen from peak inter-storey drifts envelope and peak displacements one (structural profile), rather than from the capacity curves represented in Figure 5.6:

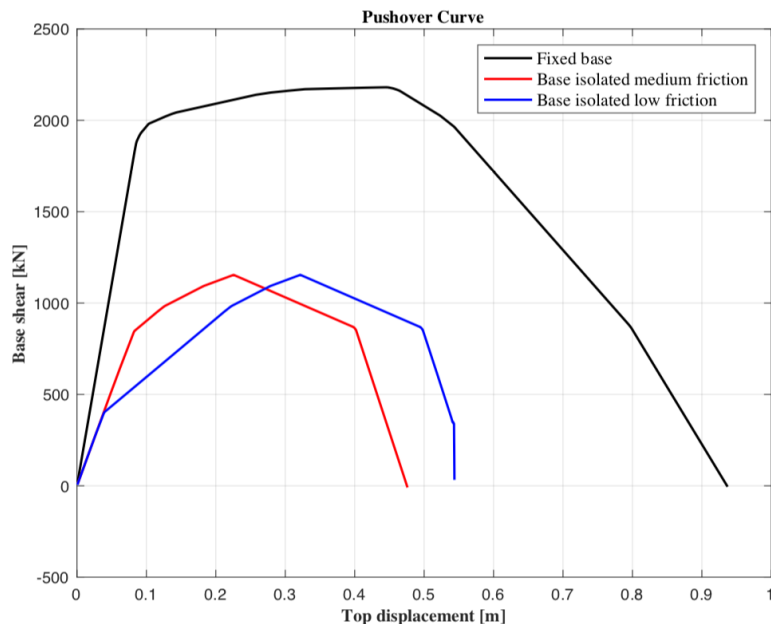


Figure 5.6: Capacity curves comparison for fixed base, base isolated with medium friction bearings and base isolated with low friction bearings

From this comparison, it is possible to understand how base isolated structures collapse at lower top displacement values with respect to fixed base: approximately 0.48 m and 0.54 m, for medium and low friction case, respectively. This can be also evaluated in terms of drift capacity -before collapse reduction: repeating the same calculations made

for the fixed base case, a value around 3.3% is obtained for both medium and low friction base isolated cases. A decrease in total base shear is also present since now, for both base isolated configurations, a peak value, approximately of $V_{is} = 1100 [kN]$, is reached before development of collapse mechanism. This demonstrates how, with the introduction of base isolation, seismic action resistance is not improved in terms of available strength but it is rather identified in an increased capacity to displaced under earthquake loading, namely in a more ductile behaviour, concentrated at the isolator level, that sustain seismic induced displacement, protecting the above superstructure. For this reason, a lower top displacement is detected with respect to the fixed base case, since it must be compatible with the selected isolator ultimate displacement capacity. Additionally, isolators are able to attenuate seismic demand through their dissipative behaviour; the resisting mechanism is so mainly based on a reduction of the seismic demand rather than on a better capacity to withstand it.

Moreover, some interesting considerations can be made by looking at the capacity curves of both base-isolated low and medium friction structural systems: these are characterized by the same first-range stiffness, obtained, respectively, as the ratio between base shear value at which isolators activate and the corresponding top displacement:

$$K_l = \frac{V_{act}}{d_{top}} = \frac{398.4}{0.039} = 10215.40 \left[\frac{kN}{m} \right] \quad (5.3)$$

$$K_m = \frac{V_{act}}{d_{top}} = \frac{848}{0.083} = 10216.87 \left[\frac{kN}{m} \right] \quad (5.4)$$

For both cases, a value around 10000 [kN/m] is obtained. This is actually associated to the superstructure contribution, when the devices are not activated yet. Low friction isolators activate for a base shear around 400 [kN], while medium friction ones for a value around 850 [kN]. The low to medium friction shear activation ratio, is estimated to be approximately equal to the corresponding friction coefficients ratio:

$$\frac{V_{act,l}}{V_{act,m}} = \frac{400}{850} \approx \frac{\mu_l}{\mu_m} = \frac{2.68}{5.66} = 0.47 \quad (5.5)$$

As anticipated before, benefits coming from the isolators' introduction can be better understood by examining the peak inter-storey drift envelopes and structural profiles comparison, reported in Figure 5.7 and Figure 5.8, for the top displacement value corresponding to the maximum base shear development, for each configuration:

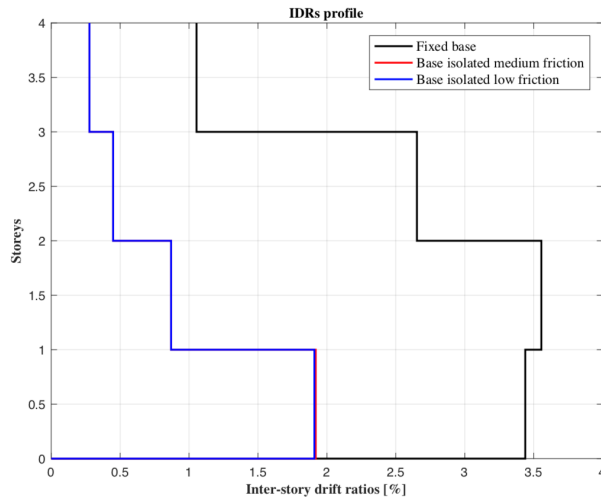


Figure 5.7: Inter-storey drift ratio comparison for fixed base, base isolated with medium friction bearings and base isolated with low friction bearings

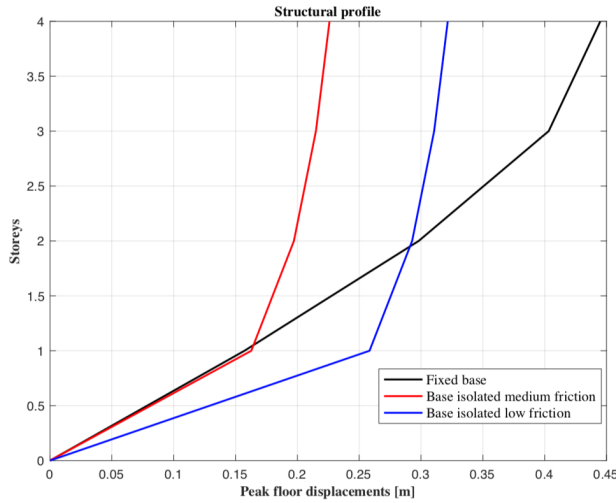


Figure 5.8: Structural profile comparison for fixed base, base isolated with medium friction bearings and base isolated with low friction bearings

From both Figure 5.7 and Figure 5.8, it is possible to notice how isolators tend to concentrate most of the inter-storey drift and peak displacement demands at the first building level, sustaining it in order to protect the superstructure above, which becomes characterised by much lower seismic demand, also distributed in a more uniform and regular fashion over all the other floors. Looking at the displaced shape in Figure 5.8, it

perfectly represents the isolation main concept of resisting seismic action thanks to the introduced devices-displacement capacity and plastic behaviour, while the rest of the structure remains in the elastic domain and displaces like a rigid body. The difference that can be noticed between medium and low friction isolators is due to the fact the latter develop the maximum base shear at a larger top displacement.

5.2. NON LINEAR RESPONSE HISTORY ANALYSIS

This analysis is performed in order to evaluate and compare the structural responses provided by the different structural solutions (i.e. the fixed-base and base-isolated one, focusing also on the variability and impact of friction coefficient), when subjected to ground shaking. This is done through the estimation of engineering demand parameters (EDP), representative of seismic performance, such as peak inter-storey drift ratios together with peak floor accelerations.

The case study building, in all different configurations, is analysed using 11 different sets of 40 ground motion records each, corresponding to 11 increasing intensity measure (IM) levels. The selected parameter to quantify the ground shaking intensity is the spectral acceleration evaluated at the fundamental period of the considered structural system, i.e. fixed base or base isolated one, indicated as $S_A(T_1)$, where:

$T_1 = 1.26 \text{ [s]}$, for the fixed base case;

$T_1 = 3.53 \text{ [s]}$, for the base isolated one, value obtained from the expression reported in section 5.1, depending on the selected friction pendulum bearings radius of curvature.

In both configurations, spectral acceleration is defined for different probabilities of exceedance (PoE) in the reference period for seismic action V_R , equal to 50 years in this case, and corresponding return period T_R . The considered values, defining the increasing intensity measure levels, are reported below:

Table 5.1: Considered intensity measures return periods and corresponding probability of exceedance in the reference period for the seismic action

PoE	0.1	0.01	0.2	0.02	0.3	0.5	0.05	0.005	0.7	0.9	0.0025
$T_R \text{ [yrs]}$	475	4975	224	2475	140	72	975	9975	42	22	19975

These values are not selected as corresponding to code-defined limit state ones, but just in order to evaluate how structural response and seismic demand vary and accumulate over the whole building, with the increasing intensity of ground shaking.

5.2.1. Ground motion records selection

A common goal of dynamic structural analysis is to predict the response of a structure subjected to ground motions having a specified spectral acceleration at a given period. This is important, for example, when coupling ground motion hazard curves from probabilistic seismic hazard analysis (PSHA) with results from non-linear response history analysis. Conditioning on S_a at only one period is desirable, because probabilistic seismic assessments benefit greatly from having a direct link to a ground motion hazard curve, defined for spectral acceleration at a single period. The response prediction is often obtained by selecting ground motions that match a target response spectrum, and using them as input to dynamic analysis. Usually, Uniform Hazard Spectrum (UHS), coming from PSHA, is employed as the target one to be matched, as was used in the NTC18 design previously discussed, but it has been demonstrated to be unsuitable for the coupling purpose mentioned before, since it conservatively implies that large-amplitude spectral values will occur at all periods within a single ground motion. An alternative, termed as Conditional Spectrum (CS), is considered. Ground motion records to be used at each intensity measure levels, are selected in order to match this newly defined response spectrum.

In order to obtain the conditional spectrum, target spectral acceleration at the considered structural configuration fundamental period, T_1 , must be determined. It is also necessary to estimate the magnitude M, distance R and number of standard deviations $\varepsilon(T_1)$ associated with the target $S_a(T_1)$. If this one is obtained from PSHA, then the M, R and $\varepsilon(T_1)$ values can be taken as the corresponding mean from disaggregation; on the other hand, in the case where simply a scenario, described in terms of M, R and $S_a(T_1)$, is evaluated, the associated $\varepsilon(T_1)$ would be the number of standard deviations by which the target $S_a(T_1)$ is larger than the median prediction given the M and R. More details on the computation of the conditional spectrum can be found in the study by (Baker, 2011) and are not described here as they go beyond the scope of this section.

Once the conditional mean spectrum is computed, it is employed in order to select the 40 records, for each intensity measure level, to be used when performing non-linear response history analysis on the different case study building configurations. This response spectrum defines the spectral shape associated with the $S_a(T_1)$ target: ground motions that match the target spectral shape can be therefore treated as representative of ground motions that naturally have the target $S_a(T_1)$ value. In order to find them, a period range over which the conditional spectrum (CS) must be matched can be established; this range would ideally include all periods to which the structural response is

sensitive and may also consider periods associated to higher mode of vibrations, as well as longer periods that affect a non-linear structure, whose first mode period has effectively lengthened due to provided plastic behaviour. For mid-rise buildings, a period range from $0.2T_1$ to $2T_1$ can represent a feasible assumption. Then, a library of ground motions can be examined to identify those that most closely match the target CS according to the below defined sum of squared errors (SSE) criterion:

$$SEE = \sum_{j=1}^n \left(\ln(S_a(T_j)) - \ln(S_{a,CSM}(T_j)) \right)^2 \quad (5.6)$$

where:

j is the index which spans over the considered period range over which ground motions response spectra must match the conditional mean one;

$\ln(S_a(T_j))$ is the ground motions spectral acceleration natural logarithm at T_j ;

$\ln(S_{a,CSM}(T_j))$ is the CS acceleration natural logarithm at T_j ;

In order to select the record' set, the sum of squares criterion must be employed so that the ones with the smallest *SEE* values, are considered.

This approach, actually, can be more effective if ground motion scaling is allowed, so that it is used to make the ground motion spectral amplitudes approximately equal the target amplitude. The above mentioned criterion gives now back the scaled records which most closely match the target. The simplest way to deal with scaling process is to define a scaling factor for each ground motion, so that its spectral acceleration at the fundamental period perfectly matches the target one from conditioned mean spectrum:

$$s_F = \frac{s_{a,CSM}(T_1)}{s_a(T_1)} \quad (5.7)$$

This is the simplest approach and, as said, leads to the definition of a number of records whose corresponding response spectra all have a “pinch” at the structural configuration-fundamental period T_1 , meaning that the scaling ensures that they are all equal at that point and also equal to the conditional mean spectrum.

As an example, in Figure 5.9 and Figure 5.10, the 40 records associated response spectra matching the target conditional mean one, at the structural configuration first period, are represented for both fixed base and base isolation solutions and an arbitrary chosen intensity measure level:

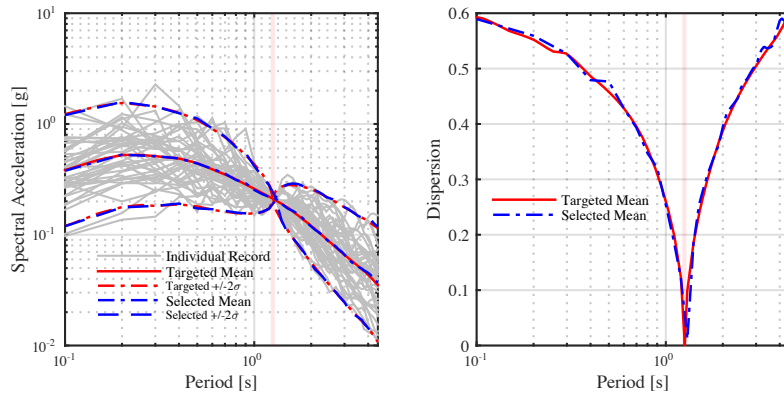


Figure 5.9: Fixed base conditioned mean spectrum method for 0.1 probability of exceedance in 50 years

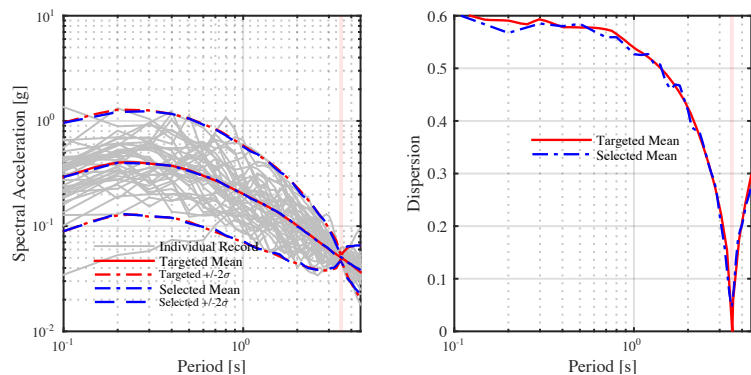


Figure 5.10: Base isolated conditioned mean spectrum method for 0.1 probability of exceedance in 50 years

Herein, a comparison between fixed base and base isolated record selection, referred to the same IM level is provided showing how the different fundamental period values lead to a different spectral matching that happens at lower values of spectral acceleration for the base isolated configurations, both low and medium friction, since they are represented by the same fundamental period, having chosen friction pendulum bearings with radius of curvature equal to 3.1 m, in both cases.

5.2.2. Results discussion

Structural configurations are then analysed under the 11 set of ground motions, each one defined for each IM level, and the before defined engineering demand parameters are recorded. To assess seismic response and compare this among the different cases, it is

not so useful to consider record by record response, but it is better to evaluate the median response parameters and compare these values. In order to do this, a lognormal distribution fitting, for each selected response parameter, is assumed over all the 40 records for each set, so that the median value is provided, actually considering only the non-collapsing ground motions. That is, the ones that do not cause structural collapse. This is due to the fact that, in the following chapter, seismic induced direct economic losses will be estimated assuming that structural collapse mechanism, namely the exceedance of the before defined drift capacity, has not been developed.

The comparison between mean EDP envelopes, i.e. the plot of the corresponding peak floor values along building height, for all the configurations, are reported. Two categories, i.e. “low intensity measure levels” from 22 to 224 years return period and “high intensity measure levels” referred to the remaining values, are considered, in order to see the effects provided by base isolation and, moreover, the impact that friction coefficient variation has on the structural response. Two category-representative IM levels are chosen: the one associated to the 140 years return period T_r , for the low level case, while the 19975 years return period corresponding one, for the high level case. The remaining IM levels will also be discussed herein, and the corresponding envelopes are reported in Appendix D, in order to validate the provided conclusions and observations.

Starting from the “low level” case, the envelopes comparisons of the selected engineering demand parameters are shown in Figure 5.11 and Figure 5.12:

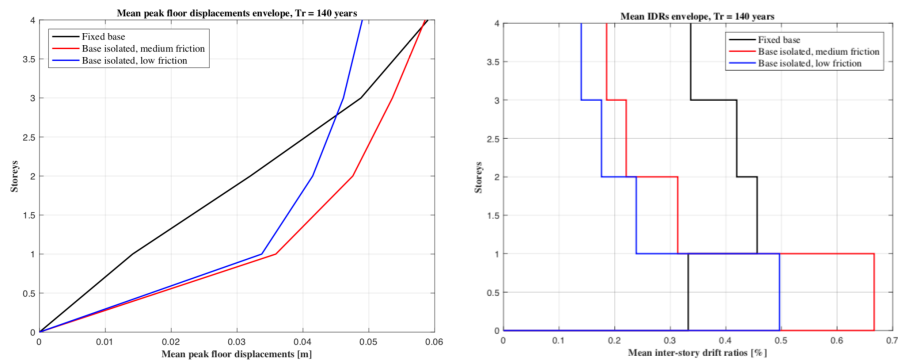


Figure 5.11: Peak floor displacements and inter-storey drift ratios envelope comparison for all the three examined structural configurations, i.e. fixed base, base isolated with medium friction pendulum bearings and base isolated with low friction pendulum bearings; 140 years return period is considered

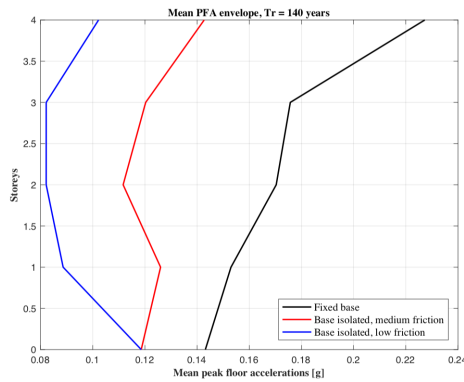


Figure 5.12: Peak floor accelerations envelope comparison for all the three examined structural configurations, i.e. fixed base, base isolated with medium friction pendulum bearings and base isolated with low friction pendulum bearings; 140 years return period is considered

In order to be able to compare structural response behaviour between fixed base and base isolated case, the considered EDP values are evaluated along the building floor levels, not directly considering their values at the isolated one.

Looking at Figure 5.11, it can be noticed how the introduction of isolators tends to increase the displacement demand at the first floor, providing quite a bigger value with respect to the fixed base case, for both medium and low friction cases, whose values, instead, are quite similar. For the other building levels, the values are still bigger, but the increase is more regular and uniform if compared with the one characterizing the fixed base solution: this demonstrates how the superstructure above the isolator plane tends to displace like a rigid body, when subjected to ground shaking. Moreover, low friction pendulum bearings provide a reduction of the top floor displacement with respect to both medium friction and fixed base case. The concept of more regular displaced shape can also be understood in particular from the inter-storey drift ratio envelope in Figure 5.11: a clear reduction is indeed present from second floor to the top one, if compared with fixed base envelope. Actually, an important issue must be remarked: the first floor drift value, with the introduction of the isolation system, is increased with respect to the fixed base one: this can be due to the high displacement contribution associated to the isolation devices, which also influence the displaced shape trend discussed before. The increase is much more relevant for medium friction isolators, while low friction ones are able to control it a bit, obtaining values closer to the fixed base ones but still higher.

Looking at Figure 5.12, it is possible to notice how peak floor accelerations are reduced at all structural levels; a more uniform and regular trend, with respect to the fixed-base case, is obtained along the building height, especially at the second and third floors. Moreover, a clear reduction is also present when moving from medium to low friction devices.

These considerations are valid, in general, for all the low intensity measure levels, namely the ones till the return period value of 224 years, when fixed-base and base-isolated solutions, with low friction pendulum bearings, are considered. Actually, using the medium friction devices, the problem of higher first floor inter-storey drift ratio still persists, also for higher intensity measures, meaning that this solution is effective in reducing the inter-storey drift seismic induced demand at all superstructure levels, except for the first one. For this reason, an alternative solution based on low friction devices is considered. This can be justified by also remarking on how this problem will influence the following part of story-based building-specific loss estimation procedure, for which the first floor drift sensitive associated economic losses, when using the medium friction pendulum bearings, will be higher not only than the low friction ones but also than the losses provided by drift sensitive damageable components in the fixed-base case. On the other hand, due to peak floor accelerations reduction, which is always present, at each IM level, the losses associated to acceleration sensitive components will decrease.

In order to validate these conclusions, the EDP envelope comparisons for the 72 years return periods, are also reported in Figure 5.13 and Figure 5.14:

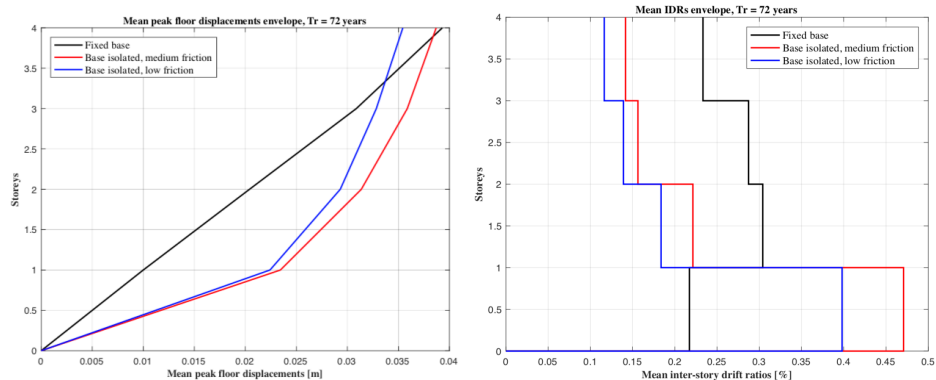


Figure 5.13: Peak floor displacements and peak inter-storey drift ratios envelope comparison for all the three examined structural configurations, i.e. fixed base, base isolated with medium friction pendulum bearings and base isolated with low friction pendulum bearings; 72 years return period is considered

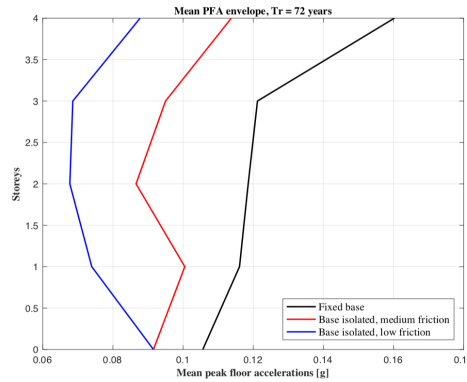


Figure 5.14: Peak floor accelerations envelope comparison for all the three examined structural configurations, i.e. fixed base, base isolated with medium friction pendulum bearings and base isolated with low friction pendulum bearings; 72 years return period is considered

The same trend can be detected by looking at the envelope comparisons associated to the 224 years return period, which is defined as the last one of the “low intensity measure level” category, reported in Appendix D.

Considering instead the 22 and 42 years return periods, namely the lowest two used to perform non-linear response history analysis, the provided engineering demand parameter envelope comparisons, present in Appendix D, show a more pronounced problem in terms first level inter-storey drift ratio, which results largely higher for both base-isolated configurations with respect to fixed-base one. This emphasizes how this issue is mainly related to very low intensity measure levels, rather than higher ones. Moreover, using medium friction pendulum bearings, the peak floor accelerations envelope assumes a quite different trend in these two cases, with some values higher than the fixed base ones: the before mentioned reduction over the whole building height is still present only if low friction devices are used.

Moving to the high intensity measure levels category, as an example, results corresponding to the 19975 years return period are shown in Figure 5.15 and Figure 5.16, in order to mainly evaluate how friction coefficient variability affects structural response:

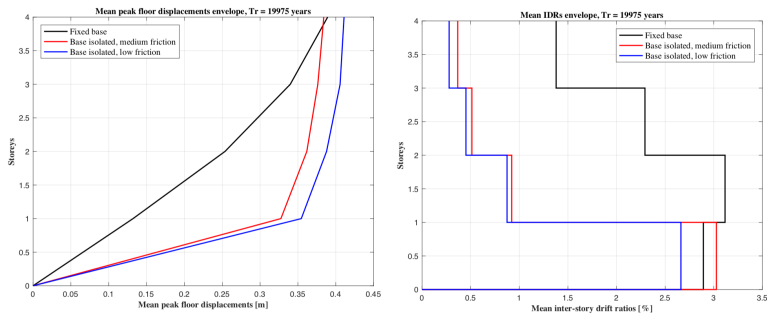


Figure 5.15: : Peak floor displacements and peak inter-storey drift ratios envelope comparison for all the three examined structural configurations, i.e. fixed base, base isolated with medium friction pendulum bearings and base isolated with low friction pendulum bearings; 19975 years return period is considered

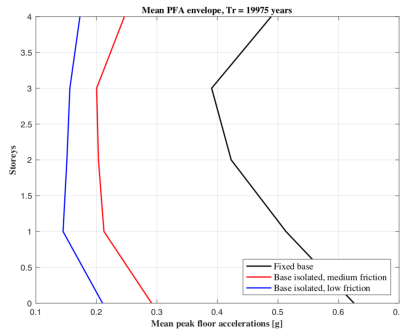


Figure 5.16: Peak floor accelerations envelope comparison for all the three examined structural configurations, i.e. fixed base, base isolated with medium friction pendulum bearings and base isolated with low friction pendulum bearings; 19975 years return period is considered

From these figures, it is possible to draw the same considerations as before for the peak floor displacements envelope, i.e. the displaced shape, which are still valid in this case of higher IM level. Actually, for the latter, a more evident decrease of the corresponding EDP is present from second floor to the roof, with respect to the before examined cases. Moreover, the plot assumes a more regular and uniform trend from first floor on. In terms of peak inter-storey drift ratios, the same problem is present for the base isolated system with medium friction devices, since the first floor values is higher than the fixed-base one. On the other hand, from Figure 5.15, it can be appreciated how the use of low friction pendulum bearings leads to the mitigation of this problem, coming up with a first floor drift ratio lower also than the fixed-base one. As regards peak floor accelerations envelope, in Figure 5.16, it can be noticed how, with the increase of the considered IM level, the reduction becomes more pronounced with respect to fixed-base solution using both isolation configurations: low friction isolators still reduce more than medium friction ones, as valid also for the lower IM levels. An additional interesting consideration

can be made: differently from the case before, peak ground acceleration (PGA) values are different between base-isolated solutions. At first impact this may appear strange, but is due to the fact that, for the examined IM level, moving from medium to low friction devices, provides a change in the non-collapsing case.

A different trend in peak floor displacement values was observed for 9975 and 4975 years return periods: in these cases, the use of medium friction devices led to a larger reduction in terms of the aforementioned EDP with respect not only to fixed-base solution but also to seismic isolated one, when low friction pendulum bearings are used. This, actually can be seen also from Figure 5.15. For 2475 and 975 years return periods, the observed trend is still valid while the 475 years return period, on the other hand, is characterized by the usual trend for which the use of low friction devices provides a higher decrease of floor displacement demand.

A summary of the general observations, coming from structural response comparison, is reported next:

- the base-isolated configuration with medium friction devices is characterized by a first storey peak drift value higher than the fixed-base one, for all IM levels. This issue will have relevant consequences in the loss estimation procedure, meaning that, even if base isolation is used, medium friction devices are not able to reduce the first storey loss associated to drift sensitive damageable components, both structural and non-structural. Herein, the use of low friction isolators comes into play so that this problem is removed for all higher intensity measure levels, but still remains present, even if the drift value is reduced with respect to the one provided by medium friction pendulum bearings, for the lowest IM levels;
- for other building floors, from second one up to the roof, the use of base isolation provides a considerable reduction of inter-storey drift ratios, giving the structure a more regular and uniform displaced shape, similar to a rigid body when subjected to ground shaking;
- this regularity can also be ensured by looking at peak floor displacements envelope, since the increase from the second floor level is not as pronounced as in the fixed-base case. Actually, it has to be underlined how, peak displacement at first floor is bigger for base-isolated configurations, due to the isolator contribution which attenuate seismic demand displacing when subjected to ground shaking. Another important observation can be made: with the IM level increase, medium friction devices are able to reduce more the provided displacements rather than low friction ones. The opposite trend is present for low IM levels;

- lastly, in terms of peak floor accelerations, a considerable reduction is present along all the building height, when using seismic isolation, with respect to the traditional fixed-base configuration. In the central part of the envelope, especially for higher IM level, a more uniform trend is detected, meaning that there is not so much difference, between subsequent levels, in the provided peak floor accelerations. On the other hand, an increase in the roof acceleration values is always present, both with medium and low friction devices: the latter are actually able to mitigate a bit this phenomenon. In general, seismic isolation provides a considerable reduction of peak floor acceleration demand, and this will also reduce the corresponding direct economic losses, associated to acceleration sensitive non-structural components, both when medium friction and low friction pendulum bearings are used.

All designed configurations structural response and seismic performance have been assessed and compared through non-linear response history analysis for increasing IM levels, associated to different return periods and corresponding probability of exceedance in the seismic action reference period. As an example, the EDP envelopes comparison for two IM levels, are provided and discussed in order to derive the most relevant considerations about seismic isolation effects and friction coefficient variability impact. For a more detailed overview about all the NRHA outputs, table with engineering demand parameters (EDP) values and envelope comparison plots are reported in Appendix D. In the following chapter, the mean EDP values along building height will be used to enter the corresponding floor dependant engineering demand parameter-damage variable (EDP-DV) function, for the considered damageable component, in order to estimate the provided seismically induced expected floor loss.



6. LOSS ESTIMATION PROCEDURE

This chapter deals presents available methods to estimate seismic induced direct economic losses from the obtained engineering demand parameters (EDPs) when non-linear response history analysis is performed to evaluate ground shaking structural response. First, a general overview about the relevance and impact that economic losses have on structural seismic performance is given, together with a brief dissertation on the previous research works and methods, available in the literature, used to estimate them. Then, the general framework of the storey-based building specific loss estimation procedure, developed by (Ramirez, 2009), is presented emphasizing the use of the so-called engineering demand parameter-damage variable (EDP-DV) functions, directly relating the structural response, coming from dynamic analysis in terms of defined parameters such as peak inter-storey drift ratio and/or peak floor accelerations, with the induced direct economic losses. As the procedure name itself indicates, they depend on the building geometry and structural behaviour, its occupancy and the considered floor level, assuming the presence of three damageable components, as already specified in this document, namely (i) structural drift sensitive elements, (ii) non-structural drift sensitive elements and (iii) non-structural acceleration sensitive ones. Then, the functions to be used for the different configurations of the case study building are specified.

Despite significant improvements in seismic design codes, such as the presence of better detailing requirements that translate in an improved earthquake performance of modern buildings compared to older structures, important shortcomings still exist. One of the inherent and underlying issues with current structural design practice is that seismic performance is not explicitly quantified and results to be of an inconsistent level since building codes mostly rely on prescriptive criteria when defining it. Some studies, such as (Krawinkler, 2004), (Aslani, 2005) and (Mitrani-Reiser, 2007), propose an innovative way of quantifying earthquake performance through the estimation of seismic induced direct economic losses, used as a metric to evaluate how well structural systems respond when subjected to ground shaking. This represents also an attempt of looking for a better connection between engineering and society, where building owner's main concern is the protection of life, when describing the performance of a building. Quantifying it through the definition of EDPs, i.e. inter-storey drift ratios or peak floor accelerations, to be checked with respect to code-defined threshold values, does not represent a method which can comply with the aim mentioned before. Herein, the evaluation of direct monetary losses comes into play as something that can be better understood not only by

designers but also by general decision-makers and, on the other hand, can be linked to the definition of an acceptable probability level for which a structure maintains its functionality after and/or during an earthquake, according to its occupancy, when a certain amount of losses is developed.

The importance and relevance of economic losses within the seismic performance framework was demonstrated by different recently-occurred earthquakes. As an example, some of them are mentioned in the reference paper by (Ramirez, 2009), showing how, though the produced levels of ground motion intensity were considered relatively moderate, buildings experienced extensive structural damage and a loss of functionality, requiring substantial repairs, even if occupant life safety was preserved.

Another mentioned example of paramount importance of how current design procedures do not comply with building owners' and users' needs, is represented by the non-structural damage sustained by the Olive View Hospital during the 1994 Northridge earthquake. Located in Sylmar, California, this six-storey structure was designed beyond minimum building code requirements in response to the structural failure of the previous Olive View Hospital building during the 1971 San Fernando earthquake. The replacement structure's lateral force resisting systems consisted of a combination of moment frames with concrete and steel plate shear walls. Although the building only experienced minor structural damage during the Northridge event, substantial non-structural damage was provided. Particularly, sprinkler heads, rigidly constrained by ceilings, ruptured when their connecting piping experienced large displacements. The resulting water leakage caused hospital downtime, so that the facility, not only was unable to treat injuries resulting from the earthquake, but also 377 patients being treated at the time of the earthquake had to be evacuated (Hall, 1995). While the structure conformed to building code standards for hospitals, the non-structural damage resulted in the loss of functionality of an essential facility, directly after a seismic event. This demonstrates how structural design using prescriptive existing codes is not enough to ensure a satisfactory seismic performance, leading to the development of preliminary documents (Vision 2000, FEMA 273 & FEMA 356) that attempt to provide some guidance on how to achieve different levels of performance that help stakeholders and design professionals make better and more informed decisions that meet building-specific needs. Actually, the performance levels defined in these documents were often qualitative, not well-defined and, consequently, open to subjectivity, demonstrating the clear need for better quantitative measures of structural performance during seismic ground motions and improved methodologies to estimate it. The Pacific Earthquake Engineering Research (PEER) Centre conducted significant research in this field, formulating a framework that quantifies performance in metrics that are more relevant to stakeholders, namely, deaths (loss of life), dollars (economic losses) and downtime (temporary loss of use of the facility). The proposed methodology uses a probabilistic approach to estimate damage

and the corresponding losses based on the seismic hazard and structural response. This is just an example, since many building-specific direct economic loss estimation methods have advanced in recent years. However, the process to calculate losses can become complex because of the type and amount of required computations, forcing structural engineers to devote extra time towards detailed loss estimations in addition to the structural design. Thus, there is a need for simplifying the procedure in order to minimize the required computational effort; following this idea, the methodology developed by (Ramirez, 2009), described in Section 6.2, leads to a clear simplification, “simplifying” the loss estimation process to utilise pre-defined functions with the dynamic-analysis obtained EDPs and directly obtain corresponding floor losses.

6.1. AVAILABLE LOSS ESTIMATION PROCEDURES

Current loss estimation methodologies can be firstly divided in two main categories: (i) methodologies for regional loss estimation and (ii) methodologies for building-specific loss estimation. Since the scope of this section is just to provide the reader with a general overview about the already developed loss estimation methods and due to the fact that regional methods do not provide the necessary level of detail required by performance-based earthquake engineering, they are not presented herein.

One of the first building-specific loss estimation methodologies was developed by (Scholl, 1982), leading to an improvement to both empirical and theoretical aspect. The latter include an in depth study of developing damage functions for a variety of building components, based on experimental test data: three example buildings (the Bank of California Building and two hotel buildings) damaged during the 1971 San Fernando earthquake were used to illustrate the damage-prediction methodology. In order to develop the theoretical motion-damage relationships, only elastic analyses in combination with response spectrum analysis (using spectral displacement as the spectral ordinate) were used to estimate structural response at each floor of each considered building. The resulting relationships evaluated damage using a damage factor, defined as the ratio between the repair costs induced by earthquake damage and the replacement value of the building. Actually, it required component damage functions (i.e. component fragility functions), to estimate damage on a component-by-component basis, reason for which a research lead by (Kutsu, 1982) had been considered in conjunction with this study in order to collect laboratory test data to estimate damage in various high-rise building components, so that the proposed component-based methodology could be implemented. The evaluated elements included: RC structural members (beams, columns and shear walls), steel frames, masonry walls, drywall partitions and glazing. Based on published building cost data, the study also statistically determined proportions of construction costs for these components. This information was then used in combination with the damage functions to calculate the overall damage factor of the component (damage as percentage of the replacement values of the component). These relationships

are limited because the analyses used do not capture higher-mode effects and damage due to nonlinear behaviour.

The second is a scenario-based loss estimation methodology – assessing monetary losses of a building from its structural response from a particular earthquake ground motion – introduced by (Gunturi S. and Shah, 1993). Damage to building components, categorized into structural, non-structural and contents elements, was calculated by obtaining structural response parameters, at each storey, from a nonlinear time history analysis, by scaling the record to peak ground acceleration (PGA) levels of 0.4g, 0.5g and 0.6g. The response parameters were related to damage levels for each component and loss was calculated per storey and summed to get the total building loss. An energy-based damage index, developed by (Park, 1985), was used to estimate damage in structural elements, while peak inter-storey drift and peak floor accelerations were used to assess non-structural damage. Several strategies to map these damage indices to monetary losses were tried, (i) one included a probabilistic approach based on the available data at the time the study was published, while the other (ii) consisted in a deterministic mapping primarily based on expert opinion and was used for practical applications. Although the study examined damage variation with different ground motions for one considered building, the frequency at which ground motions occur was not accounted for.

(Porter, 2001) described a fully probabilistic assembly-based framework. It also incorporates the uncertainty coming from estimating building damage and the associated repair costs, which in previously presented approaches had not been considered. Monte Carlo simulation was used to predict building-specific relationships between expected loss and seismic intensity, namely the vulnerability curves. Techniques to develop fragility functions for common building assemblies were presented and used to predict losses for an example office building. Ground motions were simulated using the ARMA model to generate the number of artificial time histories necessary to run structural analyses. Depending on the structural response parameter of interest, the study used both linear and non-linear dynamic analyses to compute peak structural responses. A simplified, deterministic sensitivity analysis was also conducted to investigate which sources of uncertainty have the largest effect on loss results; the uncertainty of the ground motion intensity was found to have the largest influence. Moreover, no attempt was made to explicitly compute the probability of collapse.

The last presented approach, as part of the PEER centre's effort to establish performance-based assessment methods, is the one developed by (Aslani, 2005): it consists in a component-based methodology that incorporated the effects of collapse on monetary loss by explicitly estimating the probability of collapse at increasing levels of ground motion intensity. Both side-way collapse and loss of vertical capacity were integrated into the calculation of seismic-induced expected losses; on the other hand,

losses due to building demolition, resulting from large residual inter-storey drifts, were not considered. This investigation also proposed techniques to disaggregate building losses to identify the components that most significantly contribute to the it. Moreover, a method incorporating the effect of correlations into calculating the dispersion associated with these losses at the component-level, was presented. Values of component cost correlations were unavailable so building-level cost data was used to approximate these correlation coefficients. Needed component fragilities were developed and applied to an existing seven-storey non-ductile RC moment frame building, used as an example. Damage of components was primarily estimated with minimal consideration of any dependent losses between spatially interacting components, treating them independently and assuming that they would not have any effect on the overall losses due to non-collapse. In coordination with this research, PEER's component-based loss estimation methodologies were also developed and implemented by (Mitrani-Reiser, 2007), through the definition of a computer program, named the MATLAB Damage and Loss Analysis (MDLA) toolbox, able to implement the PEER loss estimation framework. This program was then used in an investigation to benchmark the performance of a 4-storey ductile reinforced concrete moment resisting frame office building, which conformed to modern seismic codes. Mean losses, as a function of ground motion intensity level, and expected annual losses, were calculated for multiple design variants to examine how different structural and modelling parameters influenced monetary losses. The design variants only consisted of 4-storey structures and consequently losses for structures of different heights were not examined. Losses due to non-collapse were calculated on a component-by-component basis including only losses from components with available fragility functions. The considered ones included beams, columns, slab-column joints, partitions, glazing, sprinklers and elevators. An attempt was made to account for dependent losses of spatially interacting components by including the replacement cost of the dependent component in the repair cost of the other component. However, this approach results in counting the loss of the dependent component twice.

These presented procedures are some of the available ones, taken as representative for the possible different aspects that can characterize losses estimation methods. Although they have advanced substantially in recent years, some limitations and drawbacks still remain present and are pointed out below:

- inter-dependency between components losses: the economic losses of certain building components can be a function of the damage state of another element. In the above mentioned methods, these are ignored, as done by (Aslani, 2005), or double-counted, leading so to an overestimation. Actually, methods able to account for this interaction, coming up with a more precise and refined loss estimation, are not yet available;

- unfortunately, many components found in a building's inventory do have not corresponding defined fragility functions, so that a probabilistically-based damage estimation can be performed for all of them. Some of the previous studies have either ignored these components or treated these as rugged, namely as elements that do not develop any type of damage before collapse; actually this is not always a reasonable assumption. Other studies, (Aslani, 2005) for example, used generic fragility functions initially developed for regional methods. However, the data employed to obtain them is not well documented and relies heavily on expert opinion that has still to be validated;
- modern structures are designed to behave in the plastic domain having a suitable ductility capacity to protect life-safety by preventing collapse. However, residual inter-storey drifts, large enough to require post-earthquake building's demolition, can be provided. While some previous works were able to account, separately, for losses due to non-collapse or to collapse, limited research is conducted in order to look for an approach able to include economic losses provided by structural demolition. In particular, the probability that the building will be demolished due to excessive permanent residual drifts, as a function of the probability that these values exceed a defined threshold, for a given IM level, has not been incorporated into the current loss estimation framework, yet;
- although previous studies have established the need of using multiple ground motions to account for probabilistic nature of structural response, the ideal number of records to be used in loss analysis is not well defined yet. In order to determine the required number of ground motions, it is firstly needed to evaluate its influence on obtained response parameter correlation coefficients. For all the configurations of the case study building examined in the presented work, the 11 sets of 40 records each, associated to increasing levels of IM, are considered, actually accounting only for the non-collapsing records. This means that only the non-collapse expected economic losses are evaluated;
- losses for a range of design variations building classes, such as mid-rise RC moment resisting frame ones, have not been evaluated yet. Benchmarking them, for an entire structural category, can help identify possible trends and establish how well these types of buildings perform when subjected to seismic action;
- current building-specific loss estimation methods require a large amount of computations, making completely unpractical hand prediction of losses. To facilitate this procedure, computer tools are needed so that the attention can be focused on input of data and outputs, i.e. expected losses, estimation, rather than on the predicting process itself.

The storey-based building-specific loss estimation procedure, developed by (Ramirez, 2009), tends to overcome some of these drawbacks, proposing itself as an innovative and

more practical approach. Mostly, it works on the last point, leading to a clear simplification of the loss estimation or computation made possible by the use of EDP-DV functions.

6.2. STOREY-BASED BUILDING SPECIFIC LOSS ESTIMATION METHOD

This approach simplifies the fully probabilistic PEER framework, used to quantitatively assess structural seismic performance in terms of economic losses, downtime and number of fatalities, as innovative metrics. Essentially, the PEER methodology is divided into four basic steps:

1. definition of site ground motion seismic hazard;
2. assess structural response from performed dynamic analysis;
3. estimate seismic-induced damage of building components;
4. evaluation of associated repair costs.

The result of each stage serves as input to the following one; mathematically, if the involved metrics are considered to be random variables, in agreement with the fully probabilistic assumptions, they can be aggregated using the theorem of total probability, coming up with this expression, commonly known as PEER integral:

$$\lambda(DV) = \iiint G(DV|DM) dG(DM|EDP) dG(EDP|IM) d\lambda(IM) \quad (6.1)$$

where:

IM, EDP, DM and DV respectively stand for the selected intensity measure, engineering demand parameter, damage measure and decision variable;

$G[X|Y]$ denotes the complementary cumulative distribution function of the random variable X conditioned on Y occurrence;

λ denotes the mean annual occurrence rate of the considered random variable.

The first stage uses probabilistic seismic hazard analysis to generate a seismic hazard curve, defining the frequency of exceeding a ground motion IM for the considered site. The second stage involves using structural response analysis to compute EDPs, such as inter-storey drift and peak floor accelerations, and the collapse capacity of the examined structure. The third step produces damage measures (DMs) using fragility functions, which are cumulative distribution functions relating EDPs to the probability of exceeding

a defined limit state or entering the corresponding damage state. The fourth and final stage establishes decision variables (DVs), in this case economic losses based on repair and replacement costs of damaged building components, which stakeholders can use to help them make more informed design decisions.

Within this presented framework, the storey-based loss estimation procedure is introduced in order to simplify the losses computation part “overcoming” the third step of the PEER framework as represented below:

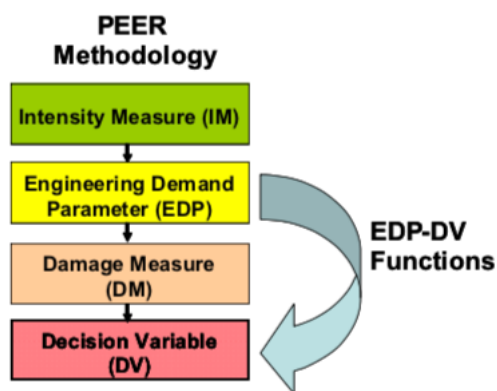


Figure 6.1: Simplified PEER framework according to storey-based building specific loss estimation procedure

This can be achieved with the development of certain functions, termed EDP-DV functions, which, according to their acronym, relate the structural response described in terms of selected EDPs directly to the seismic induced direct economic losses (DVs). These functions reduce the amount of computation by integrating fragility functions with repair costs beforehand and reduce the amount of data required to be tracked by making assumptions regarding the building's inventory as function of its occupancy and structural system. Moreover, they are particularly useful when assessing seismic performance during schematic design because many important design decisions, such as the type of lateral force resisting system, are made during this stage, when much of the building's inventory is still uncertain or unknown.

Herein the use of EDP-DV functions is explained from the analytical point of view and compared with the previously introduced component-based loss estimation methodology. According to the latter, the third and the last steps of PEER approach involve building-specific damage and losses, developed at the component level, as follows:

$$L_T = \sum_{j=1}^n L_j \quad (6.2)$$

where:

n is the total number of components present in the building; each component considered in the analysis is assigned fragility function, if available, to estimate damage, based on structural response level;

L_T is the total loss, while L_j is the j^{th} component loss; note that all of them are random variables.

Actually, the total amount of losses, conditioned on a certain ground motion intensity, can be expressed as the summation of two contributions, namely the losses due to structural collapse and the ones due to non-collapse, multiplied by the respectively probabilities of having developed the mechanism or not:

$$E[L_T|IM] = E[L_T|NC, IM]P(NC|IM) + E[L_T|C, IM]P(C|IM) \quad (6.3)$$

where:

$E[L_T|NC, IM]$ is the total building loss when no collapse is provided, for ground motion IM level;

$P(NC|IM)$ is the probability of non-structural collapse conditioned on the occurrence of an earthquake with ground motion IM level;

Same consideration can be done for the terms related to structural collapse; to be more precise these contributions are not accounted for, since the attention is mainly focused on expected losses due to non-collapse, for all the present components.

$$E[L_T|NC, IM] = E\left[\sum_{j=1}^n (L_j|NC, IM)\right] = \sum_{j=1}^n E[L_j|NC, IM] \quad (6.4)$$

with:

$E[L_j|NC, IM]$ expected loss for the j^{th} component given that collapse has not occurred at intensity measure IM; L_j is the component-associated loss defined as corresponding cost of repair or replacement;

Using the theorem of total probability, the resulting expected loss from non-structural collapse can be expressed as follow:

$$E[L_j|NC, IM] = \int_0^\infty E[L_j|NC, EDP_j] |dP(EDP_j > edp_j|NC, IM)| \quad (6.5)$$

where:

$E[L_j|NC, EDP_j]$ is the considered component expected loss when it is subjected to a certain EDP, obtained from structural response analysis;

$P(EDP_j > edp_j|NC, IM)$ is the probability of exceeding the defined EDP, in the component j, given that structural collapse has not occurred for a ground motion intensity level IM;

The first term is a function of the component's repair cost according to the provided damage state. The probability of being in a certain damage state, evaluated from component-associated fragility curves and related with the probability of exceeding the corresponding limit state, has to be accounted for, as shown below:

$$E[L_j|NC, EDP_j] = \sum_{i=1}^m E[L_j|NC, DS_i] P(DS = ds_i|NC, EDP_j) \quad (6.6)$$

where:

m is the number of damage states defined for the j component;

$E[L_j|NC, DS_i]$ is the component expected loss when the damage state DS_i has been reached, given non-structural collapse;

$P(DS = ds_i|NC, EDP_j)$ is the probability, for the j component, of being in each considered damage when subjected to the engineering demand parameter EDP_j , provided by non-structural collapse. This value can be directly read from each component-specific fragility functions.

Considering the general framework of the component-based method, the advantages and simplifications of the use of EDP-DV functions are pointed out. The first step consists in eliminating the third PEER stage of damage estimation by combining information from loss functions and fragility ones, as shown in Figure 6.1. Actually, this would require the definition of fragility functions and expected repair or replacement costs, for each

component; something that, as specified also before, is not possible for all of them due to lack of available data. However, if these costs are normalized by their corresponding replacement value a_j , the problem no longer exists and computations can be performed without the need to provide this data for each damage state. Factoring out and then eliminating the coefficient a_j on both sides of the equation above, this becomes as follows:

$$a_j E'[L_j | NC, EDP_j] = a_j \sum_{i=1}^m E'[L_j | NC, DS_i] P(DS = ds_i | NC, EDP_j) \quad (6.7)$$

Where, now, both expected losses are normalized by the component replacement value.

The second step deals with the estimation of a storey-associated loss, summing the individual component contributions in order to come up with the entire storey loss for all building levels. To be precise, this summation requires inventorying the number of components and corresponding values; here the introduced simplification comes into play since EDP-DV functions can be formulated assuming that components of the same type are grouped together and experience the same level of damage, for example all partitions in the same storey are characterized by the same damage state. The loss for each component type can be calculated multiplying the normalized expected loss by its value relative to the entire storey one b_j , namely the total value of the same components divided by the total value of the considered floor. Summing the component types present in the entire storey, the following expression is obtained:

$$E'[L_{story} | NC, EDP_k] = \sum_{j=1}^m b_j E'[L_j | NC, EDP_j] \quad (6.8)$$

where:

$E'[L_{story} | NC, EDP_k]$ is the total storey expected loss, normalized by its replacement value, conditioned on the k^{th} engineering demand parameter representing structural response when no collapse occurs.

The actual monetary value of the total expected loss for the considered story is expressed as follows:

$$E[L_{story} | NC, EDP_k] = c_l E'[L_{story} | NC, EDP_k] \quad (6.9)$$

having that:

$E[L_{story} | NC, EDP_k]$ is the storey economic loss expressed in dollars \$;

c_l is the assumed total storey replacement value, also expressed in dollars \$.

Once the loss is expressed in these terms, repair costs or replacement values are no longer required for each component, but rather establish the total value of the storey, so that the component loss can be determined by means of the coefficient b_j defined before. This is how generic EDP-DV functions are expressed. It is important to notice how, in general, floor losses are conditioned on the EDP provided by structural response and used to estimate them: EDP sensitivity is defined in terms of which EDP type is used in order to assess building-component damage state. For the case study application, as already pointed out, the presence of three different damageable components is assumed all over the building levels, so that the total expected storey loss can be determined summing up these three contributions. The considered components are:

- drift sensitive structural elements;
- drift sensitive non-structural elements;
- acceleration sensitive non-structural elements;

The selected EDPs characterising damage so are the peak inter-storey drift ratio and peak floor acceleration. Moreover, a distinction between structural and non-structural elements is considered since the amount of developed damage can be different, for the same structural response parameter. It is assumed that damage to the former is mainly caused by inter-storey drift, i.e. the peak floor acceleration sensitivity is neglected.

6.2.1. EDP-DV functions

Peak inter-storey drift ratios and peak floor accelerations are the selected EDPs to evaluate seismic induced direct economic losses for the three assumed damageable components, using EDP-DV functions. They are expressed in terms of selected EDP along the horizontal axis and expected storey loss, normalized by the storey replacement value, along the vertical one. In order to determine them, typical cost distributions for a given building occupancy and structural system, must be known and, according to (Ramirez, 2009), the source chosen to establish these values, to be used in the case study application, was the 2007 RS Means Square Foot Costs, (Balboni, 2007). However, this publication gives cost distributions for the entire building rather than the distribution at the storey level, which actually is the required one since EDP-DV functions are defined for the considered floor. Some assumptions on how costs vary along the height need to be made so that building cost distribution can be translated into storey ones; this will strongly depend on building occupancy and, particularly, on how building components are distributed amongst the different floors.

Herein are presented EDP-DV functions, defined for typical office buildings, that will be used, as shown in Chapter 7, in order to evaluate and compare the seismic performance of all the case study model structural configurations. Although different storey cost distributions could be generated for different building levels, the used number can be limited to comply with the following assumptions:

- the entire building is used for office space, namely it is not considered a mixed-use facility;
- the first floor value has a clear difference with respect to other ones since as the main entrance, the layout, facades and finishes are typically different at this level;
- the top floor value, typically defined as the building roof, is significantly different from the others because here are usually located most of the building mechanical electrical and plumbing (MEP) equipment and also includes any equipment that may be placed in a mechanical penthouse;
- the remaining intermediate floors are all dedicated to office use only, reason for which they will have the same storey cost distribution.

According to these prescriptions, three different types of EDP-DV functions, i.e. (i) first storey ones, (ii) top floor ones and (iii) intermediate level ones are defined for each one of the three damageable component groups. Their different shapes and trends will take into account the story-dependant distribution of these components along the building height.

From (Ramirez, 2009), a typical cost distribution for a commercial office building is reported in Figure 6.2:

Component Group	Building Distribution (% of total bldg value)	Story Distribution (% of story value)		
		1st Floor	Typical Floor	Top Floor
A. SUBSTRUCTURE	2.3%	0.0%	0.0%	0.0%
B. SHELL				
B10 Superstructure	17.6%	17.9%	18.5%	15.4%
B20 Exterior Enclosure	16.3%	18.8%	16.2%	16.9%
B30 Roofing	0.6%	0.0%	0.0%	4.5%
C. INTERIORS	19.4%	20.7%	21.4%	11.1%
D. SERVICES				
D10 Conveying	9.5%	9.1%	9.4%	11.8%
D20 Plumbing	1.9%	1.9%	1.9%	2.0%
D30 HVAC	13.0%	12.3%	12.7%	17.6%
D40 Fire Protection	2.6%	2.6%	2.7%	2.8%
D50 Electrical	16.8%	16.6%	17.2%	17.9%
	100%	100%	100%	100%

Figure 6.2: Building cost distribution assuming commercial office occupancy, from RS Mean Square Root Costs (2007)

As an example, in Figure 6.3 from (Ramirez, 2009), cost distribution for a typical floor in a commercial office building is defined by further dividing the cost of each component group into individual elements.

Building Height: Floor Type:		Mid-rise Typical Floor		
Component	Seismic Sensitivity	Fragility Group	Normalized costs	
B. SHELL				
B10 Superstructure	robust			
Slab	Rugged		8.2%	
Beam-column Assembly	IDR	Structural	7.2%	18.5%
Slab-column Assembly	IDR	Structural	3.1%	
B20 Exterior Enclosure				
Exterior Walls	IDR	Partitions	9.1%	
Exterior Windows	IDR	Windows	6.2%	16.2%
Exterior Doors	IDR	Partitions	1.0%	
B30 Roofing				
Roof Coverings	Rugged		0.0%	
Roof Openings	Rugged		0.0%	0.0%
C. INTERIORS				
Partitions with finishes	IDR	Partitions	4.5%	
Interior Doors	IDR	Partitions	1.9%	
Fittings	IDR	Generic-Drift	0.6%	
Stair Construction	IDR	Generic-Drift	1.9%	
Floor Finishes - 60% carpet	IDR	DS3 Partition-like	4.4%	21.4%
30% vinyl composite tile	Rugged		2.2%	
10% ceramic tile	Rugged		0.7%	
Ceiling Finishes	PFA	Ceilings	5.1%	
D. SERVICES				
D10 Conveying				
Elevators & Lifts	IDR	Generic-Drift	0.9%	
	PFA	Generic-Accl	8.5%	9.4%
D20 Plumbing				
Plumbing Fixtures	IDR	DS3 Partition-like	0.9%	
	Rugged		1.1%	1.9%
D30 HVAC				
Terminal & Package Units	PFA	Generic-Accl	9.5%	
	IDR	Generic-Drift	3.2%	12.7%
Other HVAC Sys. & Equipment			–	
D40 Fire Protection				
Sprinklers	PFA	Generic-Accl	2.0%	
Standpipes	IDR	Generic-Drift	0.7%	2.7%
D50 Electrical				
Electrical Service/Distribution	PFA	Generic-Accl	1.5%	
Lighting & Branch Wiring	Rugged		1.1%	
Lighting & Branch Wiring	PFA	Generic-Accl	5.1%	
Lighting & Branch Wiring	IDR	DS3 Partition-like	4.5%	17.2%
Communications & Security	Rugged		1.0%	
Communications & Security	PFA	Generic-Accl	1.5%	
Communications & Security	IDR	DS3 Partition-like	2.5%	
		$\Sigma =$	100%	100%

Figure 6.3: Components cost distribution for a typical floor in a commercial office building

The distribution of costs for each component group has been primarily based on engineering judgement; several of the components are assumed to be damaged only if the entire structure has developed a collapse mechanism, i.e. they are termed as rugged and they do not contribute to non-collapse induced losses.

For the scope of the presented work, it is enough to give the reader a general idea of the loss estimation framework behind the use of EDP-DV functions, whereas more detailed information on how these functions are actually obtained from building cost distribution are not discussed, since this goes beyond the scope of this dissertation. The storey-based building specific loss estimation procedure, using the EDP-DV functions reported before for the selected building occupancy, has to be performed for all the case study model structural configurations in order to assess and compare their seismic performance.



UNIVERSITÀ
DI PAVIA



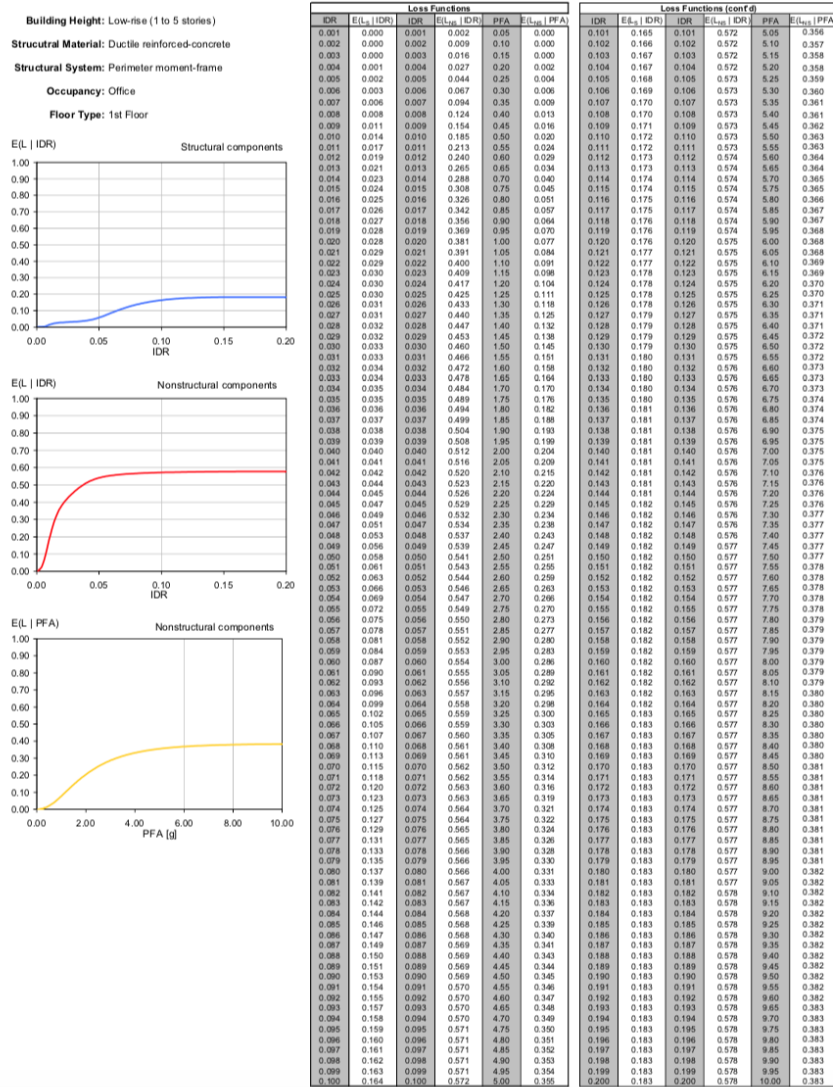
7. APPLICATION TO THE CASE STUDY BUILDING

In this chapter, the presented storey-based building specific loss estimation procedure is employed through the use of EDP-DV functions, dependant on the considered floor level and defined for the commercial office building occupancy, in order to assess and compare the seismic performance of the three case study model configurations, i.e. the fixed-base one and the two base-isolated ones, with medium friction pendulum bearings and with low friction devices. The mean EDPs, namely peak inter-storey drift ratios and peak floor accelerations, obtained from Section 5.2.2, where non-linear response history analysis were performed, using the 11 sets of 40 ground motions each, associated to increasing levels of IM, are now used to enter the corresponding floor EDP-DV functions, for the considered damageable component, so that the induced direct expected economic loss, normalized by the storey replacement value, can be obtained. This is repeated for all building floors and for all IM levels, coming up with the total expected economic loss values along building height, obtained from the summations of the three damageable components contributions, at each storey. These values are then summed up in order to determine the total building loss for the considered IM level; the impact that different floors have on the total amount of induced loss is accounted for, through the introduction of weighting coefficients. Vulnerability and loss curves are then determined for all the three case study model configurations and compared to evaluate eventually present benefits due to the use seismic isolation. The last step is the computation of the expected annual loss (EAL), given by the area beneath the just obtained loss curve, selected as the governing performance metric which defines the suitability or not of the considered structural system. It is then checked if this loss is able to comply with the performance objectives initially defined according to the conceptual seismic design approach, by means of the comparison with the targeted value established in Section 4.2.1.

Firstly, suitable EDP-DV functions must be selected according to the geometrical and material properties of the examined configurations, given that building occupancy has been set as commercial office one. From (Ramirez, 2009), functions for low-rise (1 to 5 storeys), ductile RC perimeter moment resisting frames are chosen and reported in

Appendix E, referred to first, typical and roof floor, for three damageable components, namely structural drift sensitive, non-structural drift and acceleration sensitive, in all cases. As an example, the tabulated values and associated curves for the first floor case are shown in Figure 7.1:

EDP-DV Function Data



The EDP floor values, in terms of inter-storey drift ratio and peak floor acceleration, used to enter the above represented EDP-DV functions, for the considered building level and corresponding damageable component, are, for each IM, the mean ones, assuming a lognormal fitting, over the non-collapsing records among the total 40, constituting the whole ground motions set. They are obtained and discussed in section 5.2.2 and reported in Appendix D for further clarifications. Then, entering the corresponding curve, the expected floor losses, normalized by floor replacement cost, are derived for each damageable component. The provided results are discussed and compared for the three configurations showing similar trends with the corresponding EDPs, according to the selected IM level and considered building floor.

7.1. EXPECTED FLOOR LOSSES DISCUSSION

The IM level referred to a probability of exceedance of 10% in 50 years (reference period for the seismic action determined in Section 2.1), with corresponding 475-year return period, is considered and the mean EDP induced expected losses are evaluated and compared for the three case study model configurations, as shown in Figure 7.2 and Figure 7.3:

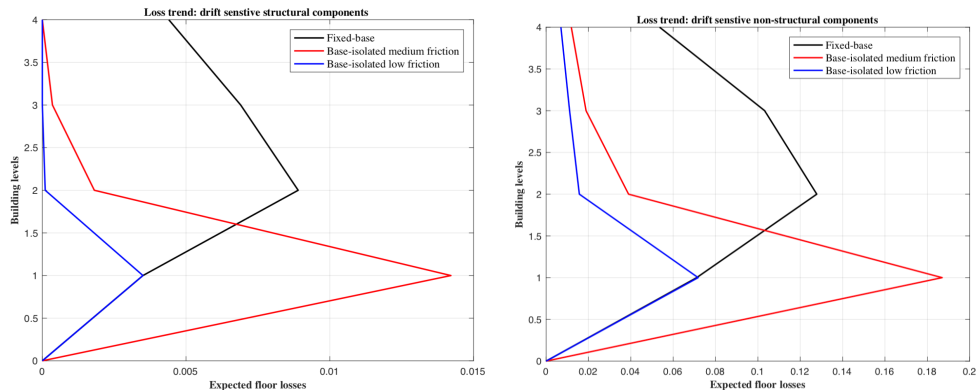


Figure 7.2: Drift sensitive structural (left) and non-structural (right) component expected floor losses, for 475-year return period IM level

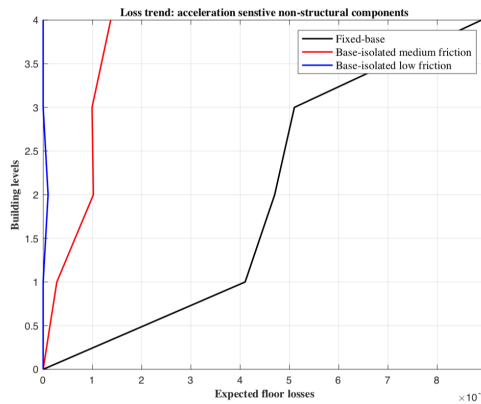


Figure 7.3: Acceleration sensitive non-structural components expected floor losses, for 475-year return period IM level

As pointed out in section 5.2.2, the first floor high drift for the base-isolated configuration, when medium friction pendulum bearings are used, results here in a significantly increase of the corresponding loss values, associated to structural and non-structural drift sensitive components, with respect to both fixed-base and low friction base-isolated case. This can be clearly observed by looking at Figure 7.2. Moreover, moving from medium to low friction devices, the first storey drift-related loss is reduced to a value practically equal to the fixed-base case, while for all the other levels, base isolation provides a significant reduction and, along the building height, the trend becomes more uniform and regular. On the other hand, in terms of acceleration sensitive non-structural losses, base isolation, in both of its configurations, is effective in reducing them along the entire building height, with respect to the fixed-base case, due to lower peak floor acceleration structural demands. In general, the first floor loss due to non-structural drift sensitive elements has the highest impact when summation is performed to obtain the total storey loss value. In particular, considering structural and non-structural elements, the same inter-storey drift value is used to enter the corresponding EDP-DV function, however completely different values of expected loss are obtained, namely much higher for the second component group, which thus results more damageable than the structural one, when subjected to the the same inter-storey drift seismic induced demand. This also denotes a higher first floor contribution, with respect to the others, when determining the total building loss. For the latter step, floor dependent weighting coefficients are established in order to “weight” the corresponding loss, when summed with the others, to determine the total one. Each building level has its own impact on the global amount. In the examined case-study configurations, these values are assumed to be equal to 0.3, 0.25 and 0.2, respectively for first, second and third floors, i.e. typical floors and lastly for the roof, showing compatibility also with the EDP-DV functions’ definition. In order to validate these observations, the comparison plot in

terms of total expected floor losses, i.e. summation of the three damageable component contributions, is shown in Figure 7.4:

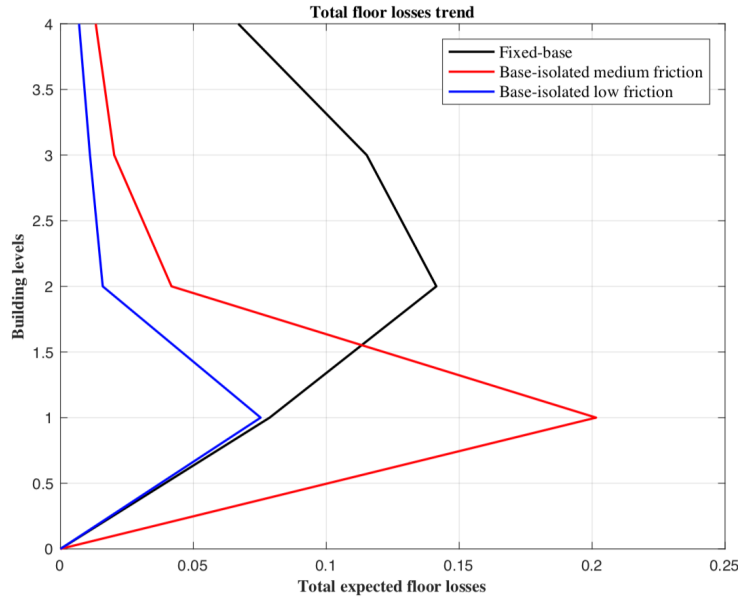


Figure 7.4: Total expected floor losses for 475-year return period IM level

The base-isolated case, with medium friction devices, provides a significantly higher first floor total expected loss with respect to the low friction counterpart, which is mainly due to the high contributions coming from non-structural drift sensitive component group, as specified before. The use of low friction devices represents hence a reasonable solution in order to mitigate the excessive first storey drift, resulting also in a first floor total loss lower than the fixed-base configuration. For all the other levels, seismic isolation is able to considerably reduce the total seismic induced losses, due to the relevant decrease outlined in terms of non-structural acceleration sensitive contribution.

Actually, for low IM levels, namely the ones associated to return periods up to 224 years, high losses at first floor are also present for the base-isolated solution when using low friction devices. This can be clearly observed in Figures from 7.5 to 7.7, which illustrates the results for a 50% probability of exceedance in 50 years, i.e. 72 years return period.

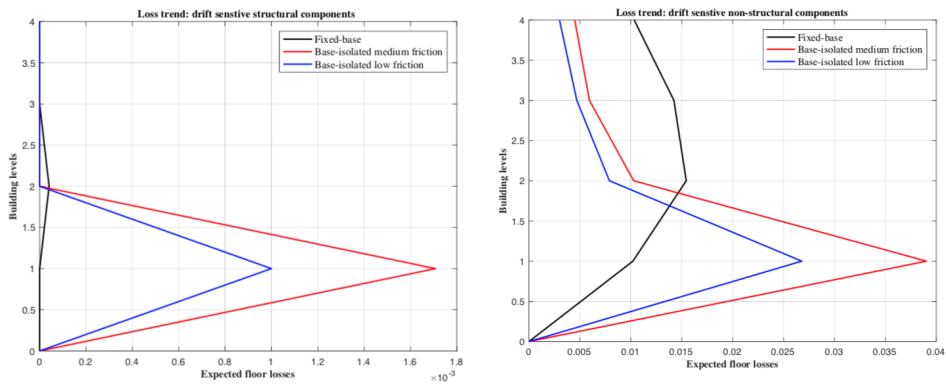


Figure 7.5: Drift sensitive structural (left) and non-structural (right) component expected floor losses, for 72-year return period IM level

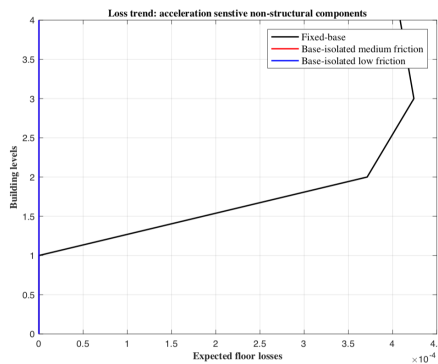


Figure 7.6: Acceleration sensitive non-structural components expected floor losses, for 72-year return period IM level

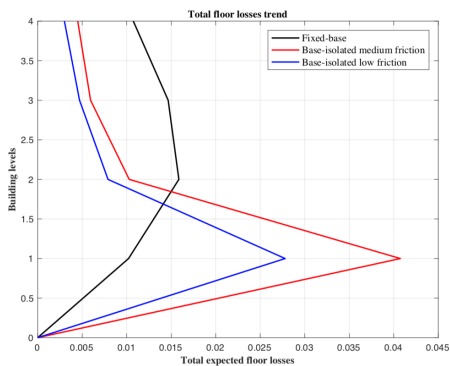


Figure 7.7: Total expected floor losses for 72-year return period IM level

In general, total floor expected losses, from Figure 7.7, and the ones associated with each damageable component, due to the reduced seismic demand, in terms of inter-storey drift ratios and peak floor accelerations, are lower than the the 475-year case (look at Figure 7.5 and Figure 7.6). However, it is possible to notice how the increase in first floor loss, associated to drift-sensitive structural and non-structural elements, is much more pronounced with respect to fixed-base case, for both base isolated solutions. The low friction one mitigates the problem a bit, although not enough to completely remove it, since a higher value is still present. Particularly, it is valid for structural element associated losses, which are almost equal to zero, for the fixed-base case, along building height. This has a great influence on the resulting total floor expected loss, mostly in terms of non-structural drift sensitive contribution which, due to high damageability of these elements, with respect to the structural ones, when subjected to the same seismic induced demand, provide much higher losses. As pointed out also in the case before, the use of base isolation strongly reduces the amount of losses due to non-structural acceleration sensitive components. Now, for both isolated cases, the corresponding losses over the entire building height are equal to 0, meaning that the presence of these elements does not affect the total amount of provided losses at each floor, due to ground shaking. For the fixed-base configuration, these values are not exactly equal to zero but still very low. Indeed, in general, with the reduction of ground shaking intensity, non-structural acceleration sensitive components will not have relevant influence on the seismic induced losses, due to a more pronounced decrease of acceleration demand and to the fact that these elements are less prone to provide damage and losses than drift sensitive ones, especially the non-structural ones.

With the increase of ground shaking intensity, the contribution of base isolation in reducing floor losses becomes more evident, particularly when low friction pendulum bearings are used rather than medium friction ones for which first floor problem, having higher losses due to drift sensitive components, remain present. As an example, the results provided by the 19975 years return period ground shaking are reported in Figures from 7.8 to 7.10:

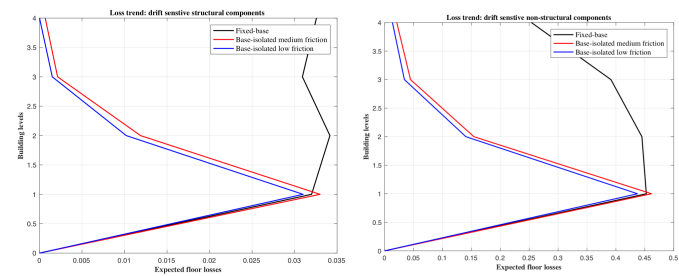


Figure 7.8: Drift sensitive structural (left) and non-structural (right) component expected floor losses, for 19975-year return period IM level

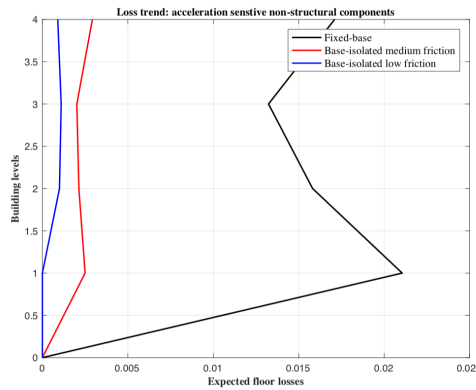


Figure 7.9: Acceleration sensitive non-structural components expected floor losses, for 19975-year return period IM level

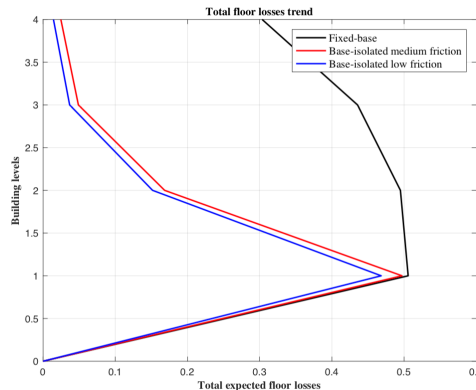


Figure 7.10: Total expected floor losses for 19975-year return period IM level

The first aspect to notice is how, using both base-isolated configurations, the total amount of floor expected losses, reported in Figure 7.10, is reduced along the entire building height, with respect to the fixed-base case. First floor reduction is present, even if not in a quite relevant way, also when medium friction devices are used, while at other levels it becomes more pronounced. This is mainly due to the strong reduction that base isolation provides in terms of peak floor acceleration demand and corresponding expected losses, associated to non-structural acceleration sensitive components. Figure 7.9 indicates how this can be quantified as more than 10%, balancing the still present higher first floor expected loss value due to drift sensitive components, with the use of

medium friction pendulum bearings (look at Figure 7.8). Furthermore, due to the larger inter-story drift demands with respect to lower ground shaking intensity cases, the structural and non-structural drift sensitive losses are still higher for the latter, but the overall difference is reduced. This means that, with the demand increase, the damageability is quite the same, while for low demands, it is much higher for non-structural components; this can also be seen by looking at the corresponding EDP-DV functions reported in Figure 7.1.

A summary of all the general observations is reported below. The comparison plots for the remaining IM levels are shown in Appendix F.

- the use of an isolation system, both with medium and low friction devices, leads to a clear reduction, with respect to fixed-base case, of acceleration sensitive non-structural components expected losses, over the entire building height, and for all IM levels. This is due to the induced seismic demand reduction, in terms of peak floor accelerations, and becomes more pronounced with the increase of ground shaking intensity. Indeed, for low levels, a decrease still can be detected, but also the fixed-base configuration provides very low values, which are close to zero;
- the large first floor inter-storey drift demands, when using base isolation system, reflects in an expected loss increase, at this level, related to drift sensitive components, both structural and non-structural. When medium friction devices are employed, this remains present for all IM levels, and it is particularly evident for the mid and low ones associated, respectively 475, 975 and 2475 years and 22, 42, 72, 140 and 224 years return periods. As an example, in the first mentioned case, the expected losses due to structural and non-structural components, from Figure 7.2, are almost three times larger than the ones provided by fixed-base and base-isolated one, when using low friction pendulum bearings. This starts reducing gradually with the increase of ground shaking, however, also for the highest ones (i.e. 19975, 9975 and 4975 years return period) it is still a bit higher;
- the use of low friction pendulum bearings is thus a promising alternative to address this issue, leading to a better seismic performance, especially for mid-level ground shakings, namely given by 475, 975 and 2475 years return period. In these cases, first floor losses due to drift sensitive components are much lower than the ones provided by the use of medium friction devices, but also reduced with respect to the fixed-base ones. For the highest IM levels (i.e. 19975, 9975 and 4975 years return period) a reduction is still present but not so much pronounced. However, the problem remains unsolved for the lowest ones, i.e. 22, 42, 72, 140 and also 224 years return period; for the first three ones the difference is higher but the provided loss values are not so much relevant, also

for the fixed-base case while, for the remaining, values closer to the fixed-base solution are provided;

- in general, non-structural drift sensitive components, when employing the representative EDP-DV functions, result more damageable, for the same inter-storey drift induced demand, than structural ones. This is particularly evident for low levels of ground shaking whereas reduced difference in expected losses is observed for higher IM levels in which the damageability becomes quite the same, but still larger for non-structural elements;
- looking at the total floor expected loss comparison, it is possible to notice how, in general, drift sensitive contributions lead to higher loss at first floor if compared to the fixed-base one, particularly when medium friction devices are employed in the base-isolated case. This increase is present also with low friction pendulum bearings for the low levels of ground shaking while it becomes a reduction for the remaining ones, also with respect to fixed-base configuration. However, for three cases of high intensity measure level, associated to the 19975, 9975 and 4975 years return periods, also using medium friction isolators leads to first floor total expected loss reduction, albeit low. This is due to the benefits coming from the clear decrease in the demand on the non-structural acceleration sensitive components, over the entire building height, when base isolation is used.

Following this discussion, the above defined weighting coefficients, namely 0.3, 0.25 and 0.2, respectively for first, second and third floors, i.e. typical floors and lastly for the roof, are used multiplying the corresponding loss, and are summed in order to obtain a total building expected loss value, normalized by the storey replacement value, for the selected IM level. The obtained results for each case study model configuration are reported in Figures 7.11 to 7.13:

Tr [yrs]	22	42	72	140	224	475	975	2475	4975	9975	19975
EL	0.0031	0.0077	0.0128	0.0277	0.0457	0.1011	0.1656	0.2760	0.3519	0.4186	0.4450

Figure 7.11: Total building expected losses for the fixed base configuration

Tr [yrs]	22	42	72	140	224	475	975	2475	4975	9975	19975
EL	0.0042	0.0086	0.0172	0.0353	0.0532	0.0786	0.1044	0.1476	0.1702	0.1989	0.2084

Figure 7.12: Total building expected losses for the base isolated configuration, using medium friction pendulum bearings

Tr [yrs]	22	42	72	140	224	475	975	2475	4975	9975	19975
EL	0.0040	0.0073	0.0121	0.0192	0.0239	0.0307	0.0473	0.0800	0.1431	0.1764	0.2014

Figure 7.13: Total building expected losses for the base isolated configuration, using low friction pendulum bearings

The corresponding vulnerability curves, representing the total building expected loss versus the increasing level of ground shaking IM level are provided and compared for the three different case study model configurations, as shown in Figure 7.14:

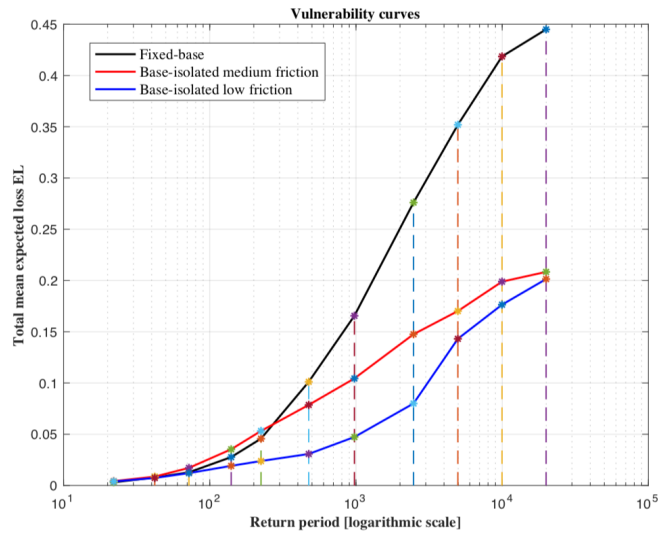


Figure 7.14: Vulnerability curves comparison for the three case-study model configurations

The analysis of the vulnerability curves comparison together with the results presented before enables the evaluation of the effectiveness of the base isolation system introduction, in order to improve case study building seismic performance. The following are the most important considerations that can be made:

- the use of medium friction pendulum bearings provides higher total expected building losses, with respect to the fixed-base configuration, for return periods from 22 to 224 years, showing how the presence of significantly larger first floor drift sensitive, structural and non-structural losses, has a great impact on the overall structural seismic performance, especially for the lowest IM levels. On the other hand, for the remaining return periods, corresponding to more severe ground shaking intensity, a clear reduction can be observed, sometimes resulting in a half of the provided total loss by the fixed-base solution;
- the alternative solution of low friction devices provides a higher total expected building loss only for the first return period value, while for all the others a significant reduction is present, becoming more and more pronounced with the increase of the IM level. This demonstrates the clear improvement that can be achieved, in terms of global structural seismic performance, when this solution is employed, not only with respect to the fixed-base configuration but also to

the one where medium friction isolators are introduced. However, this improvement, with respect to the latter, tends to saturate for the highest return periods meaning that the total expected building losses are quite similar;

- a final consideration that can be made is on how the medium and low levels of ground shaking are the ones that mostly create issues when medium friction pendulum bearings are used, not leading to an improvement in the global seismic performance. On the other hand, they behave well under more severe IM levels, showing their effectiveness. Actually, this represents an aspect deserving future research, related to the great impact that the friction coefficient variation has on the global structural response and seismic performance evaluated through loss estimation procedures.

7.2. LOSS CURVES AND EAL DEFINITION

The final step of the presented work consists of determining the loss curves for the three case-study building configurations, i.e. the curves showing the present trend between total building expected loss normalized by replacement value, and mean annual probability of exceeding a defined ground motion intensity. In order to obtain this parameter, the Poisson process assumption for modelling the seismic hazard and its occurrence comes into play. Having the probability of exceeding a certain IM level in a given time window, i.e. 50 years, the corresponding mean annual frequency of exceedance, namely the Poisson process mean rate, is determined with the following expression:

$$\lambda = - \left(\frac{\ln(1 - poE)}{T} \right) \quad (7.1)$$

where:

poE is the probability of exceedance of a certain IM level in the reference period T , equal to 50 years;

λ is the corresponding mean annual frequency of exceeding the considered IM level.

Once this has been determined, the associated annual probability of exceedance, which is the parameter actually present in the loss curves, is obtained using the Poisson process relationship, as follows:

$$poE_a = 1 - e^{-(\lambda t)} \quad (7.2)$$

where:

t is the considered time window, now equal to 1 year, since the annual probability of exceedance, poE_a , has to be computed.

The resulting loss curves are shown in Figure 7.15:

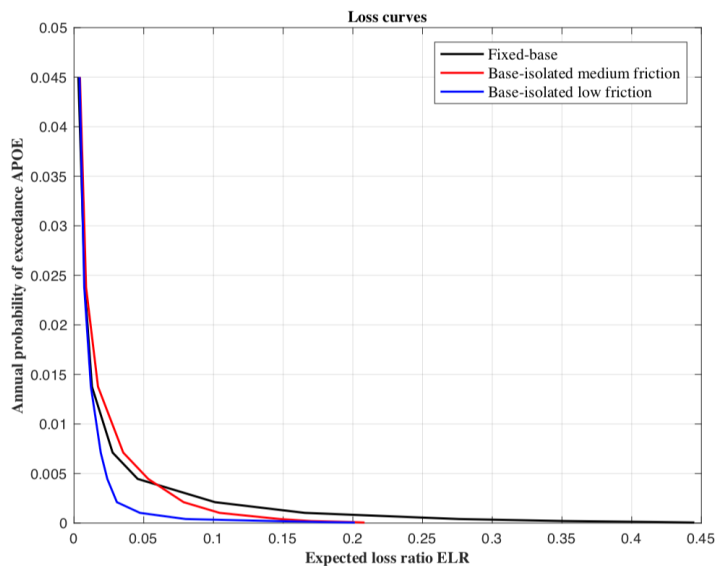


Figure 7.15: Loss curves comparison for the three case-study model configurations

Using these curves, the seismic performance metric the expected annual loss (EAL) can be determined for the three case study model configurations, as the area beneath the corresponding loss curve, evaluated using the trapezoidal rule of integration. The results obtained were:

- $EAL_{FB} = 0.1051\%$, for the fixed-base system;
- $EAL_{BI,mf} = 0.0961\%$, for the base-isolated system, using medium friction pendulum bearings;
- $EAL_{BI,lf} = 0.0582\%$, for the base-isolated system, using low friction pendulum bearings;

These values must be checked with the expected annual loss threshold (0.07%), outlined in Section 4.2.1, in order to verify if the considered structural system is able to validate the conclusions driven by the conceptual seismic design approach, according to which base isolation was preliminary selected as the recommended and feasible structural solution to comply with the serviceability limit state performance objectives.

The EAL results indicate how the fixed-base structural system provides an expected annual loss that clearly exceeds the imposed threshold, meaning that the conceptual seismic design conclusions are validated: it was not possible to design a traditional fixed-base structural system able to comply with the set up performance objectives at the serviceability limit state since, as pointed out in Section 4.2.2, there is no feasible initial period range and corresponding space of possible solutions compatible with the design response spectrum in the ADRS format.

On the other hand, this can be achieved for the base-isolated configuration using friction pendulum bearings whose effect, in terms of the serviceability limit state considerations, was to reduce the design response spectrum, obtaining an “overdamped” one. In order to demonstrate this conclusion, two different isolation systems, using medium and low friction devices, were designed according to NTC18 requirements and their seismic performance assessed through non-linear response history analysis and losses estimation procedure. At the end, comparing the provided expected loss values with the targeted one, it is possible to understand how, even if it is an *a priori* feasible solution, the one characterized by the medium friction pendulum bearings is not able to fulfil the defined performance requirements. The isolators efficiency is not enough to decrease the induced EAL to a value lower than the defined threshold. Low friction pendulum bearings, instead, are able to improve global structural response and seismic performance coming up with a final expected annual loss value much lower than the medium friction and fixed base case ones, which respects the defined threshold equal to 0.07%. In parallel, this also validates the conceptual seismic design initial conclusion, according to which a feasible period range and solutions’ space exist if base isolation is employed, showing how CSD can be used as a qualitative method for the choice of the structural typology to be used if loss-based performance requirements are to be satisfied.



8. CONCLUSIONS AND FUTURE DEVELOPMENTS

The presented thesis research focused on the improvement, in terms of expected annual loss (EAL), that seismic isolation provides to a reinforced concrete (RC) frame's structural performance when subjected to earthquake action; the considered case study model was a bi-dimensional RC moment resisting frame located at L'Aquila, chosen as one of the most seismic-prone sites in Italy. A conceptual seismic design (CSD) approach was used within the framework of performance-based earthquake engineering (PBEE) in order to support the choice for seismic isolation, showing how it is a feasible and recommended design solution, as opposed to a fixed-base structure. Friction pendulum bearing (FPB) isolators were employed in two different configurations: (i) medium friction and (ii) low friction devices, selected from an Italian manufacturer's catalogue, following a vertical capacity versus demand comparison criterion, being still at a preliminary design step.

To do this, performance objectives that drive the seismic design were set in terms of expected loss ratios, associated with three different limit states, corresponding to three ground motion return periods, and target EAL, equal to 0.07%, not to be exceeded. Pre-defined EDP-DV functions were used to determine the structural EDPs corresponding to the serviceability limit state (SLS) expected loss ratios associated to each damageable component assumed to be present in all building levels, namely structural drift sensitive, non-structural drift sensitive and acceleration sensitive ones. Minimum peak inter-storey drift and peak floor acceleration were the SLS design parameters to be converted into spectral values, used to enter the design response spectrum in the ADRS format verifying if a feasible initial period range and corresponding space of feasible solutions exists or not, for the selected structural system. Each of these considerations do not depend on the chosen configuration; as the same SLS design parameters were defined. For the fixed-base traditional solution this could not be verified, while for both base-isolated configurations a feasible period range with corresponding solutions' space was qualitatively determined given the spectral reduction provided by the isolators. This means that only the latter solution was theoretically able to comply with the defined performance objectives.

In order to validate these pre-design conclusions, both fixed-base and base-isolated, with medium and low friction pendulum bearings, configurations were designed for L'Aquila seismic hazard in agreement with the respectively present NTC18 requirements. Their

structural response was evaluated through NRHA using 11 sets of 40 records each, associated with increasing IM levels. Mean floor EDPs, over only the non-collapsing records, in terms of peak inter-storey drift ratios and peak floor accelerations, were used as input in the pre-defined EDP-DV functions to estimate seismic induced expected economic floor losses for each damageable component group. Summing them over the entire building height, a total expected loss was determined for each IM level. Seismic performance was evaluated through the comparison of vulnerability curves between fixed-base and base-isolated cases, focusing also on the impact that friction coefficient variation, from low to medium friction devices, has on structural response. Moreover, loss curves and associated EAL, defined as the governing performance metric, were determined. This demonstrated how the use of a base-isolated structural solution, with low friction pendulum bearings, leads to the fulfilment of the above defined performance objectives, i.e. having an EAL below the imposed target, while the fixed-base one does not, confirming what was anticipated by the CSD approach.

In terms of future developments within this framework, following the obtained conclusions, there are two main aspects on which future research could focus:

- the first addresses the use of the CSD approach for base-isolated structures. In this work it has been employed mainly in a qualitative way as a discriminant method between feasible and unfeasible structural solutions, with respect to the fulfilment of defined performance objectives (in this case in terms of EAL at SLS, though still in a preliminary stage of the seismic design). This results in a qualitative definition of a feasible period range and corresponding feasible solutions' space, compatible with the overdamped design response spectrum in the ADRS format. A practical quantification at this stage is still absent for base-isolated structures, reason for which research may be developed to obtain an actual initial period range within which the base-isolated fundamental structural one must fall. Moreover, this can pave the way also to ultimate limit state (ULS) considerations, already developed for fixed-base systems, for base-isolated structures, so that a corresponding feasible backbone curve, complying with additional defined performance requirements at ULS, can be determined. This would fully extend the CSD framework to base-isolated systems, providing, according to the basic idea of this approach, a conceptual and not detailed seismic design, in terms of the basic geometrical frame dimensions;
- the second refers to the influence friction coefficient variation has on structural response. Initially, it was thought that, in general, the use of an isolation system would lead to a substantial improvement of the structural response and seismic performance, with a consequent reduction of seismic induced expected floor losses. On the contrary, this work has shown how medium friction pendulum bearings were not necessarily able to ensure this anticipated improvement due to

the fact that they do not have enough effectiveness to reduce the provide EAL below the targeted value. Some further design optimisation may have been performed but this demonstrates how experience in this direction is required for the use of base isolation in seismic design. Moreover, a certain trade-off between structural improvement and realization costs, that are usually higher with respect to a traditional fixed-base system, must be accounted for. Only with the use of low friction devices, SLS performance objectives are met, due to the clear reduction in both seismic demands and induced losses with respect to the medium friction case. Further research and studies may focus on this topic in order to better understand how structural response metrics vary with friction coefficient when a base-isolated system, using friction pendulum bearings, is designed.

Finally, following the idea of PBEE, CSD is employed as a validation instrument, for the selected structural system to be designed, focusing on different metrics, used to evaluate seismic performance, and performance objectives that must be met. These are expressed in terms of expected loss ratio and expected annual loss rather than the typically employed engineering demand parameters, such as inter-story drift ratios or peak floor accelerations, able to “communicate” not only with engineers and designers but also with society and general decision-makers, who may be more interested in economic losses when trying to assess structural seismic performance. In this sense, a further development comes into play looking not only at direct economic losses but also at indirect ones, such as downtime, to be incorporated in this framework through a more refined expected loss ratio definition at each limit state. This will be a function of the considered building, its occupancy and mostly its important and relevance in the society, which influence the nominal life with respect to which it should be designed. Research on methods able to suitably estimate them, with the increase of structural damage under earthquake action, can be performed.



REFERENCES

2007 RS Means Square Foot Costs [Book] / auth. Balboni B.. - Kingston, MA : [s.n.], 2007.

A Model Code for the Displacement-Based Seismic Design of Structures [Book] / auth. T.J. Sullivan M.J.N. Priestley, G.M. Calvi. - 2012.

An Ounce of Prevention: Probabilistic Loss Estimation for Performance-based Earthquake Engineering [Report] / auth. Mitrani-Reiser J. and Beck, J. / Department of Civil Engineering and Applied Mechanics ; California Institute of Technology. - 2007.

Assembly-based vulnerability of buildings and its uses in seismic performance evaluation and risk management decision-making [Report] : Technical Report No. 309 / auth. Porter K.A., and Kiremidjian, A.S. / John A. Blume Earthquake Engineering Center, Standford University. - Standford, CA : [s.n.], 2001.

Assessing Seismic Collapse Safety of Modern Reinforced Concrete Frame Buildings [Journal] / auth. Haselton C.B., and Deierlein, G. G., // PEER Report. - 2007.

Building-specific Earthquake Damage Estimation [Report] : Ph.D. Thesis / auth. Gunturi S. and Shah H. / John A. Blume Earthquake Engineering Center, Standford University. - Standford, CA : [s.n.], 1993.

Building-Specific Loss Estimation Methods & Tools for Simplified Performance-Based Earthquake Engineering [Report] / auth. Ramirez C.M., and Miranda, E. / Departement of Civil and Environmental Engineering ; Standford University. - 2009.

Calibration of Model to Simulate Response of Reinforced Concrete Beam-Columns to Collapse [Journal] / auth. Curt B. Haselton Abbie B. Liel, Sarah C. Taylor-Lange, and Gregory G. Deierlein // ACI Structural Journal . - 2016.

Conceptual seismic design in performance-based earthquake engineering. [Journal] / auth. O'Reilly GJ Calci GM. // Earthquake Engng Struct Dyn.. - 2019. - pp. 48-389-411.

Conditional Mean Spectrum: Tool for ground motion selection [Journal] / auth. Baker J.W. // Journal of Structural Engineering. - 2011.

Development of Damage Functions for High-rise Building Components [Report] / auth. Kutsu O., Miller, D.D., and Brokken, S.T. / John A. Blume & Associates. - San Francisco, CA : [s.n.], 1982.

Existing buildings: The New Italian Provisions for Probabilistic Seismic Assessment. [Journal] / auth. Pinto PE Franchin P. // Ansal A, ed. Perspectives on European Earthquake Engineering and Seismology. - 2014.

Hysteretic Models that Incorporate Strength and Stiffness Deterioration [Journal] / auth. Ibarra L. F., Medina R. A. and and Krawinkler H. // Earthquake Engineering & Structural Dynamics. - 2005.

Mechanistic seismic damage model for reinforced concrete [Journal] / auth. Park Y.J., and Ang, A.H.S. // ASCE Journal of Structural Engineering. - 1985.

Northridge earthquake of January 17, 1994 [Report] / auth. Hall J.F. / Earthquake Engineering Research Institute. - 1995.

Performance-Based Earthquake Engineering [Book Section] / auth. Krawinkler H. and Miranda, E. // Earthquake Engineering: From Engineering Seismology to Performance-Based Engineering / book auth. Bertero Y. Borzognia and V.. - [s.l.] : CRC Press, 2004.

Probabilistic basis for 2000 SAC Federal Emergency Management Agency steel moment frame guidelines. [Journal] / auth. Cornell CA Jalayer F, Hamburger RO, Foutch DA. // Journal of Structural Engineering.. - 2002.

Probabilistic Earthquake Loss Estimation and Loss Disaggregation in Buildings [Report] : Report No. 157 / auth. Aslani H. and Miranda, E. / John A. Blume Earthquake Engineering Center, Standford University. - 2005.

Progress and challenges in seismic performance assessment [Journal] / auth. Cornell CA Krawinkler H. // PEER Center News. - 2000.

Seismic Damage Assessment for High-rise Building [Report] / auth. Scholl R.E., Kustu, O., Perry, C.L., and Zanetti, J.M. / John A. Blume & Associates. - San Francisco, CA : [s.n.], 1982.

Seismic Design of Reinforced Concrete and Masonry Buildings [Book] / auth. T. Paulay M.J.N. Priestley. - 1992.



UNIVERSITÀ
DI PAVIA



APPENDIX A

This Appendix contains the beam and column demands, in terms of bending moment (M), shear (V) and axial force (N), due to distributed gravity loads and lateral forces together with their seismic combination. The maximum values used in the design are bold.

Beam demands are reported for each floor level, from the first to the roof, respectively in terms of bending moment, shear and axial force.

Beam 5111-5211-5311		From left support to right one								
Load		Ma [kNm]	Mb [kNm]	Mc [kNm]	Md [kNm]	Me [kNm]	Mf [kNm]	Mg [kNm]	Mh [kNm]	Mi [kNm]
Floor (G and Q combined)		-130.7	77.1	-147.3	-144.1	71.9	-144.1	-147.3	77.1	-130.7
Seismic (Lateral forces)		585.7	0.2	-584.2	592.1	1.2	-591.1	579.3	0.6	-578.6
Seismic combination		455	77.3	-731.5	448	73.1	-735.2	432	77.7	-709.3

Beam 5112-5212-5312		From left support to right one								
Load		Ma [kNm]	Mb [kNm]	Mc [kNm]	Md [kNm]	Me [kNm]	Mf [kNm]	Mg [kNm]	Mh [kNm]	Mi [kNm]
Floor (G and Q combined)		-138.7	75.9	-141.6	-143.9	72.1	-143.9	-141.6	75.9	-138.7
Seismic (Lateral forces)		578.1	0.9	-576.6	590.7	-0.4	-589.9	572.5	0.2	-572.2
Seismic combination		439.4	76.8	-718.2	446.8	71.7	-733.8	430.9	76.1	-710.9

Beam 5113-5213-5313		From left support to right one								
Load		Ma [kNm]	Mb [kNm]	Mc [kNm]	Md [kNm]	Me [kNm]	Mf [kNm]	Mg [kNm]	Mh [kNm]	Mi [kNm]
Floor (G and Q combined)		-142.9	75.2	-138.7	-143.6	72.4	-143.6	-138.7	75.2	-142.9
Seismic (Lateral forces)		418.7	1.1	-417.5	435.3	1	-434.7	414.6	0	-414.5
Seismic combination		275.8	76.3	-556.2	291.7	73.4	-578.3	275.9	75.2	-557.4

Beam 5114-5214-5314		From left support to right one								
Load		Ma [kNm]	Mb [kNm]	Mc [kNm]	Md [kNm]	Me [kNm]	Mf [kNm]	Mg [kNm]	Mh [kNm]	Mi [kNm]
Floor (G and Q combined)		-106.6	71.5	-128.8	-125.8	63.2	-125.8	-128.8	71.5	-106.6
Seismic (Lateral forces)		236.2	0.6	-234.8	253.7	0.1	-253.4	233.6	-0.5	-234.4
Seismic combination		129.6	72.1	-363.6	127.9	63.3	-379.2	104.8	71	-341

Beam 5111-5211-5311	Va [kN]	Vc [kN]	Vd [kN]	Vf [kN]	Vg [kN]	Vi [kN]
Load						
Floor (G and Q combined)	141.2	-146.8	144	-144	146.8	-141.2
Seismic (Lateral forces)	-195	-195	-197.2	-197.2	-193	-193
Seismic combination	-53.8	-341.8	-53.2	-341.2	-46.2	-334.2

Beam 5112-5212-5312	Va [kN]	Vc [kN]	Vd [kN]	Vf [kN]	Vg [kN]	Vi [kN]
Load						
Floor (G and Q combined)	143.5	-144.5	144	-144	144.5	-143.5
Seismic (Lateral forces)	-192.4	-192.4	-196.8	-196.8	-190.8	-190.8
Seismic combination	-48.9	-336.9	-52.8	-340.8	-46.3	-334.3

Beam 5113-5213-5313	Va [kN]	Vc [kN]	Vd [kN]	Vf [kN]	Vg [kN]	Vi [kN]
Load						
Floor (G and Q combined)	144.7	-143.3	144	-144	143.3	-144.7
Seismic (Lateral forces)	-139.4	-139.4	-145	-145	-138.2	-138.2
Seismic combination	5.3	-282.7	-1	-289	5.1	-282.9

Beam 5114-5214-5314	Va [kN]	Vc [kN]	Vd [kN]	Vf [kN]	Vg [kN]	Vi [kN]
Load						
Floor (G and Q combined)	122.3	-129.7	126	-126	129.7	-122.3
Seismic (Lateral forces)	-78.5	-78.5	-84.5	-84.5	-78	-78
Seismic combination	43.8	-208.2	41.5	-210.5	51.7	-200.3

Beam 5111-5211-5311	Positive axial load --> tension					
Load	Na [kN]	Nc [kN]	Nd [kN]	Nf [kN]	Ng [kN]	Ni [kN]
Floor (G and Q combined)	18.3	18.3	16.6	16.6	18.3	18.3
Seismic (Lateral forces)	-116.2	-116.2	-68.1	-68.1	-22.2	-22.2
Seismic combination	-97.9	-97.9	-51.5	-51.5	-3.9	-3.9

Beam 5112-5212-5312						
Load	Na [kN]	Nc [kN]	Nd [kN]	Nf [kN]	Ng [kN]	Ni [kN]
Floor (G and Q combined)	-3.3	-3.3	0.8	0.8	-3.3	-3.3
Seismic (Lateral forces)	-224.2	-224.2	-135.2	-135.2	-45.2	-45.2
Seismic combination	-227.5	-227.5	-134.4	-134.4	-48.5	-48.5

Beam 5113-5213-5313						
Load	Na [kN]	Nc [kN]	Nd [kN]	Nf [kN]	Ng [kN]	Ni [kN]
Floor (G and Q combined)	12.6	12.6	8.7	8.7	12.6	12.6
Seismic (Lateral forces)	-326.8	-326.8	-195.5	-195.5	-65.6	-65.6
Seismic combination	-314.2	-314.2	-186.8	-186.8	-53	-53

Beam 5114-5214-5314						
Load	Na [kN]	Nc [kN]	Nd [kN]	Nf [kN]	Ng [kN]	Ni [kN]
Floor (G and Q combined)	-46	-46	-44.9	-44.9	-46	-46
Seismic (Lateral forces)	-381.7	-381.7	-227.6	-227.6	-73.8	-73.8
Seismic combination	-427.7	-427.7	-272.5	-272.5	-119.8	-119.8

Column demands are reported for each floor, from the first to the roof, respectively for lateral and central columns.

Column 7111				
Load	Ma [kNm]	Mb [kNm]	V [kN]	N [kN]
Floor(G and Q combined)	28.5	-54.2	-18.4	-551.7
Seismic (Lateral forces)	-734.7	215.5	211.2	605.3
Seismic combination	-706.2	161.3	192.8	53.6

Column 7411				
Load	Ma [kNm]	Mb [kNm]	V [kN]	N [kN]
Floor(G and Q combined)	-28.5	54.2	18.4	-551.7
Seismic (Lateral forces)	-720.6	209.5	206.7	-600
Seismic combination	-749.1	263.7	225.1	-1151.7

Column 7211				
Load	Ma [kNm]	Mb [kNm]	V [kN]	N [kN]
Floor(G and Q combined)	1	-0.3	-0.3	-1122.3
Seismic (Lateral forces)	-1474.6	427.9	422.8	18.2
Seismic combination	-1473.6	427.6	422.5	-1104.1

Column 7311				
Load	Ma [kNm]	Mb [kNm]	V [kN]	N [kN]
Floor(G and Q combined)	1	-0.3	0.3	-1122.3
Seismic (Lateral forces)	-1465	423.6	419.7	-23.5
Seismic combination	-1464	423.3	420	-1145.8

Column 7112				
Load	Ma [kNm]	Mb [kNm]	V [kN]	N [kN]
Floor(G and Q combined)	76.5	-70.4	-36.7	-410.5
Seismic (Lateral forces)	-370.2	371.2	185.3	410.3
Seismic combination	-293.7	300.8	148.6	-0.2

Column 7412				
Load	Ma [kNm]	Mb [kNm]	V [kN]	N [kN]
Floor(G and Q combined)	-76.5	70.4	36.7	-410.5
Seismic (Lateral forces)	-369.2	368.8	184.5	-407
Seismic combination	-445.7	439.2	221.2	-817.5

Column 7212				
Load	Ma [kNm]	Mb [kNm]	V [kN]	N [kN]
Floor(G and Q combined)	-3.5	2.2	1.4	-831.5
Seismic (Lateral forces)	-748.4	750.5	374.7	16
Seismic combination	-751.9	752.7	376.1	-815.5

Column 7312				
Load	Ma [kNm]	Mb [kNm]	V [kN]	N [kN]
Floor(G and Q combined)	3.5	-2.2	-1.4	-831.5
Seismic (Lateral forces)	-746.8	748.1	373.7	-19.3
Seismic combination	-743.3	745.9	372.3	-850.8

Column 7113				
Load	Ma [kNm]	Mb [kNm]	V [kN]	N [kN]
Floor(G and Q combined)	68.2	-65.4	-33.4	-267
Seismic (Lateral forces)	-206.9	359.4	141.6	217.9
Seismic combination	-138.7	294	108.2	-49.1

Column 7413				
Load	Ma [kNm]	Mb [kNm]	V [kN]	N [kN]
Floor(G and Q combined)	-68.2	65.4	33.4	-267
Seismic (Lateral forces)	-203.3	353.9	139.3	-216.2
Seismic combination	-271.5	419.3	172.7	-483.2

Column 7213				
Load	Ma [kNm]	Mb [kNm]	V [kN]	N [kN]
Floor(G and Q combined)	4.4	-6.4	-2.7	-543
Seismic (Lateral forces)	-416.8	724.9	285.4	11.6
Seismic combination	-412.4	718.5	282.7	-531.4

Column 7313				
Load	Ma [kNm]	Mb [kNm]	V [kN]	N [kN]
Floor(G and Q combined)	-4.4	6.4	2.7	-543
Seismic (Lateral forces)	-414.2	720.9	283.8	-13.3
Seismic combination	-418.6	727.3	286.5	-556.3

Column 7114				
Load	Ma [kNm]	Mb [kNm]	V [kN]	N [kN]
Floor(G and Q combined)	77.5	-106.6	-46	-122.3
Seismic (Lateral forces)	-59.3	236.2	73.9	78.5
Seismic combination	18.2	129.6	27.9	-43.8

Column 7414				
Load	Ma [kNm]	Mb [kNm]	V [kN]	N [kN]
Floor(G and Q combined)	-77.5	106.6	46	-122.3
Seismic (Lateral forces)	-60.6	234.4	73.8	-78
Seismic combination	-138.1	341	119.8	-200.3

Column 7214				
Load	Ma [kNm]	Mb [kNm]	V [kN]	N [kN]
Floor(G and Q combined)	-1.5	3	1.1	-255.7
Seismic (Lateral forces)	-128	488.5	154.1	6
Seismic combination	-129.5	491.5	155.2	-249.7

Column 7314				
Load	Ma [kNm]	Mb [kNm]	V [kN]	N [kN]
Floor(G and Q combined)	1.5	-3	-1.1	-255.7
Seismic (Lateral forces)	-128.4	487	153.9	-6.5
Seismic combination	-126.9	484	152.8	-262.2



UNIVERSITÀ
DI PAVIA



APPENDIX B

This Appendix contains the most relevant properties of the designed beam and column cross sections.

	b [mm]	h [mm]	Asb [mm ²]	ρ_b [/]	Ast [mm ²]	ρ_t [/]	NTC18 7.4.6.2.1	MRd+ [kNm]	MRd- [kNm]	Mcap [kNm]
1st floor	812.8	609.6	10 ϕ 24	0.0091	10 ϕ 24	0.0091	OK	792.66	807.02	1063.4
2nd floor	812.8	609.6	10 ϕ 24	0.0091	10 ϕ 24	0.0091	OK	781.27	781.27	1063.4
3rd floor	812.8	609.6	8 ϕ 24	0.0073	8 ϕ 24	0.0073	OK	600.21	600.21	856.9
Top floor	812.8	609.6	6 ϕ 24	0.0055	6 ϕ 24	0.0055	OK	357.55	408.28	651.3

	Lp [m]	Lc [m]	γ_{Rd}	Vfloor [kN]	VEd [kN]	Asw [mm ²]	s [mm]	$\rho_{sh,r}$ [/]	VRd [kN]
1st floor	0.4584	5.0831	1.1	121.92	465.2	6 ϕ 10	125	0.0046	1499.3
2nd floor	0.4584	5.0831	1.1	121.92	460.27	6 ϕ 10	125	0.0046	1499.3
3rd floor	0.4584	5.0831	1.1	121.92	381.85	4 ϕ 10	125	0.0031	1134.4
Top floor	0.4584	5.0831	1.1	106.68	261.52	4 ϕ 10	125	0.0031	1134.4

	b [mm]	h [mm]	ν_{Ed} [/]	ν_{lim} [/]	μ_{Ed} [/]	ω [/]	As [mm ²]	ρ [/]	NTC18 7.4.6.2.2	Mcap [kNm]
1st L	812.8	762	0.068	0.65	0.058	0.1	16 ϕ 24	0.0117	OK	1337.1
1st C	812.8	965.2	0.0534	0.65	0.0712	0.13	18 ϕ 24	0.0104	OK	2210.3
2nd L	812.8	762	0.0483	0.65	0.0345	0.1	16 ϕ 24	0.0117	OK	1279.1
2nd C	812.8	965.2	0.0397	0.65	0.0363	0.1	18 ϕ 24	0.01	OK	2005.4
3rd L	812.8	762	Reinforcement ratios set equal to 0.01 to comply with NTC18 requirement. The amount of reinforcement As is determined from				16 ϕ 24	0.01	OK	1074.4
3rd C	812.8	965.2					18 ϕ 24	0.01	OK	1874.2
Top L	812.8	762					16 ϕ 24	0.01	OK	1017.7
Top C	812.8	965.2					18 ϕ 24	0.01	OK	1733.9

	γ_{Rd}	Lp [m]	Lc [m]	VEd [kN]	Asw [mm ²]	s [mm]	$\rho_{sh,r}$ [/]	VRd [kN]	
1st L	1.1	0.40	3.70	866.57	5 ϕ 10	75	0.0064	2664.4	
1st C	1.1	0.40	3.70	1432.5	7 ϕ 10	75	0.009	3855.9	
2nd L	1.1	0.38	3.24	866.57	5 ϕ 10	75	0.0064	2664.4	
2nd C	1.1	0.38	3.24	1432.5	7 ϕ 10	75	0.009	3855.9	
3rd L	1.1	0.38	3.24	795.08	4 ϕ 10	75	0.0052	1989.3	
3rd C	1.1	0.38	3.24	1387	6 ϕ 10	75	0.0077	2944.2	
Top L	1.1	0.38	3.24	795.08	4 ϕ 10	75	0.0052	1989.3	
Top C	1.1	0.38	3.24	1387	6 ϕ 10	75	0.0077	2944.2	

Column cross sections are designed for acting shear VEd, determined from the maximum moment capacity over two floor levels, differently for lateral and central columns. 1st & 2nd, 3rd & Top lateral and central are the possible shear design configurations.



APPENDIX C

In this Appendix are reported the 7 ground motion records, for each NTC18 limit state, used to check the friction pendulum bearings design.

Operational limit state (SLO) ground motions set:

SLO	Earthquake Name	Date	Mw	Fault Mechanism	Epicentral Distance [km]	EC8 Site class
	Umbria Marche	26/09/1997	6	normal	22	C
	Basso Tirreno	15/04/1978	6	oblique	18	C
	Ano Liosia	07/09/1999	6	normal	19	C
	Friuli (aftershock)	15/09/1976	6	thrust	11	C
	Umbria Marche	26/09/1997	6	normal	27	C
	Dinar	01/10/1995	6.4	normal	8	C
	Alkion	25/02/1981	6.3	normal	25	C
Mean			6.1		18.57143	

Damage limit state (SLD) ground motions set:

SLD	Earthquake Name	Date	Mw	Fault Mechanism	Epicentral Distance [km]	EC8 Site class
	Alkion	24/02/1981	6.6	normal	20	C
	Umbria Marche	26/09/1997	6	normal	22	C
	Basso Tirreno	15/04/1978	6	oblique	18	C
	Ano Liosia	07/09/1999	6	normal	19	C
	Umbria Marche	26/09/1997	6	normal	27	C
	Dinar	01/10/1995	6.4	normal	8	C
	Alkion	25/02/1981	6.3	normal	25	C
Mean			6.185714		19.85714	

Life safety limit state (SLV) ground motions set:

SLV	Earthquake Name	Date	Mw	Fault Mechanism	Epicentral Distance [km]	EC8 Site class
	Alkion	29641	6.6	normal	20	C
	Umbria Marche	35699	6	normal	22	C
	Izmit (aftershock)	36416	5.8	oblique	27	C
	Friuli (aftershock)	28018	6	thrust	9	C
	Izmit (aftershock)	36416	5.8	oblique	25	C
	Dinar	34973	6.4	normal	8	C
	Izmit (aftershock)	36416	5.8	oblique	26	C
Mean			6.05714286		19.57142857	

Collapse limit state (SLC) ground motions set:

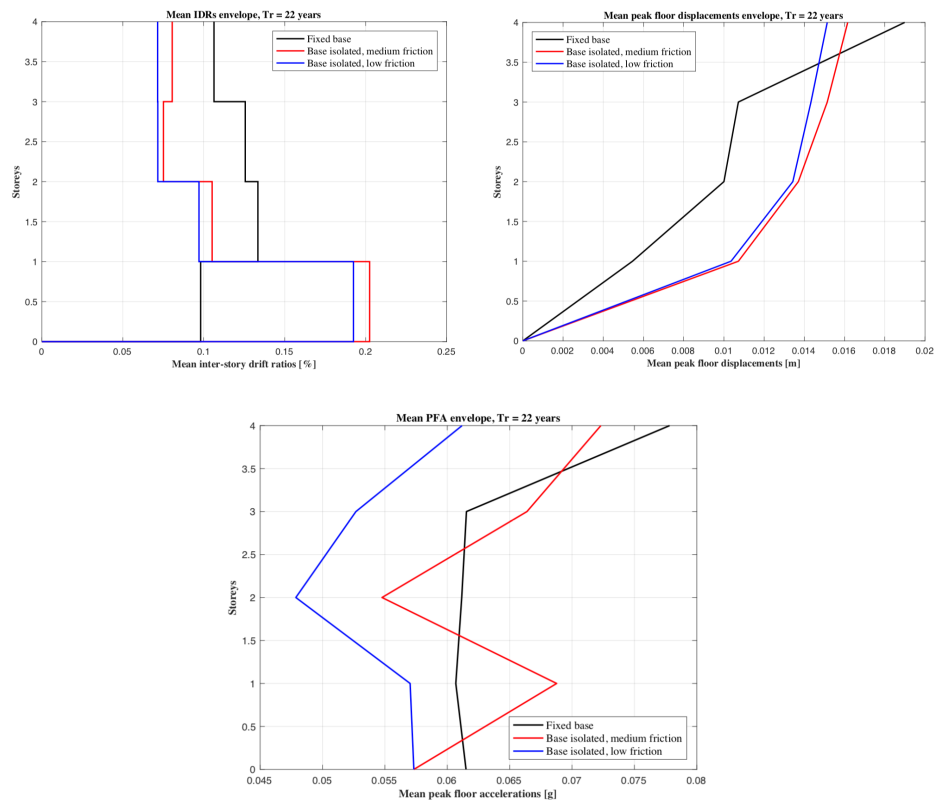
SLC	Earthquake Name	Date	Mw	Fault Mechanism	Epicentral Distance [km]	EC8 Site class
	Izmit (aftershock)	36416	5.8	oblique	27	C
	Alkion	29641	6.6	normal	19	C
	Adana	35973	6.3	strike slip	30	C
	Alkion	29642	6.3	normal	25	C
	Dinar	34973	6.4	normal	8	C
	Umbria Marche	35699	5.7	normal	25	C
	Izmit (aftershock)	36416	5.8	oblique	26	C
Mean			6.128571		22.85714	



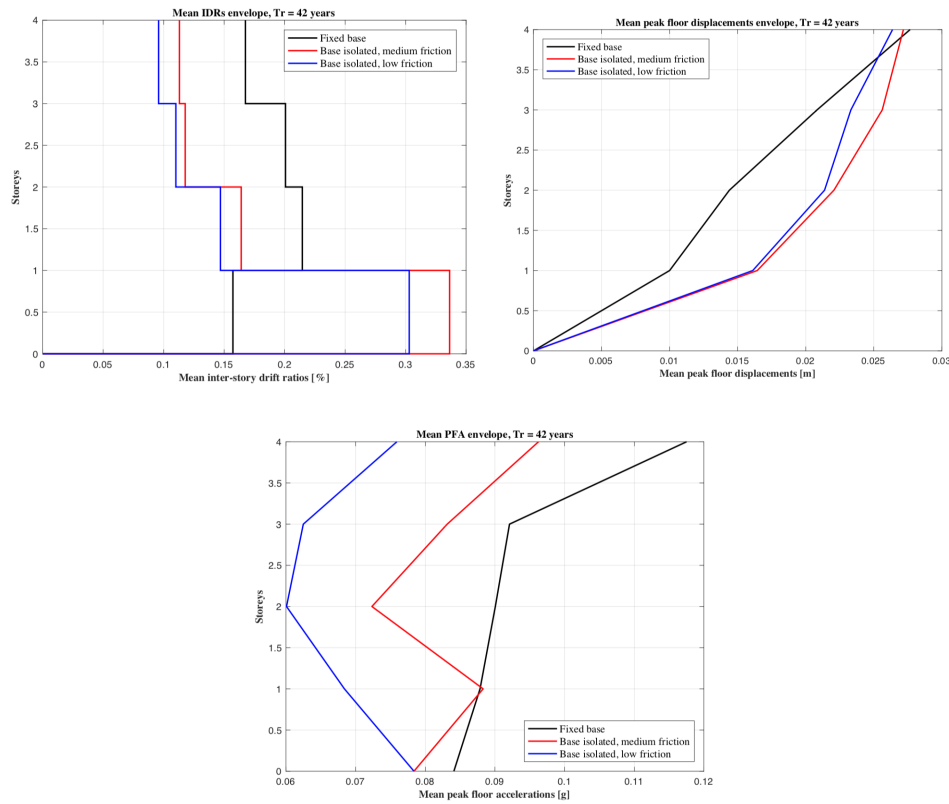
APPENDIX D

This Appendix contains the peak inter-storey drift, peak floor acceleration and peak floor displacement envelope comparisons for the remaining IM levels.

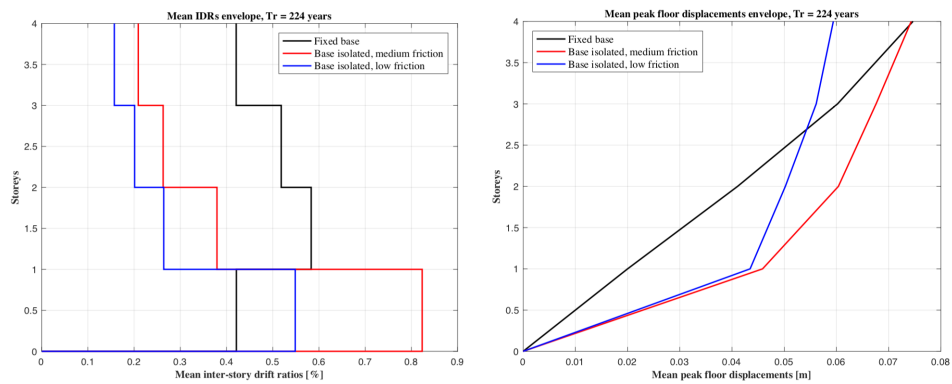
22-year return period:

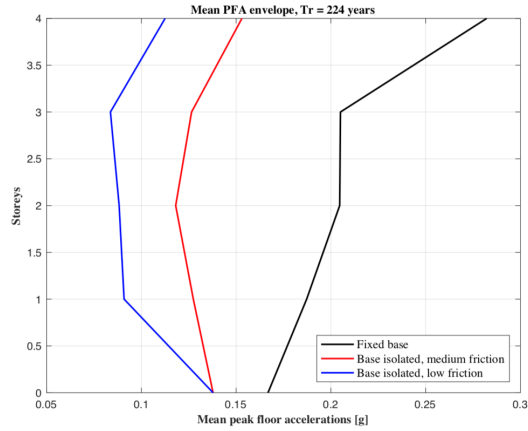


42-year return period:

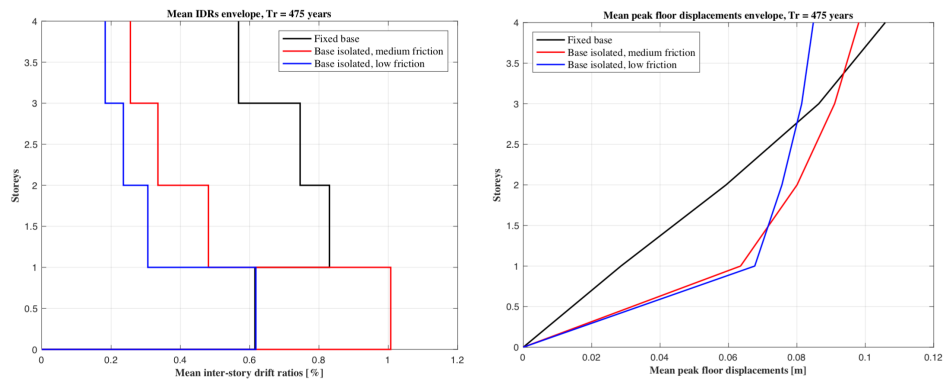


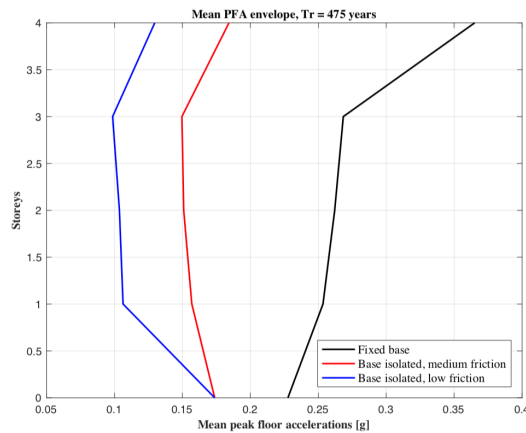
224-year return period:



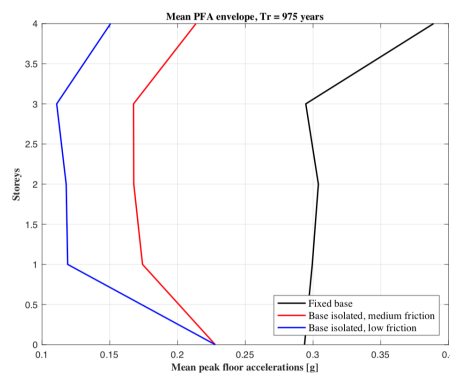
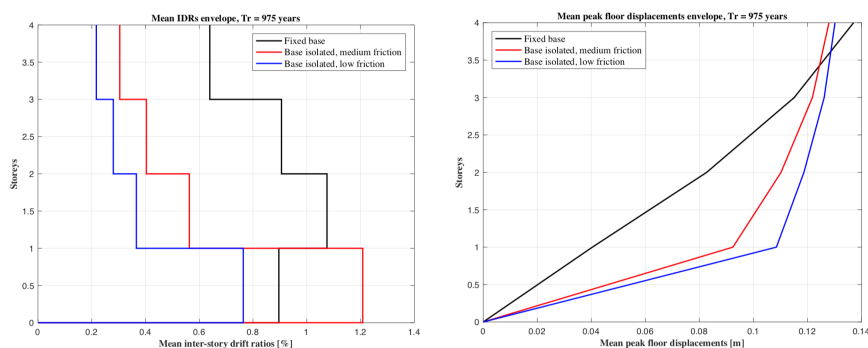


475-year return period:

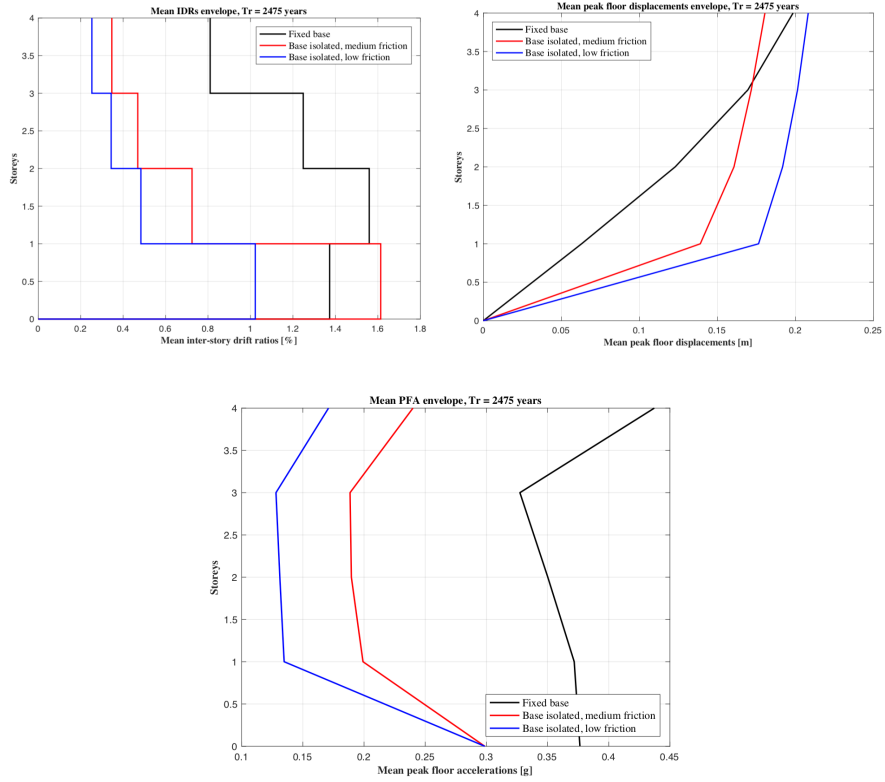




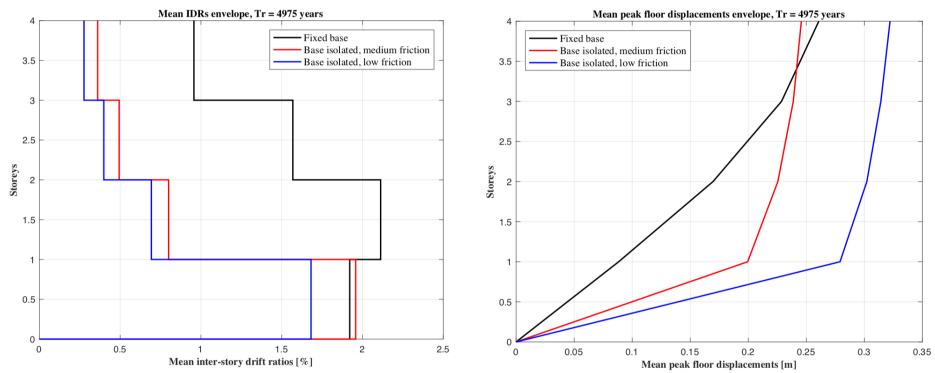
975-year return period:

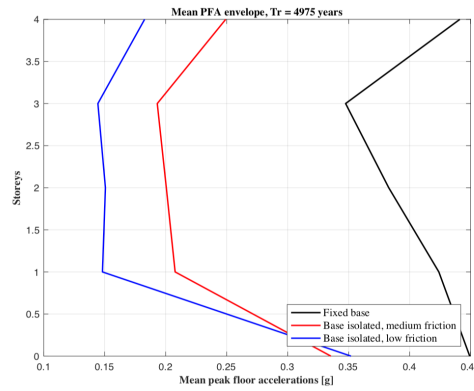


2475-year return period:

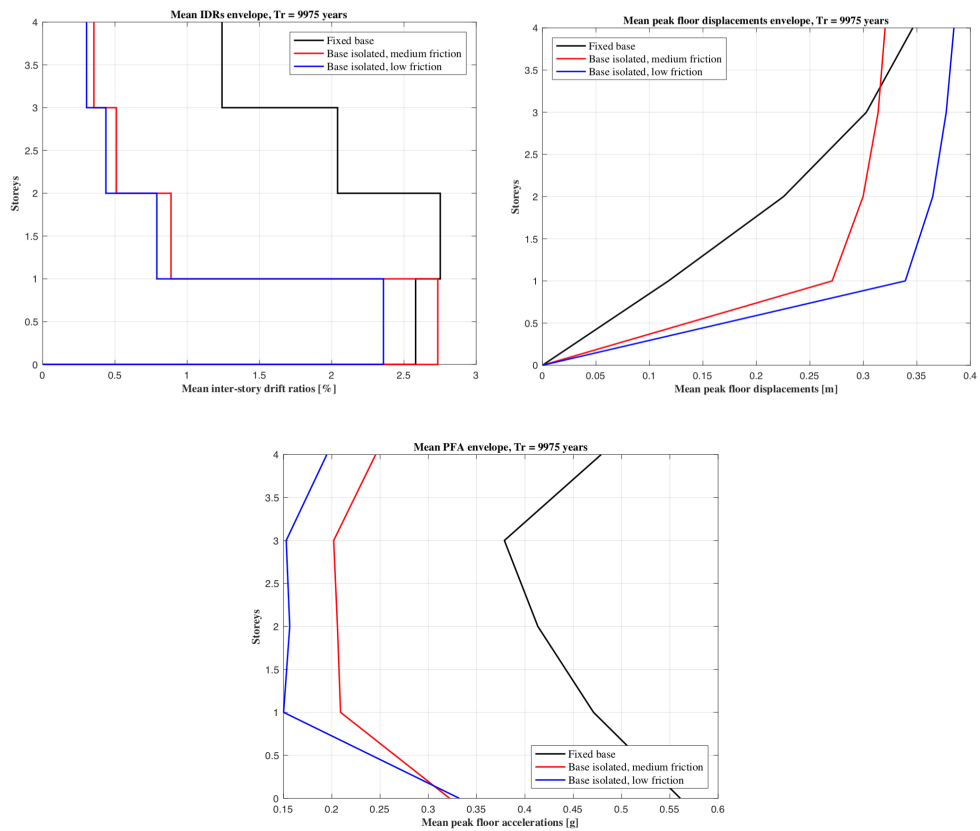


4957-year return period:





9975-year return period:





UNIVERSITÀ
DI PAVIA



IUSS

APPENDIX E

This Appendix contains the used EDP-DV functions, for low-rise ductile RC perimeter moment frames with building occupancy, from (Ramirez, 2009), respectively defined for first, typical and top floor.

EDP-DV Function Data

Building Height: Low-rise (1 to 5 stories)

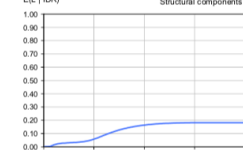
Structural Material: Ductile reinforced-concrete

Structural System: Perimeter moment-frame

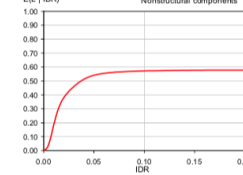
Occupancy: Office

Floor Type: 1st Floor

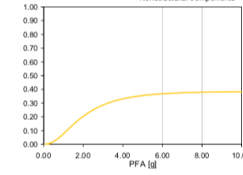
EDL | IDR Structural components



EDL | IDR Nonstructural components



EDL | PFA Nonstructural components



Loss Functions

EDL | IDR | PFA

EDP-DV Function Data

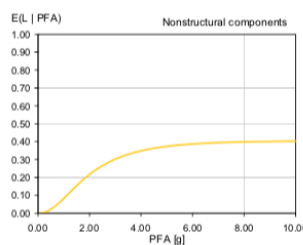
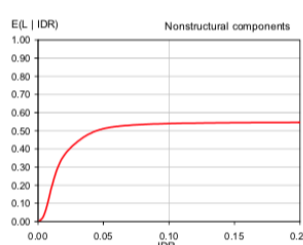
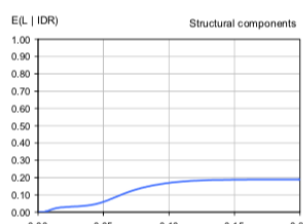
Building Height: Low-rise (1 to 5 stories)

Structural Material: Ductile reinforced-concrete

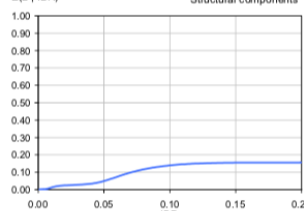
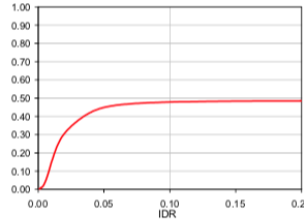
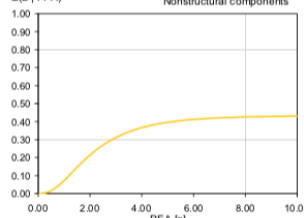
Structural System: Perimeter moment-frame

© 2010 Pearson Education, Inc.

Occupancy: Once



IDR	Loss Functions						IDR	Loss Functions (cont'd)					
	E(Loss)	I(DR)	E(Loss)	I(DR)	PFA	E(Loss) / PFA		E(Loss)	I(DR)	E(Loss)	I(DR)	PFA	E(Loss) / PFA
0.001	0.000	0.001	0.002	0.005	0.000	0.000	0.101	0.170	0.101	0.540	6.05	0.374	
0.002	0.000	0.002	0.009	0.010	0.000	0.000	0.102	0.171	0.102	0.540	5.10	0.375	
0.003	0.000	0.003	0.015	0.025	0.001	0.000	0.103	0.172	0.103	0.540	5.15	0.376	
0.004	0.001	0.005	0.026	0.045	0.002	0.000	0.104	0.173	0.104	0.540	5.20	0.377	
0.005	0.002	0.005	0.042	0.055	0.004	0.000	0.105	0.174	0.105	0.540	5.25	0.378	
0.006	0.003	0.006	0.064	0.070	0.007	0.000	0.106	0.175	0.106	0.540	5.30	0.378	
0.007	0.004	0.007	0.085	0.080	0.010	0.000	0.107	0.176	0.107	0.540	5.35	0.378	
0.008	0.005	0.008	0.119	0.140	0.010	0.000	0.108	0.177	0.108	0.541	5.40	0.380	
0.009	0.009	0.011	0.148	0.145	0.018	0.000	0.109	0.177	0.109	0.541	5.45	0.381	
0.010	0.015	0.010	0.177	0.150	0.022	0.000	0.110	0.177	0.110	0.541	5.50	0.381	
0.011	0.017	0.011	0.205	0.155	0.027	0.000	0.111	0.178	0.111	0.541	5.55	0.382	
0.012	0.020	0.012	0.231	0.160	0.032	0.000	0.112	0.179	0.112	0.541	5.60	0.382	
0.013	0.023	0.013	0.256	0.165	0.037	0.000	0.113	0.180	0.113	0.541	5.65	0.382	
0.014	0.024	0.014	0.276	0.170	0.043	0.000	0.114	0.180	0.114	0.542	5.70	0.384	
0.015	0.025	0.015	0.296	0.175	0.049	0.000	0.115	0.180	0.115	0.542	5.75	0.384	
0.016	0.026	0.016	0.313	0.180	0.055	0.000	0.116	0.181	0.116	0.542	5.80	0.384	
0.017	0.027	0.017	0.329	0.185	0.062	0.000	0.117	0.181	0.117	0.542	5.85	0.385	
0.018	0.028	0.018	0.345	0.190	0.068	0.000	0.118	0.182	0.118	0.542	5.90	0.385	
0.019	0.029	0.019	0.354	0.195	0.076	0.000	0.119	0.182	0.119	0.542	5.95	0.386	
0.020	0.029	0.020	0.365	0.160	0.083	0.000	0.120	0.183	0.120	0.542	6.00	0.387	
0.021	0.030	0.021	0.375	1.05	0.090	0.000	0.121	0.183	0.121	0.542	6.05	0.387	
0.022	0.030	0.022	0.384	1.10	0.105	0.000	0.122	0.183	0.122	0.542	6.10	0.388	
0.023	0.031	0.023	0.394	1.15	0.109	0.000	0.123	0.184	0.123	0.542	6.15	0.388	
0.024	0.031	0.024	0.400	1.20	0.112	0.000	0.124	0.184	0.124	0.543	6.20	0.389	
0.025	0.031	0.025	0.407	1.25	0.119	0.000	0.125	0.184	0.125	0.543	6.25	0.389	
0.026	0.032	0.026	0.414	1.30	0.126	0.000	0.126	0.184	0.126	0.543	6.30	0.389	
0.027	0.033	0.027	0.420	1.35	0.131	0.000	0.127	0.185	0.127	0.543	6.35	0.390	
0.028	0.033	0.028	0.427	1.40	0.138	0.000	0.128	0.185	0.128	0.543	6.40	0.390	
0.029	0.033	0.029	0.433	1.45	0.147	0.000	0.129	0.185	0.129	0.543	6.45	0.391	
0.030	0.034	0.030	0.439	1.50	0.154	0.000	0.130	0.186	0.130	0.543	6.50	0.391	
0.031	0.034	0.031	0.444	1.55	0.161	0.000	0.131	0.186	0.131	0.543	6.55	0.391	
0.032	0.034	0.032	0.449	1.60	0.169	0.000	0.132	0.186	0.132	0.543	6.60	0.391	
0.033	0.036	0.033	0.455	1.65	0.174	0.000	0.133	0.186	0.133	0.543	6.65	0.392	
0.034	0.036	0.034	0.460	1.70	0.181	0.000	0.134	0.186	0.134	0.543	6.70	0.392	
0.035	0.037	0.035	0.465	1.75	0.187	0.000	0.135	0.186	0.135	0.543	6.75	0.393	
0.036	0.037	0.036	0.470	1.80	0.193	0.000	0.136	0.187	0.136	0.543	6.80	0.393	
0.037	0.037	0.037	0.475	1.85	0.199	0.000	0.137	0.187	0.137	0.543	6.85	0.393	
0.038	0.039	0.038	0.478	1.90	0.205	0.000	0.138	0.187	0.138	0.543	6.90	0.394	
0.039	0.040	0.038	0.482	1.95	0.211	0.000	0.139	0.187	0.139	0.544	6.95	0.394	
0.040	0.041	0.040	0.486	2.00	0.217	0.000	0.140	0.187	0.140	0.544	7.00	0.394	
0.041	0.042	0.041	0.489	2.05	0.222	0.000	0.141	0.187	0.141	0.544	7.05	0.394	
0.042	0.044	0.042	0.494	2.10	0.227	0.000	0.142	0.187	0.142	0.544	7.10	0.394	
0.043	0.045	0.043	0.495	2.15	0.233	0.000	0.143	0.187	0.143	0.544	7.15	0.395	
0.044	0.047	0.044	0.498	2.20	0.238	0.000	0.144	0.187	0.144	0.544	7.20	0.395	
0.045	0.049	0.045	0.501	2.25	0.243	0.000	0.145	0.188	0.145	0.544	7.25	0.395	
0.046	0.051	0.046	0.503	2.30	0.247	0.000	0.146	0.188	0.146	0.544	7.30	0.396	
0.047	0.051	0.047	0.504	2.35	0.252	0.000	0.147	0.188	0.147	0.544	7.35	0.396	
0.048	0.048	0.050	0.507	2.40	0.257	0.000	0.148	0.188	0.148	0.544	7.40	0.396	
0.049	0.057	0.049	0.509	2.45	0.261	0.000	0.149	0.188	0.149	0.544	7.45	0.396	
0.050	0.060	0.050	0.511	2.50	0.265	0.000	0.150	0.188	0.150	0.544	7.50	0.397	
0.051	0.061	0.051	0.512	2.55	0.269	0.000	0.151	0.188	0.151	0.544	7.55	0.397	
0.052	0.064	0.052	0.514	2.60	0.274	0.000	0.152	0.188	0.152	0.544	7.60	0.397	
0.053	0.065	0.053	0.516	2.65	0.278	0.000	0.153	0.188	0.153	0.544	7.65	0.397	
0.054	0.071	0.055	0.517	2.70	0.281	0.000	0.154	0.188	0.154	0.544	7.70	0.397	
0.055	0.074	0.056	0.518	2.75	0.285	0.000	0.155	0.188	0.155	0.544	7.75	0.398	
0.056	0.075	0.057	0.519	2.80	0.289	0.000	0.156	0.188	0.156	0.544	7.80	0.398	
0.057	0.080	0.057	0.521	2.85	0.292	0.000	0.157	0.188	0.157	0.544	7.85	0.398	
0.058	0.084	0.058	0.522	2.90	0.296	0.000	0.158	0.188	0.158	0.544	7.90	0.398	
0.059	0.087	0.059	0.523	2.95	0.299	0.000	0.159	0.188	0.159	0.544	7.95	0.398	
0.060	0.090	0.060	0.523	3.00	0.302	0.000	0.160	0.188	0.160	0.544	8.00	0.398	
0.061	0.091	0.061	0.524	3.05	0.306	0.000	0.161	0.188	0.161	0.544	8.05	0.398	
0.062	0.096	0.062	0.525	3.10	0.308	0.000	0.162	0.189	0.162	0.544	8.10	0.399	
0.063	0.099	0.063	0.526	3.15	0.311	0.000	0.163	0.189	0.163	0.545	8.15	0.399	
0.064	0.102	0.064	0.526	3.15	0.314	0.000	0.164	0.189	0.164	0.545	8.20	0.399	
0.065	0.103	0.065	0.527	3.20	0.317	0.000	0.165	0.189	0.165	0.545	8.25	0.399	
0.066	0.108	0.068	0.528	3.30	0.320	0.000	0.166	0.189	0.166	0.545	8.30	0.399	
0.067	0.111	0.067	0.529	3.35	0.322	0.000	0.167	0.189	0.167	0.545	8.35	0.399	
0.068	0.114	0.068	0.529	3.40	0.324	0.000	0.168	0.189	0.168	0.545	8.40	0.399	
0.069	0.117	0.069	0.530	3.45	0.327	0.000	0.169	0.189	0.169	0.545	8.45	0.400	
0.070	0.120	0.071	0.531	3.50	0.330	0.000	0.170	0.189	0.170	0.545	8.50	0.400	
0.071	0.122	0.071	0.531	3.55	0.331	0.000	0.171	0.189	0.171	0.545	8.55	0.401	
0.072	0.124	0.072	0.531	3.60	0.333	0.000	0.172	0.189	0.172	0.545	8.60	0.400	
0.073	0.127	0.073	0.532	3.65	0.336	0.000	0.173	0.189	0.173	0.545	8.65	0.400	
0.074	0.129	0.074	0.532	3.70	0.338	0.000	0.174	0.189	0.174	0.545	8.70	0.401	
0.075	0.131	0.075	0.533	3.75	0.341	0.000	0.175	0.189	0.175	0.545	8.75	0.401	
0.076	0.134	0.076	0.533	3.80	0.341	0.000	0.176	0.189	0.176	0.545	8.80	0.400	
0.077	0.136	0.077	0.533	3.85	0.343	0.000	0.177	0.189	0.177	0.545	8.85	0.400	
0.078	0.136	0.078	0.534	3.90	0.345	0.000	0.178	0.189	0.178	0.545	8.90	0.401	
0.079	0.140	0.079	0.534	3.95	0.347	0.000	0.179	0.189	0.179	0.545	8.95	0.401	
0.080	0.144	0.081	0.535	4.05	0.350	0.000	0.180	0.189	0.181	0.545	9.05	0.401	
0.082	0.145	0.082	0.535	4.10	0.352	0.000	0.182	0.189	0.182	0.545	9.10	0.401	
0.083	0.147	0.084	0.535	4.15	0.353	0.000	0.183	0.189	0.183	0.545	9.15	0.401	
0.084	0.148	0.084	0.536	4.20	0.356	0.000	0.184	0.189	0.184	0.545	9.20	0.401	
0.085	0.150	0.085	0.536	4.25	0.358	0.000	0.185	0.189	0.185	0.545	9.25	0.401	
0.086	0.152	0.086	0.536	4.30	0.359	0.000	0.186	0.189	0.186	0.545	9.30	0.401	
0.087	0.154	0.087	0.537	4.35	0.359	0.000	0.187	0.189	0.187	0.545	9.35	0.401	
0.088	0.155	0.088	0.537	4.40	0.360	0.000	0.188	0.189	0.188	0.545	9.40	0.401	
0.089	0.156	0.089	0.537	4.45	0.362	0.000	0.189	0.189	0.189	0.545	9.45	0.401	
0.090	0.159	0.090	0.537	4.50	0.363	0.000	0.190	0.189	0.190	0.545			

EDP-DV Function Data**Building Height:** Low-rise (1 to 5 stories)**Structural Material:** Ductile reinforced-concrete**Structural System:** Perimeter moment-frame**Occupancy:** Office**Floor Type:** Top Floor**E(L | IDR)** Structural components**E(L | IDR)** Nonstructural components**E(L | PFA)** Nonstructural components

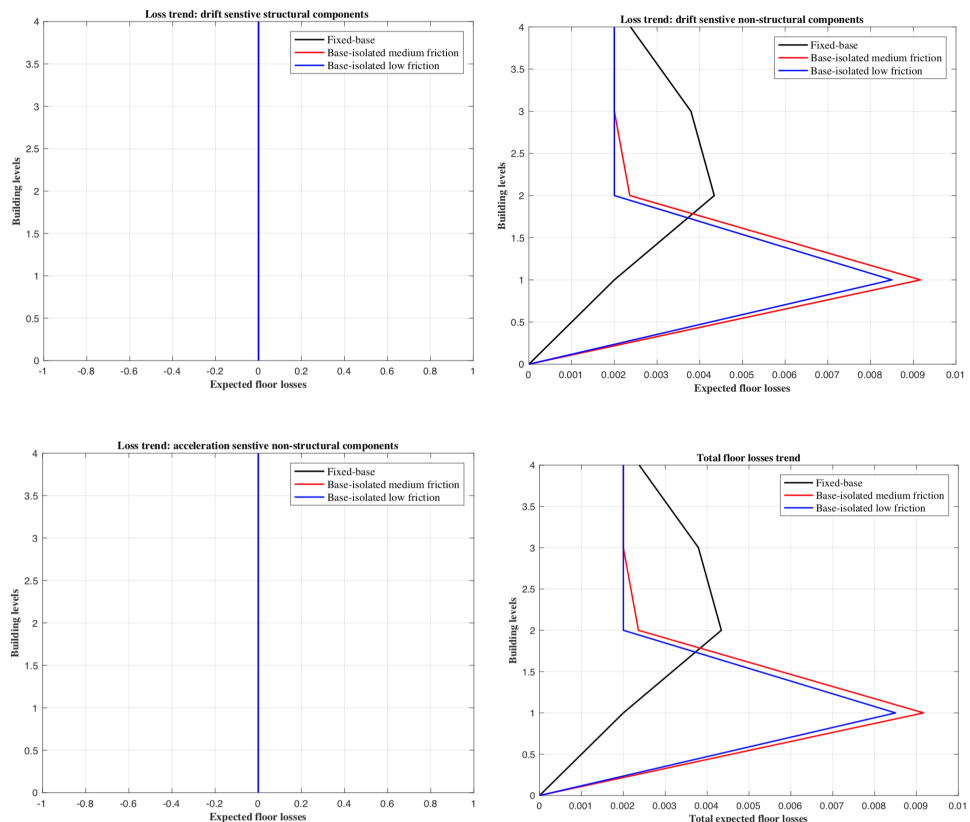
Loss Functions				Loss Functions (conf d)			
IDR	E(L ₁ IDR)	IDR	E(L ₁₀ IDR)	IDR	E(L ₁ IDR)	IDR	E(L ₁₀ PFA)
0.01	0.000	0.000	0.000	0.000	0.000	0.000	0.307
0.002	0.000	0.002	0.007	0.10	0.000	0.141	0.398
0.003	0.000	0.003	0.013	0.15	0.000	0.103	0.399
0.004	0.001	0.004	0.021	0.20	0.001	0.104	0.400
0.005	0.001	0.005	0.034	0.25	0.000	0.105	0.401
0.006	0.003	0.006	0.052	0.30	0.000	0.106	0.402
0.007	0.005	0.007	0.074	0.35	0.007	0.107	0.403
0.008	0.007	0.008	0.097	0.40	0.010	0.108	0.404
0.009	0.009	0.009	0.122	0.45	0.013	0.109	0.405
0.010	0.012	0.010	0.146	0.50	0.016	0.110	0.405
0.011	0.014	0.011	0.169	0.55	0.020	0.111	0.406
0.012	0.016	0.012	0.191	0.60	0.023	0.112	0.407
0.013	0.018	0.013	0.211	0.65	0.029	0.113	0.407
0.014	0.020	0.014	0.231	0.70	0.034	0.114	0.408
0.015	0.021	0.015	0.246	0.75	0.040	0.115	0.409
0.016	0.021	0.016	0.261	0.80	0.046	0.116	0.410
0.017	0.022	0.017	0.275	0.85	0.052	0.117	0.410
0.018	0.023	0.018	0.287	0.90	0.059	0.118	0.411
0.019	0.024	0.019	0.300	0.95	0.065	0.119	0.411
0.020	0.024	0.020	0.307	1.00	0.072	0.120	0.412
0.021	0.024	0.021	0.315	1.05	0.079	0.121	0.413
0.022	0.025	0.022	0.324	1.10	0.086	0.122	0.413
0.023	0.025	0.023	0.331	1.15	0.094	0.123	0.414
0.024	0.025	0.024	0.338	1.20	0.102	0.124	0.414
0.025	0.026	0.025	0.345	1.25	0.109	0.125	0.415
0.026	0.026	0.026	0.351	1.30	0.113	0.126	0.415
0.027	0.027	0.027	0.358	1.35	0.123	0.127	0.416
0.028	0.027	0.028	0.364	1.40	0.131	0.128	0.416
0.029	0.027	0.028	0.370	1.45	0.137	0.129	0.417
0.030	0.028	0.029	0.376	1.50	0.146	0.130	0.417
0.031	0.028	0.031	0.381	1.55	0.153	0.131	0.418
0.032	0.029	0.032	0.387	1.60	0.160	0.132	0.418
0.033	0.029	0.033	0.392	1.65	0.167	0.133	0.418
0.034	0.030	0.034	0.397	1.70	0.174	0.134	0.419
0.035	0.030	0.035	0.402	1.75	0.181	0.135	0.419
0.036	0.031	0.036	0.406	1.80	0.188	0.136	0.420
0.037	0.031	0.037	0.411	1.85	0.194	0.137	0.420
0.038	0.031	0.037	0.416	1.90	0.201	0.138	0.420
0.039	0.033	0.039	0.419	1.95	0.207	0.139	0.421
0.040	0.034	0.040	0.423	2.00	0.214	0.140	0.421
0.041	0.035	0.041	0.426	2.05	0.220	0.141	0.421
0.042	0.036	0.042	0.429	2.10	0.226	0.142	0.422
0.043	0.036	0.042	0.432	2.15	0.231	0.143	0.422
0.044	0.039	0.044	0.435	2.20	0.237	0.144	0.422
0.045	0.040	0.045	0.438	2.25	0.243	0.145	0.422
0.046	0.042	0.046	0.440	2.30	0.248	0.146	0.423
0.047	0.043	0.047	0.443	2.35	0.254	0.147	0.423
0.048	0.044	0.048	0.446	2.40	0.259	0.148	0.423
0.049	0.047	0.047	0.447	2.45	0.264	0.149	0.424
0.050	0.049	0.049	0.449	2.50	0.269	0.150	0.424
0.051	0.051	0.051	0.450	2.55	0.274	0.151	0.424
0.052	0.052	0.052	0.452	2.60	0.278	0.152	0.424
0.053	0.056	0.053	0.453	2.65	0.283	0.153	0.425
0.054	0.059	0.054	0.455	2.70	0.287	0.154	0.425
0.055	0.061	0.055	0.456	2.75	0.292	0.155	0.425
0.056	0.064	0.056	0.457	2.80	0.299	0.156	0.425
0.057	0.064	0.057	0.458	2.85	0.304	0.156	0.426
0.058	0.069	0.058	0.460	2.90	0.304	0.157	0.426
0.059	0.071	0.059	0.461	2.95	0.308	0.159	0.426
0.060	0.074	0.060	0.462	3.00	0.311	0.160	0.426
0.061	0.077	0.061	0.462	3.05	0.315	0.161	0.426
0.062	0.078	0.062	0.463	3.10	0.318	0.162	0.426
0.063	0.082	0.063	0.464	3.15	0.322	0.163	0.427
0.064	0.084	0.064	0.465	3.20	0.325	0.164	0.427
0.065	0.087	0.065	0.467	3.25	0.328	0.165	0.427
0.066	0.089	0.066	0.468	3.30	0.331	0.166	0.427
0.067	0.087	0.067	0.467	3.35	0.334	0.167	0.427
0.068	0.094	0.068	0.467	3.40	0.337	0.168	0.427
0.069	0.096	0.069	0.468	3.45	0.340	0.169	0.428
0.070	0.098	0.070	0.469	3.50	0.346	0.170	0.428
0.071	0.100	0.071	0.470	3.55	0.346	0.171	0.428
0.072	0.102	0.072	0.470	3.60	0.348	0.172	0.428
0.073	0.104	0.073	0.470	3.65	0.351	0.173	0.428
0.074	0.106	0.074	0.471	3.70	0.353	0.174	0.428
0.075	0.108	0.075	0.471	3.75	0.356	0.175	0.428
0.076	0.110	0.076	0.471	3.80	0.359	0.176	0.428
0.077	0.112	0.077	0.472	3.85	0.360	0.177	0.428
0.078	0.113	0.078	0.472	3.90	0.362	0.178	0.428
0.079	0.115	0.079	0.473	3.95	0.363	0.179	0.429
0.080	0.116	0.080	0.473	4.00	0.366	0.180	0.429
0.081	0.117	0.081	0.473	4.05	0.368	0.181	0.429
0.082	0.120	0.082	0.474	4.10	0.370	0.182	0.429
0.083	0.121	0.083	0.474	4.15	0.372	0.183	0.429
0.084	0.122	0.084	0.474	4.20	0.374	0.184	0.429
0.085	0.124	0.085	0.475	4.25	0.376	0.185	0.429
0.086	0.125	0.086	0.475	4.30	0.377	0.186	0.430
0.087	0.126	0.087	0.475	4.35	0.379	0.187	0.430
0.088	0.127	0.088	0.476	4.40	0.380	0.188	0.430
0.089	0.129	0.089	0.476	4.45	0.382	0.189	0.430
0.090	0.131	0.090	0.476	4.50	0.384	0.190	0.430
0.091	0.131	0.091	0.476	4.55	0.386	0.191	0.430
0.092	0.132	0.092	0.477	4.60	0.386	0.192	0.430
0.093	0.133	0.093	0.477	4.65	0.386	0.193	0.430
0.094	0.134	0.094	0.477	4.70	0.386	0.194	0.430
0.095	0.135	0.095	0.477	4.75	0.386	0.194	0.430
0.096	0.136	0.096	0.477	4.80	0.391	0.195	0.430
0.097	0.137	0.097	0.478	4.85	0.393	0.197	0.431
0.098	0.138	0.098	0.478	4.90	0.394	0.198	0.431
0.099	0.139	0.099	0.478	4.95	0.395	0.199	0.431
0.100	0.139	0.100	0.478	5.00	0.395	0.200	0.431



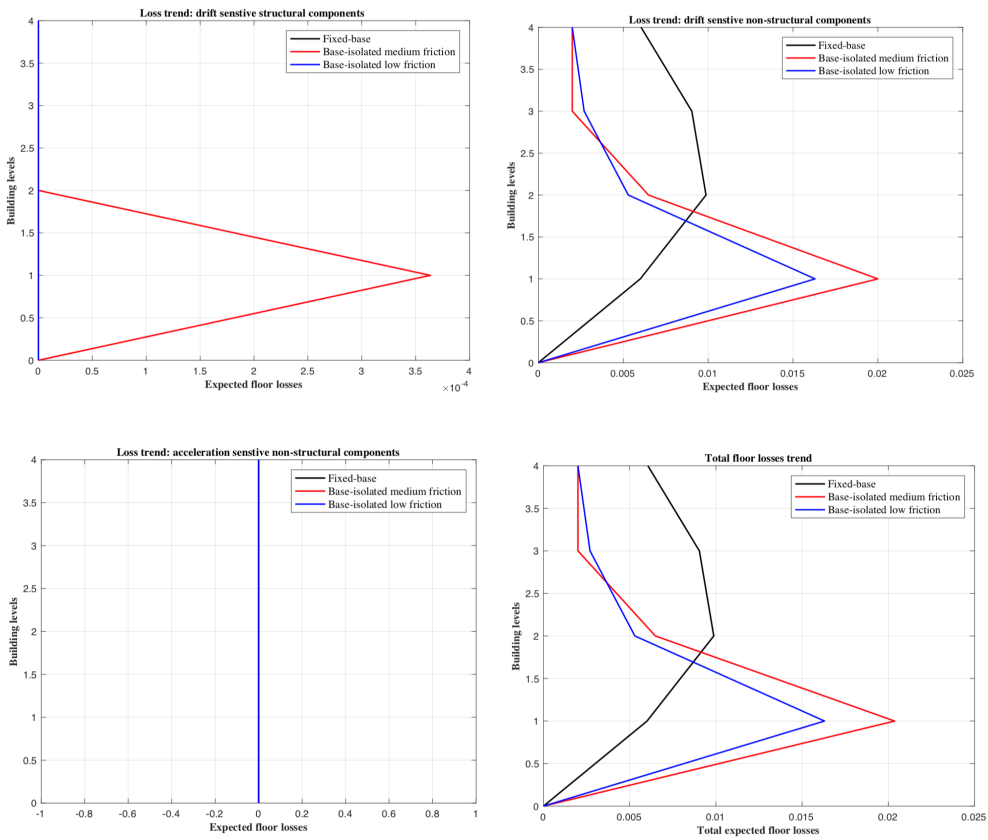
APPENDIX F

This Appendix contains the expected floor loss, for each damageable component, and total floor loss comparison for the remaining IM levels.

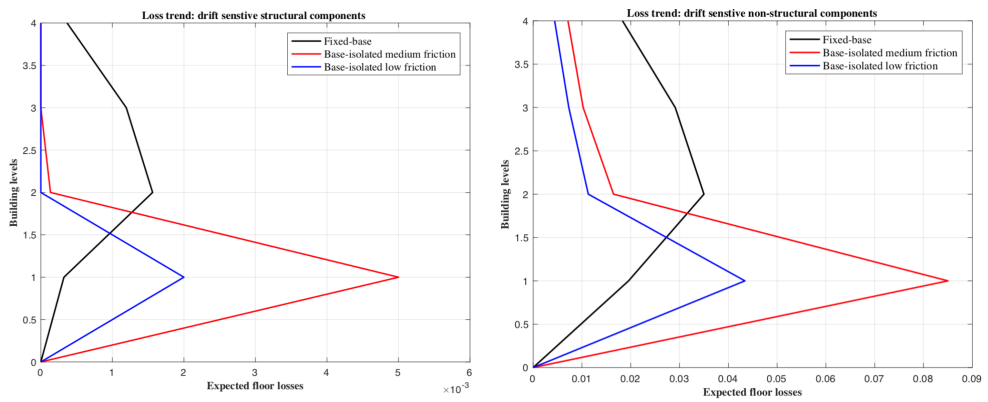
22-year return period:

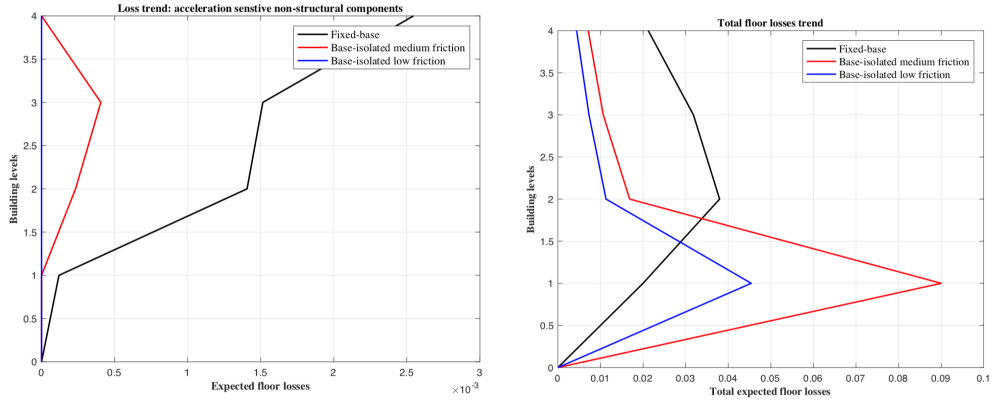


42-year return period:

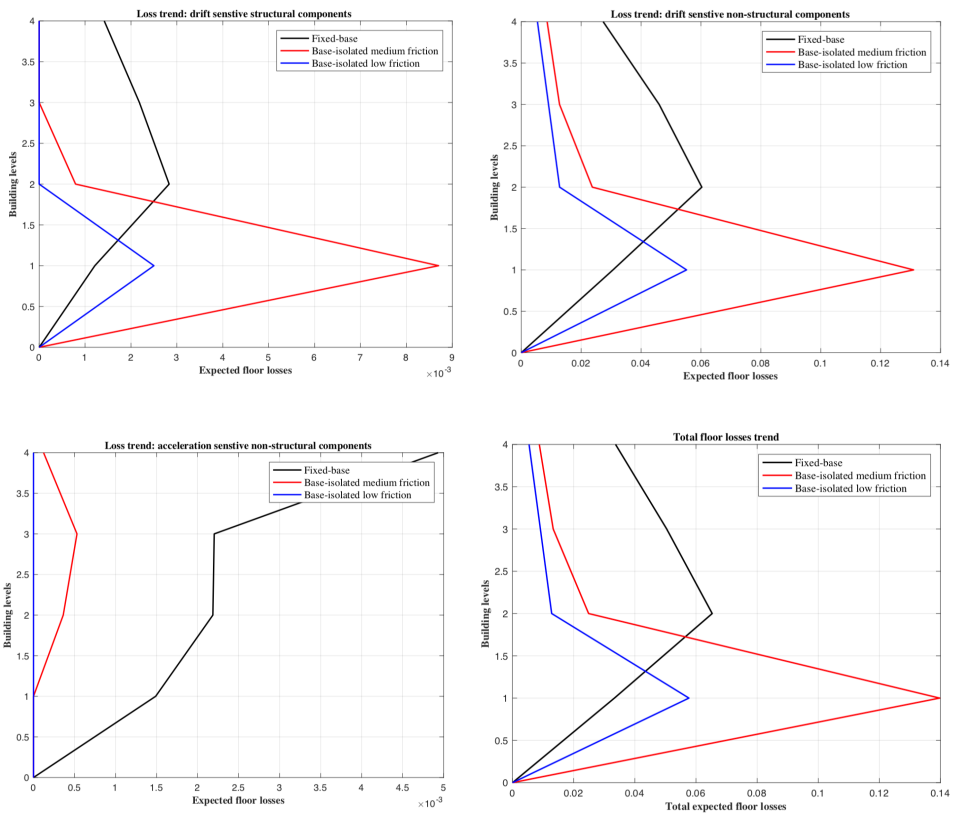


140-year return period:

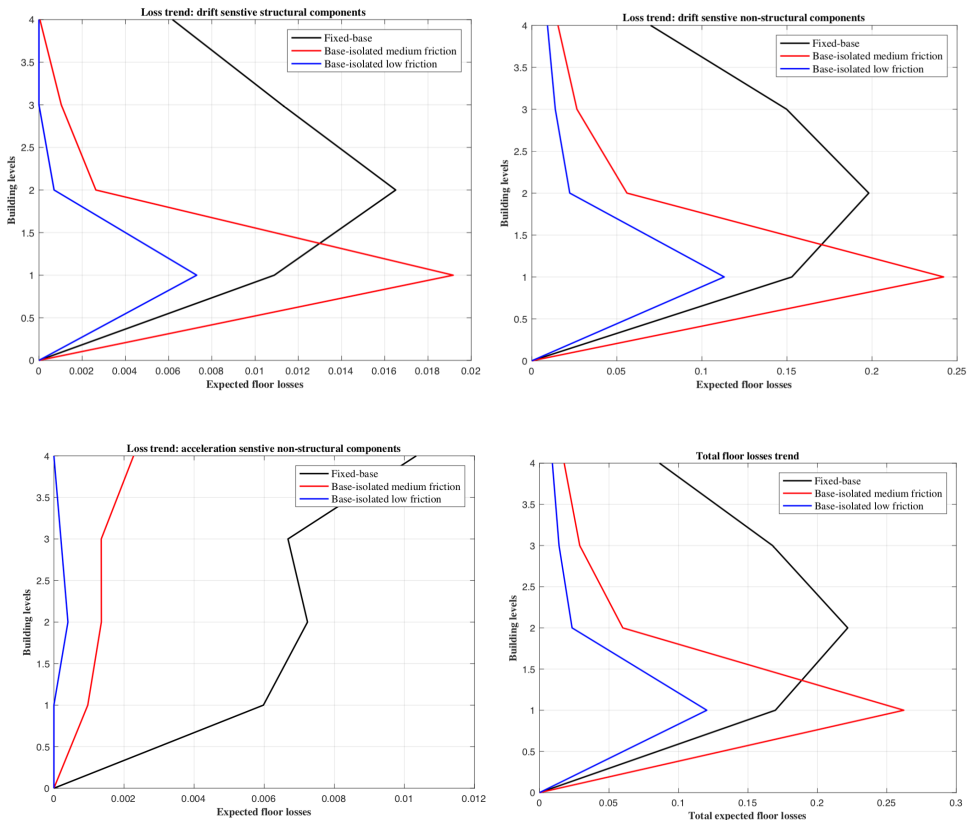




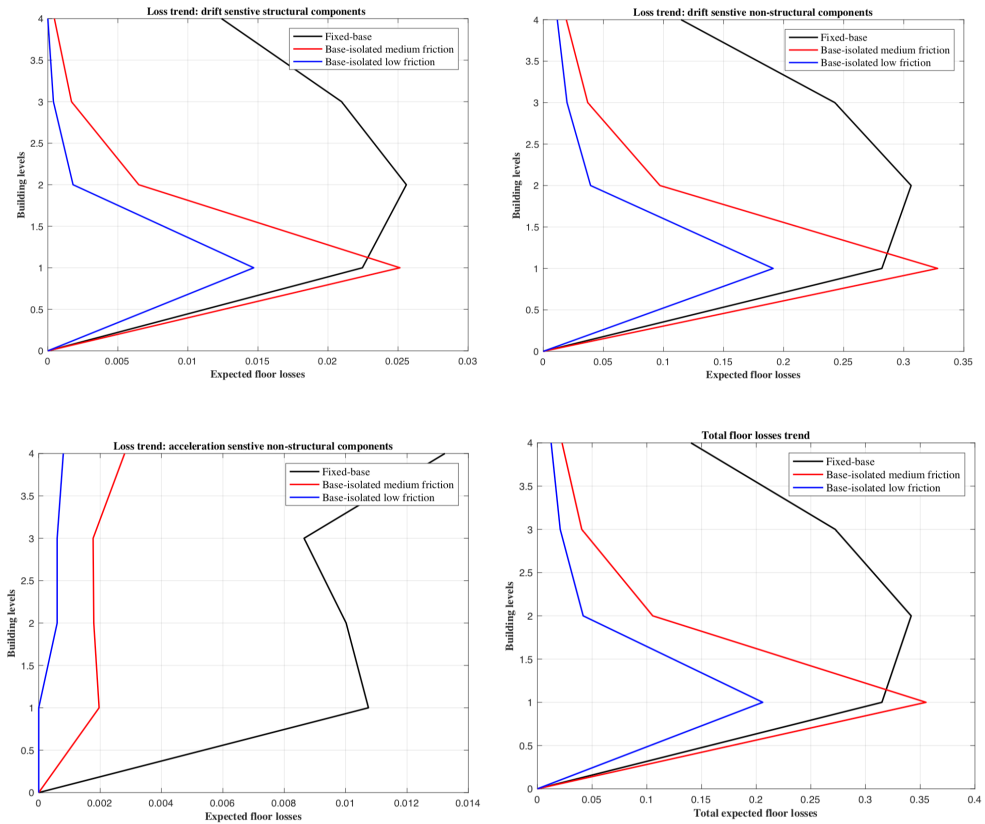
224-year return period:



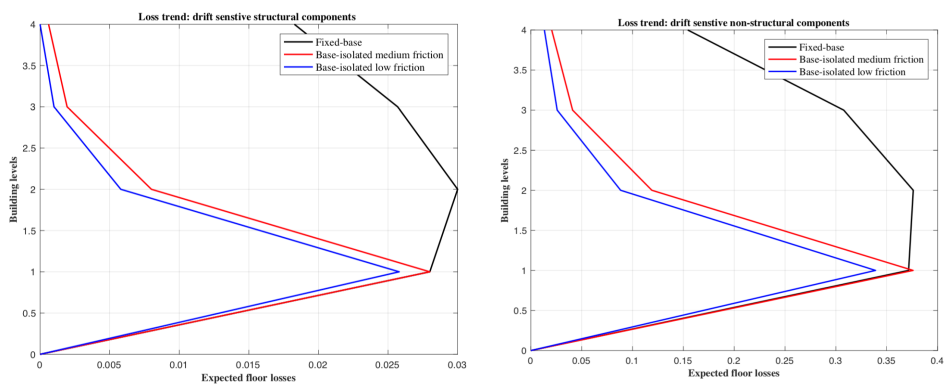
975-year return period:

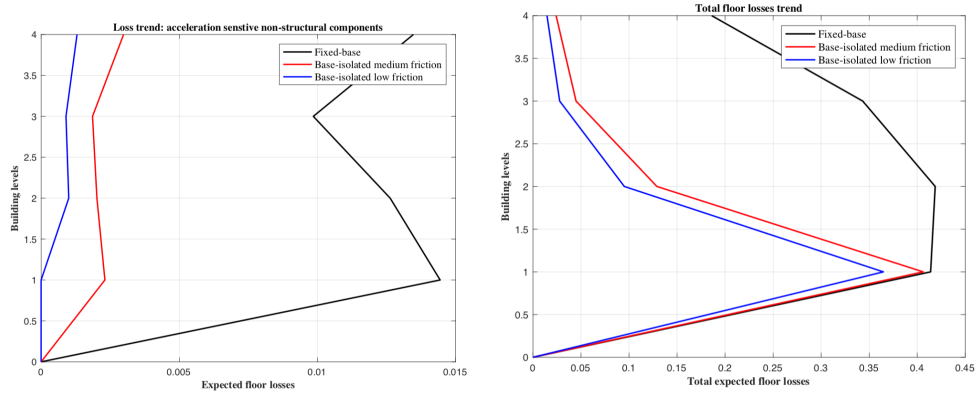


2475-year return period:



4975-year return period:





9975-year return period:

